THE USE OF TETHERS

FOR

PAYLOAD ORBITAL TRANSFER

CONTINUATION OF

INVESTIGATION OF ELECTRODYNAMIC STABILIZATION AND

CONTROL OF LONG ORBITING TETHERS

Contract NAS8-33691

Semiannual Progress Report

For the period 1 September 1981 through 28 February 1982

Volume II

Principal Investigator

Dr. Giuseppe Colombo

Co-Investigators

Dr. Manuel Martinez-Sanchez

Mr. David Arnold

Table of Contents

The Use of Tethers for Payload Orbital Transfer - Final Report on Subcontract SV1-52006 submitted to the Smithsonian Astrophysical Observatory by The Space Systems Laboratory of the Massachusetts Institute of Technology.

List of Figures

List of Figures (continued)

List of Tables

Introduction

This report presents the results of a study of "The Use of Tethers for Payload Orbital Transfer" and is Volume II of the Semi-Annual Report required by the contract. This work was carried out under Modification 5 of Contract NAS8-33691 originally titled "Investigation of Electrodynamic Stabilization and Control of Long Orbiting Tethers." Dr. Giuseppe Colombo is Principal Investigator on this contract. The Smithsonian Astrophysical Observatory (SAO), studied the dynamic behavior of the tether and the Massachusetts Institute of Technology (M.I.T.), under subcontract SVI-52006, studied the facilities and systems required for "The Use of Tethers for Payload Orbital Transfer." The results of the M.I.T. study are presented in Appendix A of this report.

The general introduction to the nature and applications of the present work can be found in the initial sections of Appendix A. The body of Appendix A contains detailed technical discussions of various tether systems. A numerical verification of some of the crucial dynamical calculations made in Appendix A is contained in the SAO work presented in the first part of this report.

Concurrent with this effort, SAO also performed, under Modification 4 of the same contract, "The Study of Certain Tether Safety Issues" also with Dr. Colombo as Principal Investigator. The results of that study are given in Volume I of this Semi-Annual Report.

The body of this report has been assembled from the monthly reports submitted under this contract revised and augmented where necessary for clarity and completeness. This report is intended to stand alone as a summary of the work done on "The Use of Tethers for Payload Orbital Transfer."

The author of this report is Mr. David A. Arnold. The author of Appendix A is Dr. Manuel Martinez-Sanchez.

2.0 Study Approach to Dynamic Behavior of the Tether

The SKYHOOK program has been used to do simulations of two cases considered in the M.I.T. study of the use of the tether for payload orbital transfer. The purpose of using SKYHOOK is to provide more detailed and realistic simulations of the cases considered in the theoretical studies done at M.I.T. In particular, there is the need to study oscillation of the system during the various operations. In the case of transporting a payload along the wire, the radial velocity introduces coriolis forces that could set up transverse oscillations of the system. These could be a problem especially as the payload approaches the end of the wire.

The use of an orbiting tether system by the Shuttle involves the operations of deployment and retrieval which may excite oscillation of the system. The SKYHOOK program has been used to verify the theoretical predictions of the orbits of the Shuttle, tether system, and payload made by M.I.T. and to determine the extent to which the results are influenced by librations of the system.

3.0 Payload Transport Along the Wire

One of the cases considered in the M.I.T. study is the transport of a payload along the tether from a heavy lower platform to an upper launching platform. A simulation has been done using the SKYHOOK program to study the dynamics of the system as the payload moves along the wire. We assume that the payload has a means of grasping the tether and controlling its speed of trans Since the net force due to the gradient of the gravitational and centripital forces is away from the center of gravity of the system, the payload will have to be dissipating energy for most of the trip from a heavy lower platform to the upper launching platform.

The simulation which has been done integrates the motion of three mass points - the base platform, the payload, and the upper launching platform. The mass of the tether is neglected. A constant transport speed of 10 m/sec has been used in this first simulation. The mass of the base platform is 300 tons, the payload is 30 tons, and the launching platform at the top is 10 tons. The altitude of the base is 300 km and the wire is 250 km long. The diameter of the wire was set to 2 mm, which is in fact not sufficient to withstand the tension load. The only effect of this assumption in the simulation is to make the wire more elastic than it would be with a thicker tether. For simplicity the integration has been started with the payload 1 km from the bottom moving at 10 m/sec. The startup phase has been neglected. The radial velocity results in coriolis forces that push the payload to the rear. Runs have been done for 100, 500, 2400, and 24000 seconds in order to approach the problem gradually in anticipation of possible instabilities.

The climbing of the payload along the wire has been simulated in the SKYHOOK program by making the natural length of each of the two wire segments a function of time. The initial lengths of the lower and upper segments of wire are chosen in such a way that they will be 1 and 249 km in length respectively when the system is stretched to equilibrium. At later times the length of the lower segments is computed as $l_1 + vt$ and the length of the upper segment is $l_1 - vt$, where v is the velocity of the payload and l_1 and l_2 are the initial lengths.

In the simulation, not too much happens in the first 100 seconds. Figure 1 shows the results for the first 500 seconds. Part a) is the in-plane motion vs. time, part b) is the tension and part c) is the radial vs. in-plane configuration at successive time intervals. Mass 1 is the lower platform, Mass 2 the upper platform, and Mass 3 the moving payload. Coriolis forces result in a displacement of the payload to the rear (positive in-plane

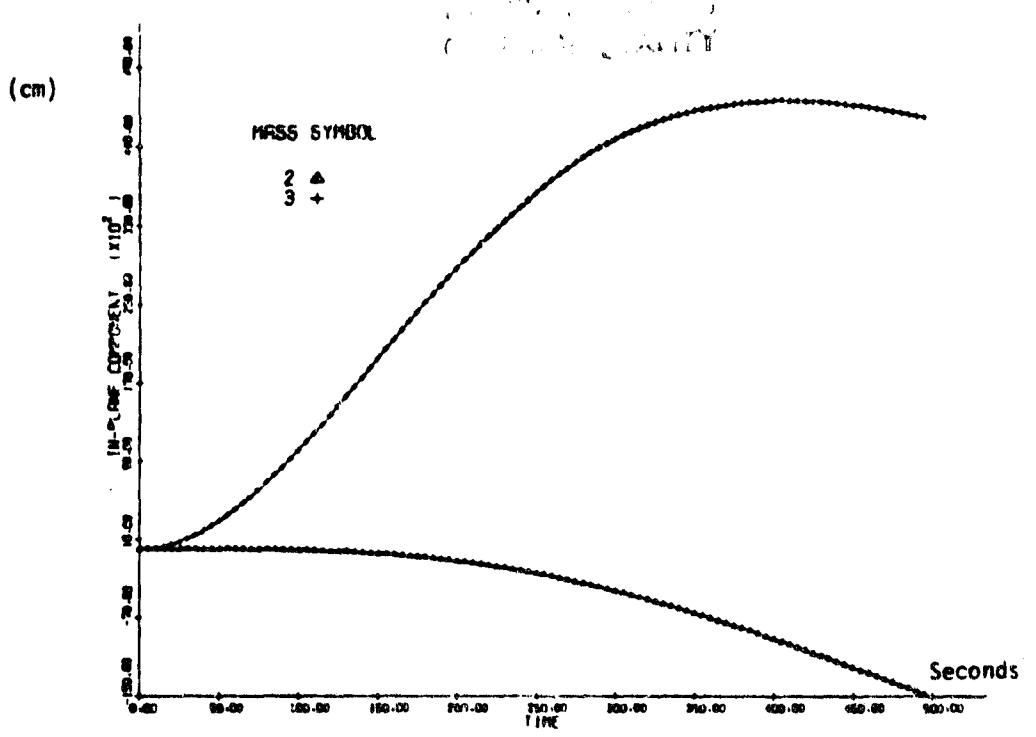

(a)

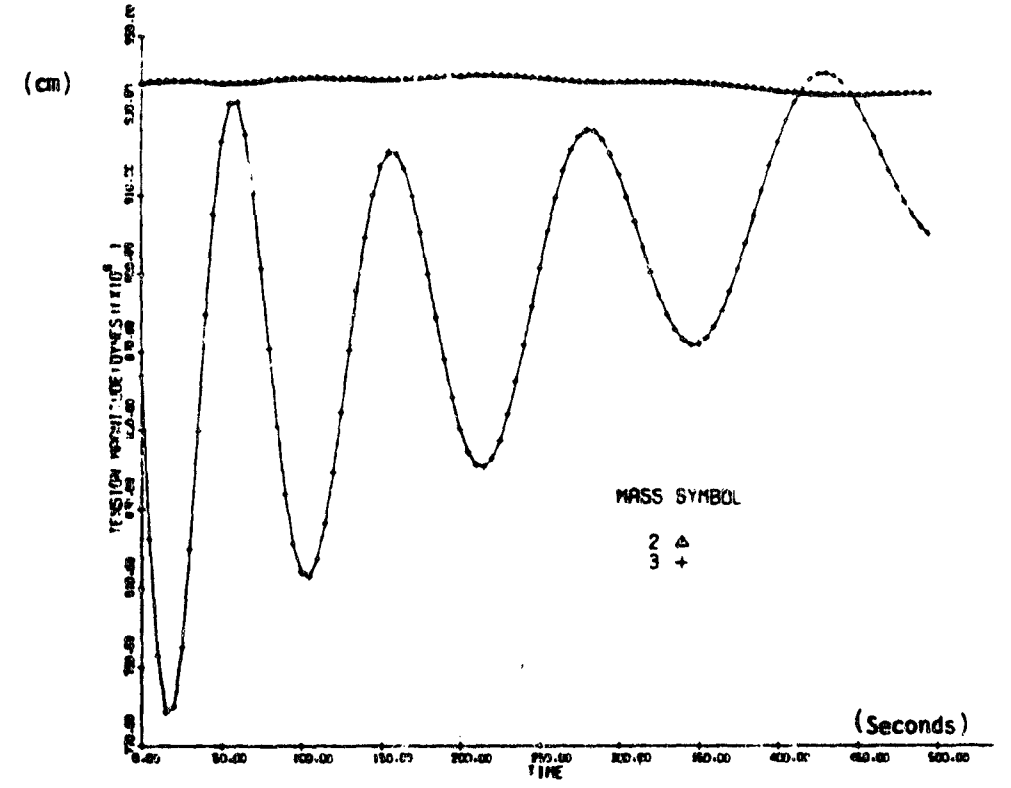

(b)

Figure 1 Motion during the first 500 seconds with a 30 ton payload climbing at 10 m/sec starting 1 km from the bottom of a 250 km wire. Part a) is the in-plane displacement of each mass vs. time, part b) is the tension and part c) (next page) is the radial vs. in-plane configuration at 5 second intervals.

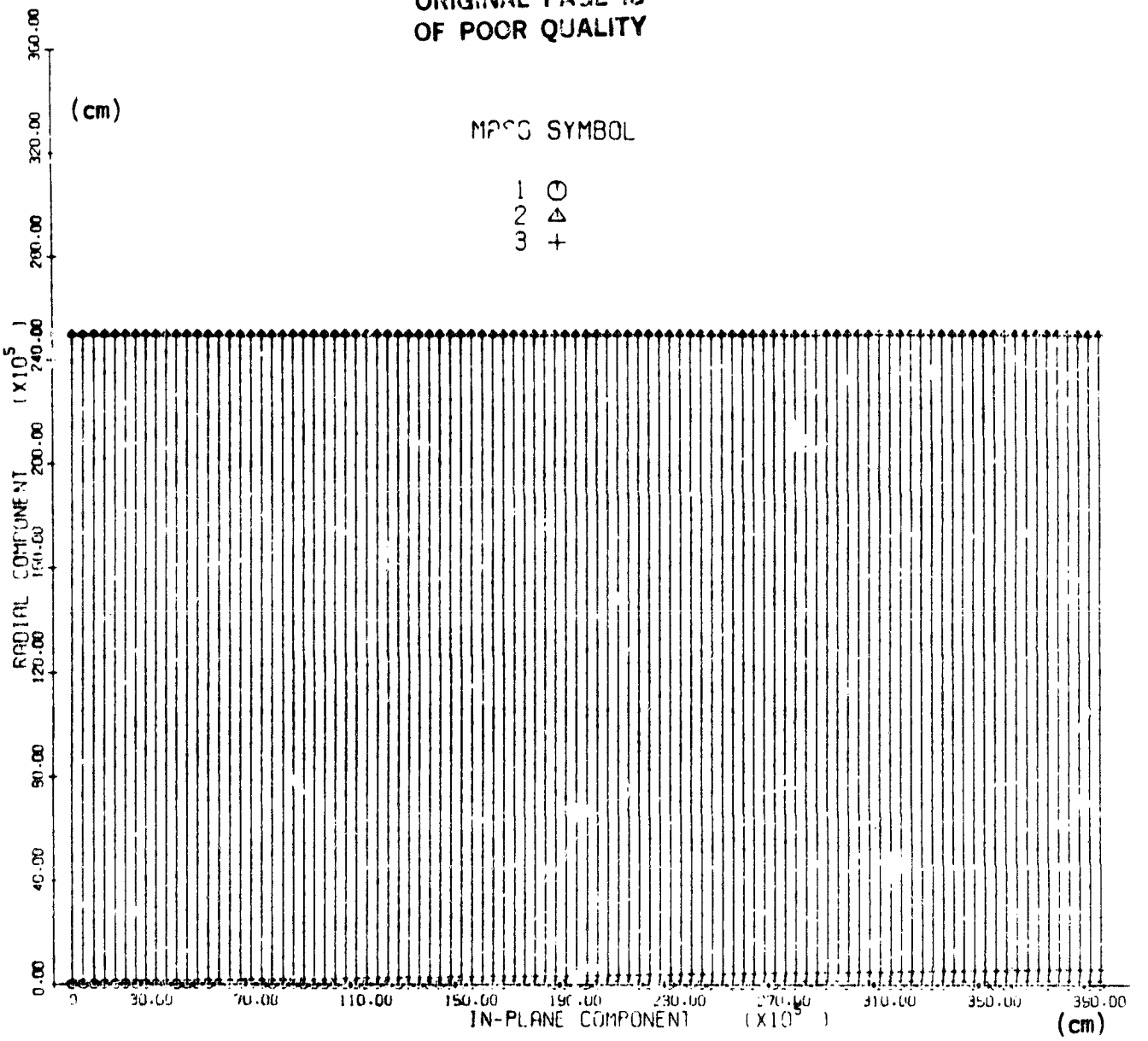

Figure 1(c). Motion during the first 500 seconds with a 30 ton payload climbing at 10 m/sec starting 1 km from the bottom of a 250 km wire- radial vs. in-plane configuration at 5 second intervals.

displacement of Mass 3 in Figure 1a). The upper platform is generally moving forward and closer to the lower platform during this time period. In Figure 1b we see that the tension in the lower segment is initially lower than that in the upper segment. This is because the center of gravity is initially about 7.44 km from the lower platform. The tension is greatest at the center of gravity in equilibrium. The payload will initially have to expend energy to get to the center of gravity and will then coast the rest of the way up. As the payload moves up, the center of gravity will shift upward and the payload will be at the center of gravity 8.06 km from the lower platform. The tension in the lower wire segment oscillates with decreasing frequency as the payload moves up the wire. The natural period for a 30 ton mass at the end of a 1 km Kevlar wire 2 mm in diameter is about 73 seconds. At 5 km the period is about 164 seconds. These numbers agree roughly with the periods seen in the plot. In 500 seconds the payload moves from 1 km to 6 km from the lower platform. Figure 1c shows the in-plane vs. radial configuration at 5 second intervals plotted at equal scale in the two axes. We see the slight bending of the wire to the right as a result of coriolis forces.

Figure 2 shows the behavior during the first 2400 seconds plotted at 25 second intervals. Part a) is the in-plane vs. time, part b) is the tension vs. time, and parts c) and d) are the in-plane vs. radial configurations at successive time intervals. In part a) we see that the upper mass which had been moving forward for the first 1000 seconds has moved to the rear and is almost in line with the payload climbing the wire. In part b) we see that the tension is now greatest in the lower section since the payload passes the center of mass of the system at about 700 seconds. The frequency of the tension oscillations is continuing to decrease as the length of the lower section of wire increases. Part c) shows the radial vs. in-plane configurations at 25 second intervals plotted at equal scale in both axes.

(a)

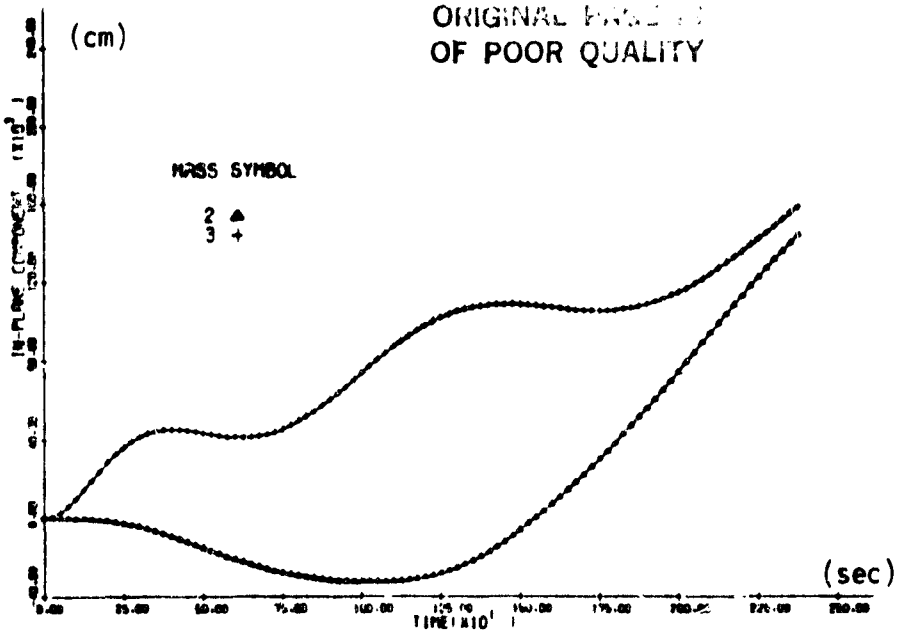

(b)

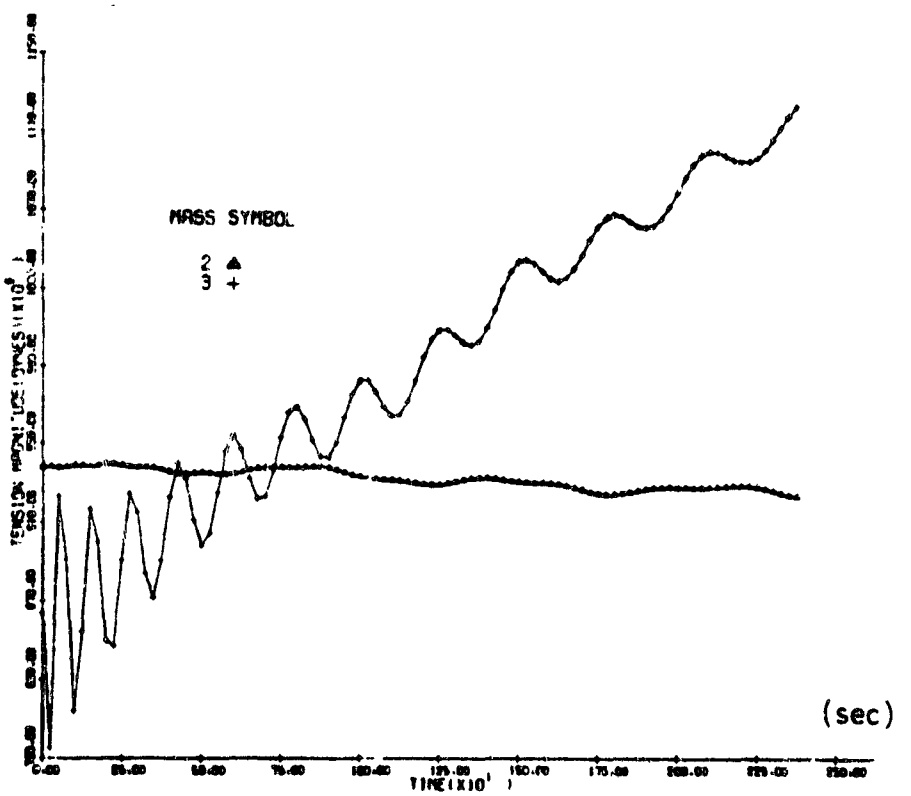

Figure 2. Motion during the first 2400 seconds of a payload climbing the tether. Part a) is the in-plane, part b) is the tension, part c) is the in-plane vs. radial at 25 second intervals plotted at equal scale in both axes, and part d) is the in-plane vs. radial with the in-plane axis expanded.

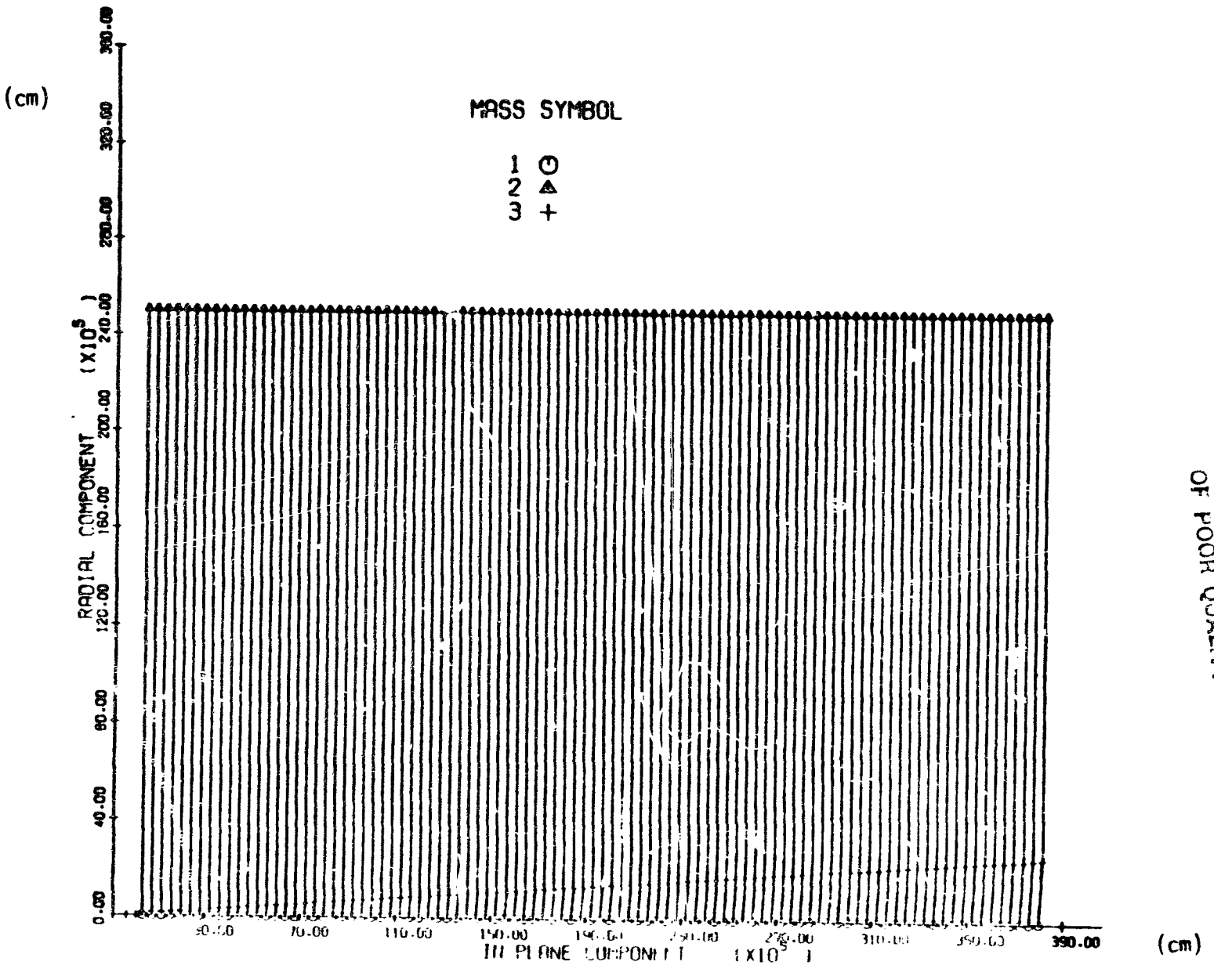

Figure 2(c). Motion during the first 2400 seconds of a payload climbing the tether - in-plane vs. radial at 25 second intervals.

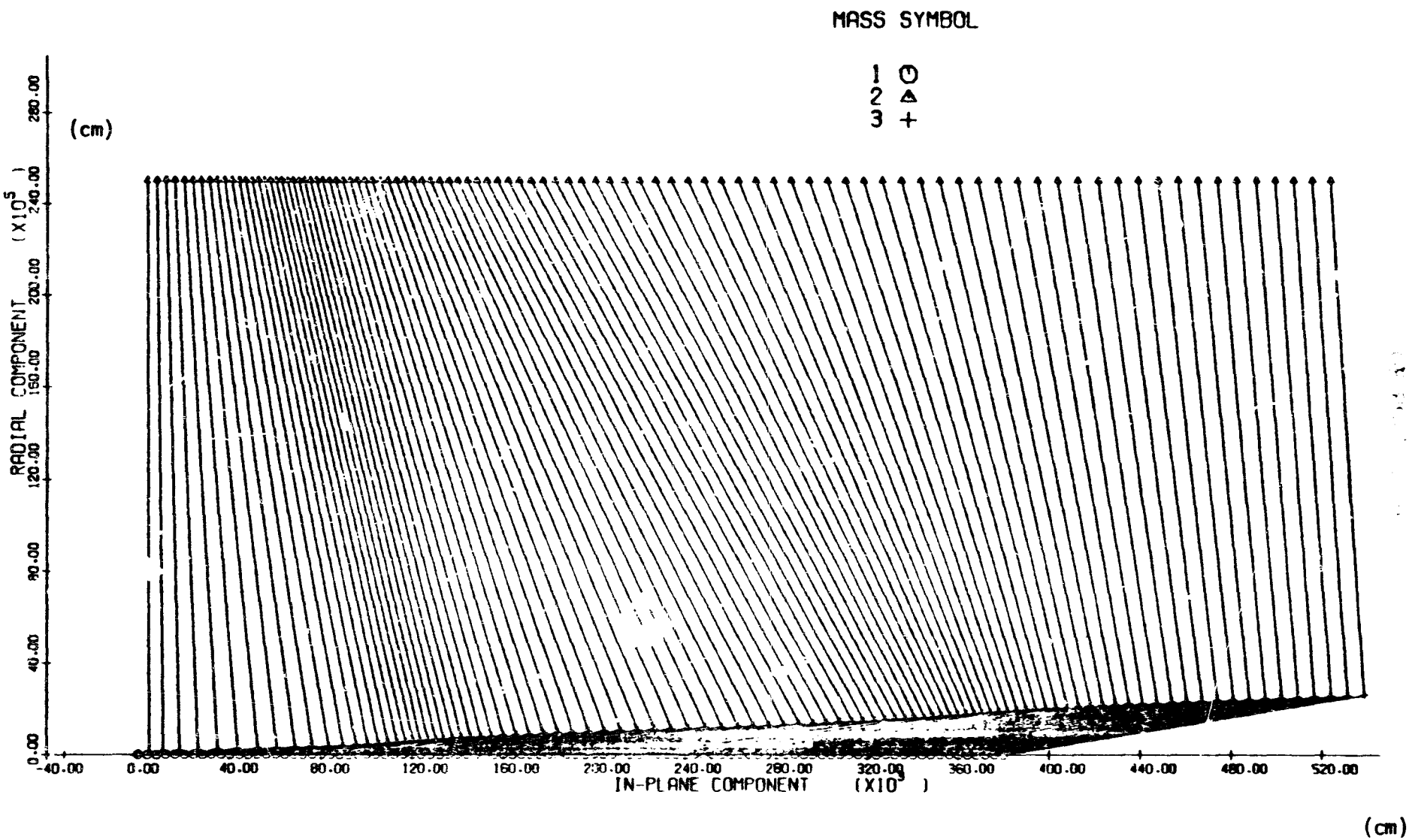

Figure 2(d). Motion during the first 2400 seconds of a payload climbing the tether - in-plane vs. radial behavior with the in-plane axis expanded.

Part d) shows the same thing with the in-plane axis expanded to show the in-plane movement with better resolution. The features described in part a) can be seen in this plot, especially the swinging of the top mass to the right near the end of the plot.

Figure 3 shows the behavior for the first 24000 seconds plotted at 250 second intervals. Part a) is the in-plane, part b) the tension, and parts c) and d) show the in-plane vs. radial configuration. The period for in-plane pendulum oscillations of a tethered system is the orbital period divided by the square root of 3. For a 300 km orbit, the orbital period is about 5430 seconds and the in-plane period is about 3135 seconds. In 24000 seconds we would expect about 7.6 cycles. This seems to agree roughly with the results seen in part a). The in-plane period is independent of length, so we do not see a change in period with time. In addition to the pendulum motion of the system as a whole we also see transverse oscillations of the payload on the wire and oscillations of the upper platform with respect to the payload. When the payload is close to the lower platform, the period of transverse oscillations of the payload is short, and the period of oscillation of the upper platform is the period for oscillations of the system as a whole. As the payload climbs, the period for transverse oscillations of the payload lengthens, and the period of oscillation of the upper platform shortens. Part b) shows the tension vs. time. The tension in the lower segment continues to increase with time as the payload climbs the wire. The lengthening of the wire seen in parts c) and d) is the result of using too small a wire diameter. The computer run halted with the diagnostic that the stepsize was too small as the length of the upper segment approached zero. The last output point was at 23750 seconds and the run ended at 23881 seconds. The last

(a)

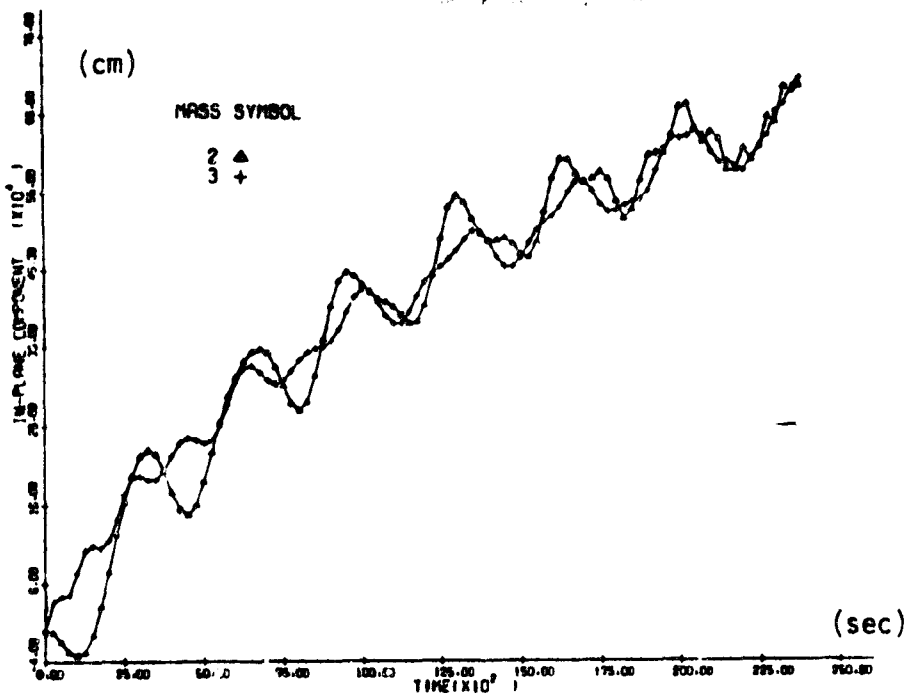

(b)

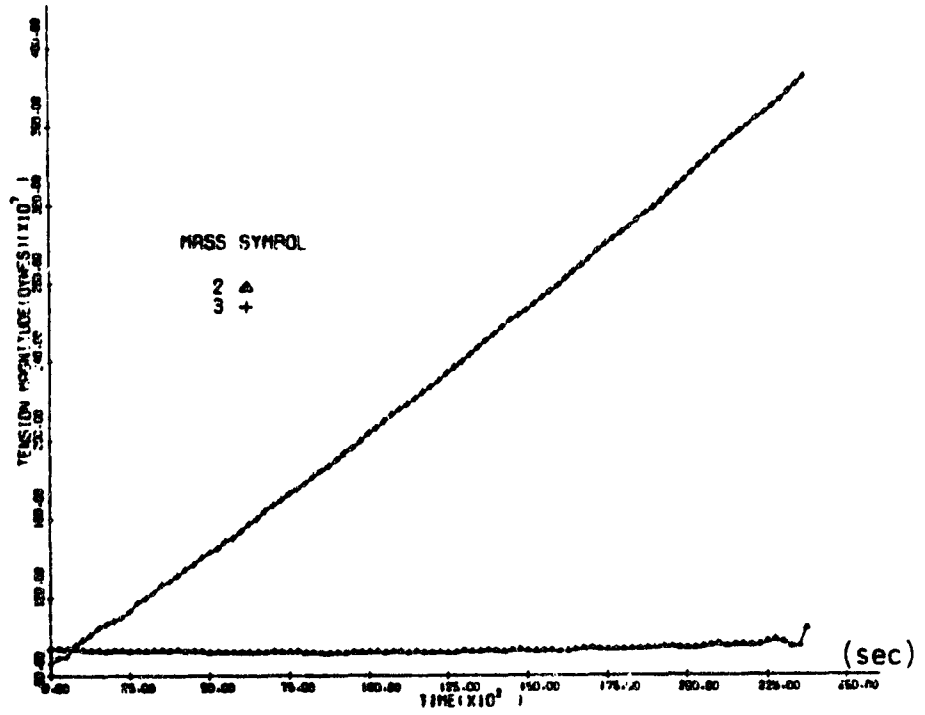

Figure 3 Motion during the first 24000 seconds of a payload climbing the tether. Part a) is the in-plane motion, part b) is the tension, part c) is the radial vs. in-plane configuration at equal scale, and part d) is the radial vs. in-plane with the in-plane axis expanded.

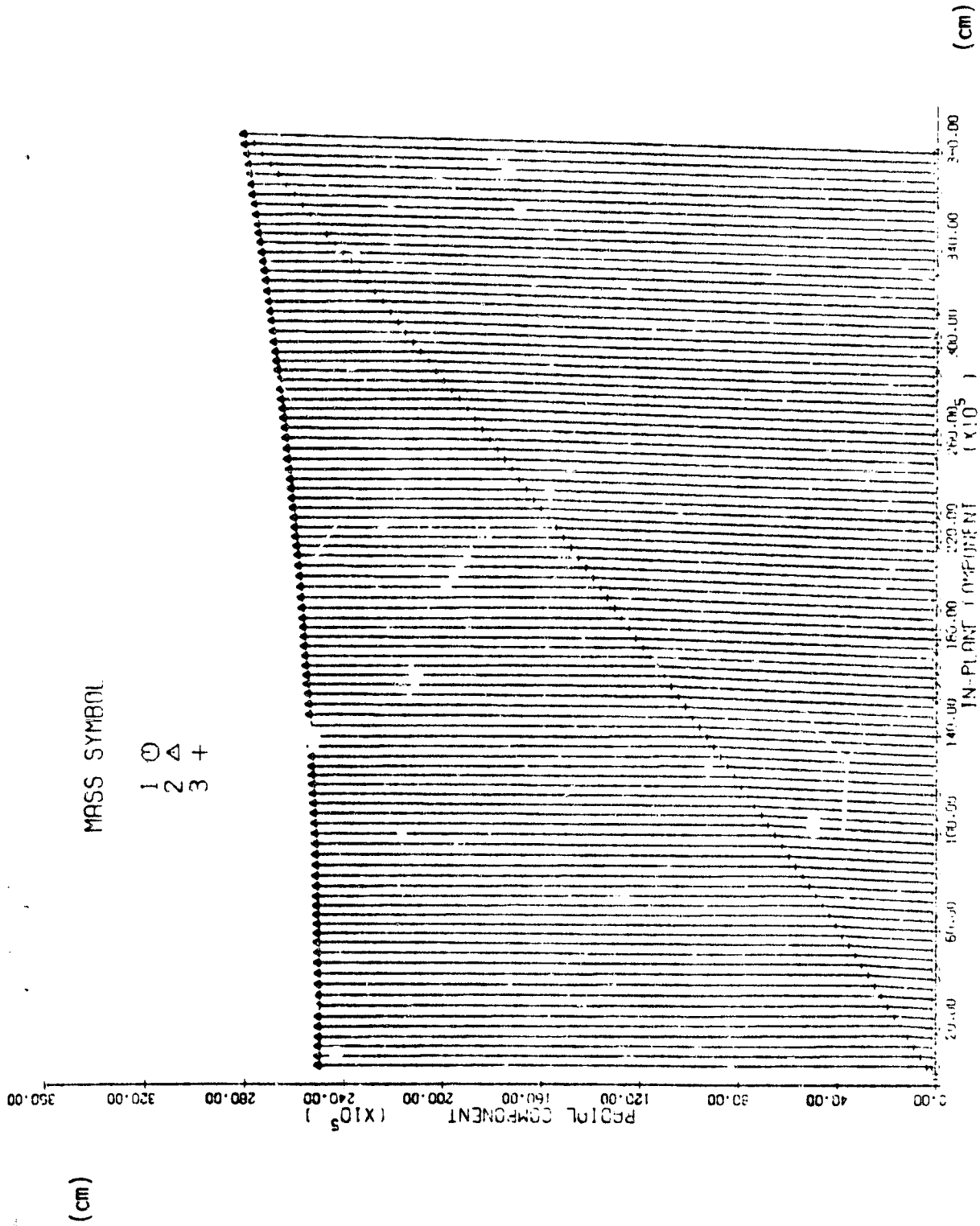

Figure 3(c). Motion during the first 24000 seconds of a payload climbing the tether - radial vs. in-plane configuration at equal scale. The tether stretches as the payload climbs because of increased gravity gradient force on the payload. (The amount of stretch is not realistic because the tether cross section used in the simulation was too small to withstand the tension which develops at the end.)

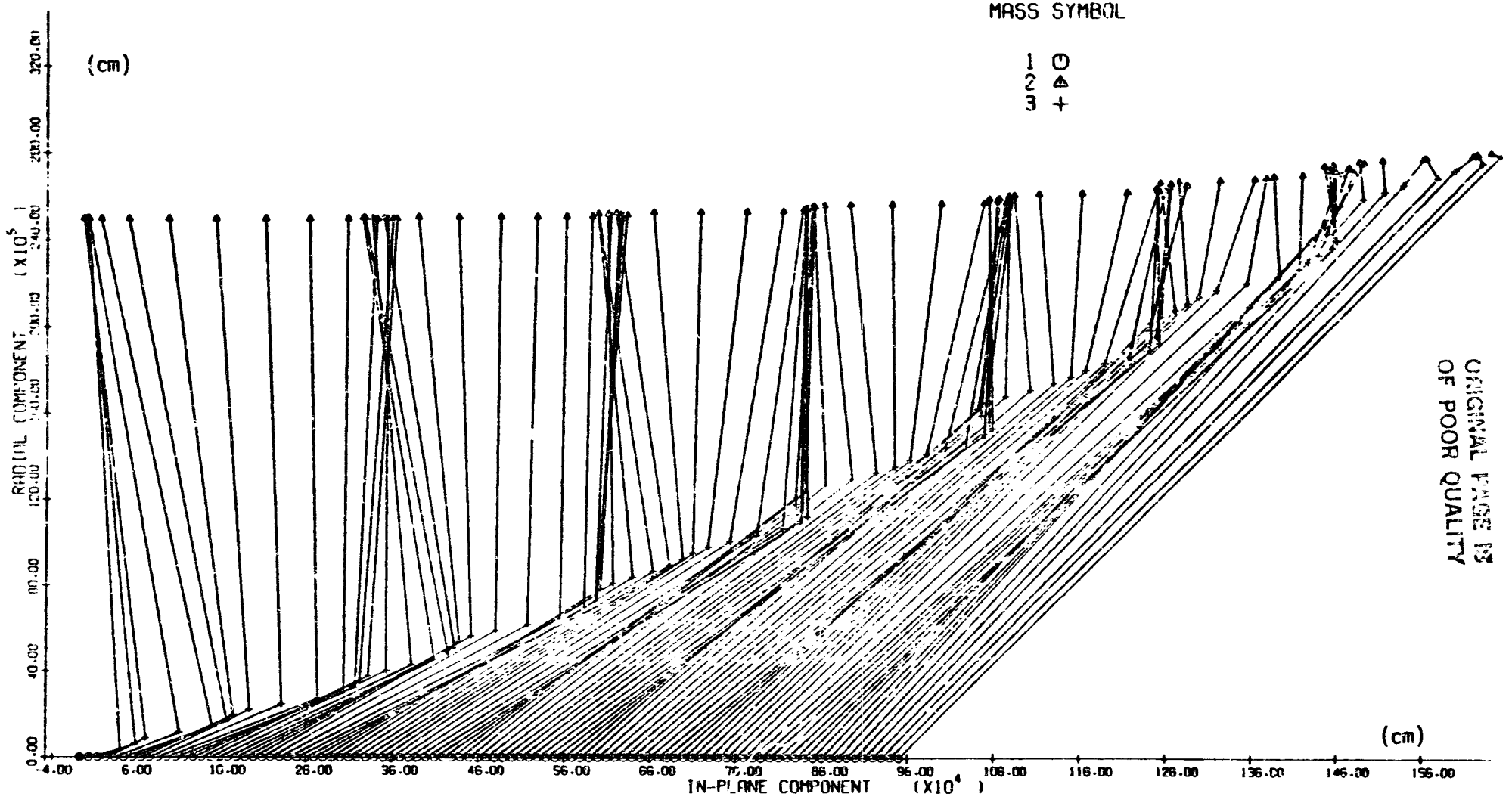

Figure 3(d). Motion during the first 24000 seconds of a payload climbing the tether - radial vs. in-plane with the in-plane axis expanded. The small oscillation of the payload and subsatellite as the payload climbs the wire is clearly seen here.

130 seconds have been rerun using the last output state vector as the initial state vector as the initial state vector of the next run. The results are plotted in Figure 4. The payload has been taken as the reference point in the plots so that we see the motion of the upper platform as viewed from the payload. Part a) is the radial component, part b) the in-plane, and part c) the in-plane vs. radial configuration. In part a) we see that the upper platform goes below the payload during the last couple of seconds. To give better resolution, the last 15 seconds have been plotted alone in Figure 5. Part a) is the radial, part b) the in-plane, and part c) the in-plane vs. radial. Part c) clearly shows the upper platform looping around the payload in the last few seconds. It is remarkable that the behavior is stable for so long. The payload would of course have to decelerate as it reaches the platform. The rate may have to be controlled to eliminate oscillations during the approach to the launching platform.

Since the dynamics of the out-of-plane component is different from that of the in-plane, a run has been done with an initial out-of-plane displacement for the wire. The platform at the top was moved 3 km and the payload 12 meters placing it in a line between the upper and lower platforms. The wire diameter in this run is 7.5 mm which is sufficient to withstand the tension load. The results for the first 23750 seconds are shown in Figure 6. The time required to reach the upper platform at 10 m/sec is 24824.7 seconds. Part a) of the Figure shows the in-plane, part b) the out-of-plane, part c) the in-plane vs. radial, and part d) the out-of-plane vs. radial. The in-plane is similar to the results seen before without the out-of-plane displacement. The out-of-plane behavior is very regular and does not show the transverse oscillation induced by

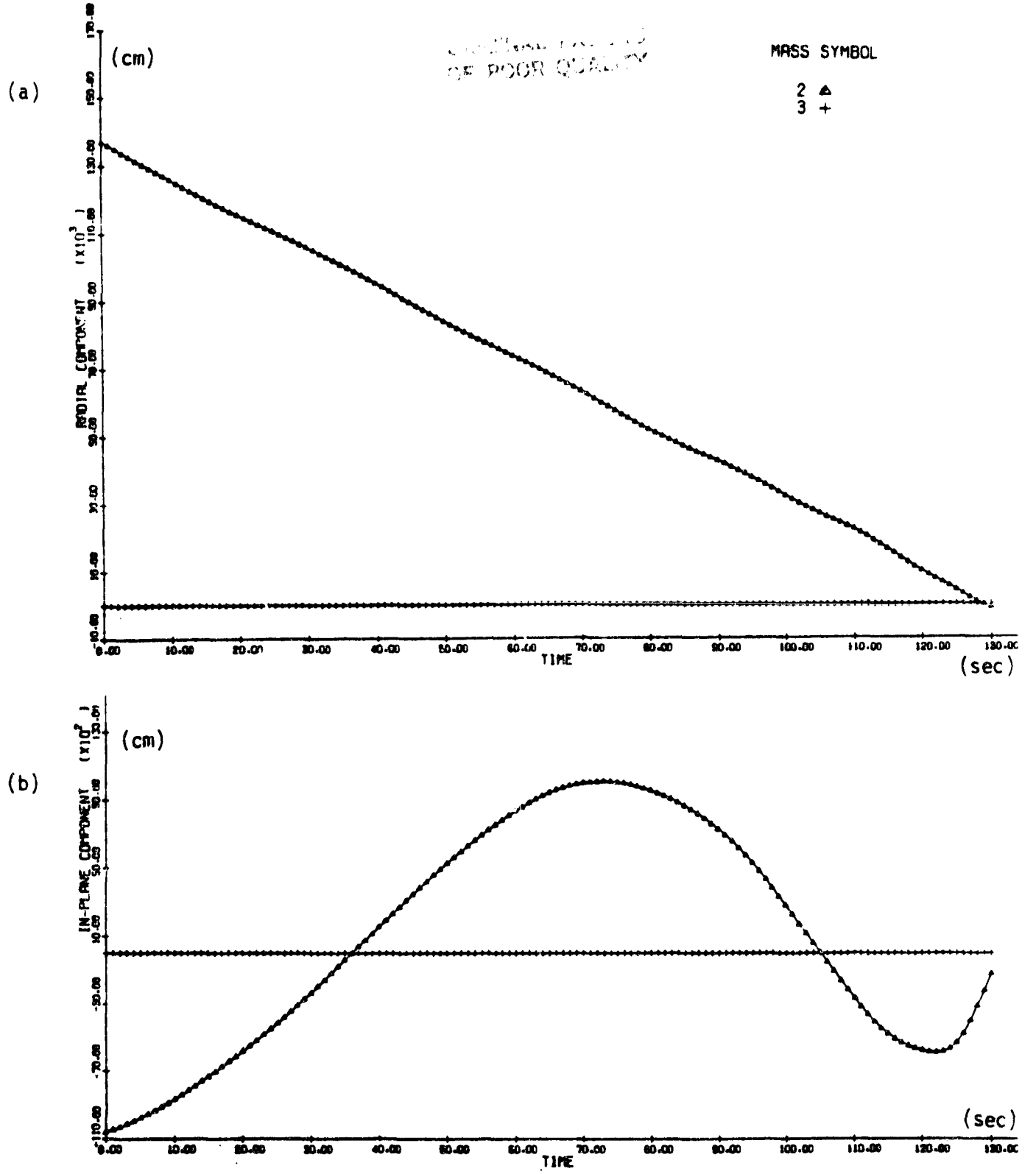

Figure 4 Last 130 seconds of a payload climbing the tether to an upper launching platform. The motion of the upper platform is shown relative to the payload climbing the wire. Part a) is the radial vs. time, part b) is the in-plane, and part c) (next page) is the in-plane vs. radial.

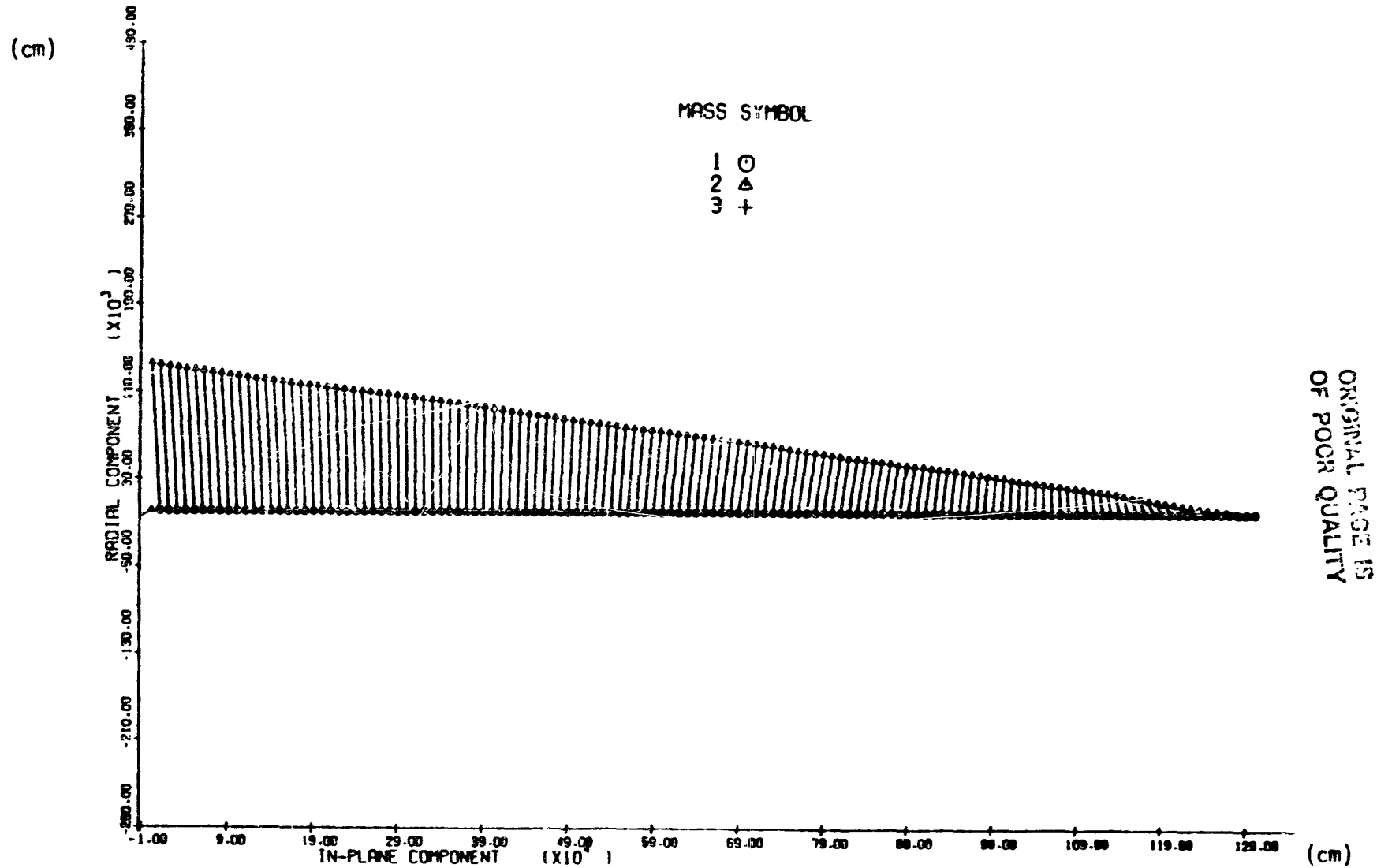

Figure 4(c). Last 130 seconds of a payload climbing the tethers to an upper launching platform. The motion of the upper platform is shown relative to the payload climbing the wire - radial vs. in-plane behavior.

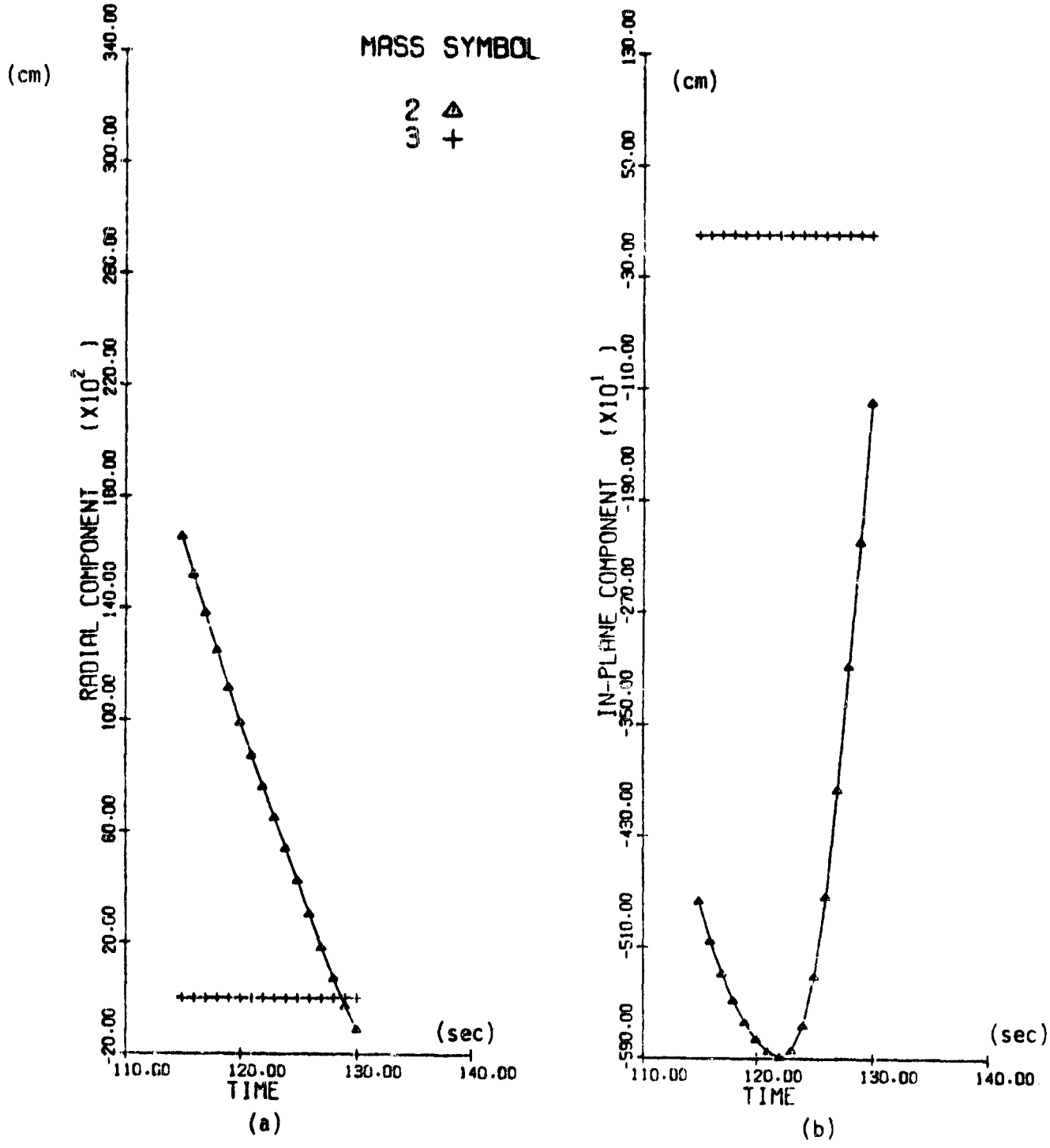

Figure 5. Last 15 seconds of a payload climbing the tether to an upper launching platform. The motion of the upper platform is shown relative to the payload climbing the wire. Part a) is the radial behavior vs. time, part b) is the in-plane behavior vs. time and part c) (next page) is the in-plane vs. radial behavior.

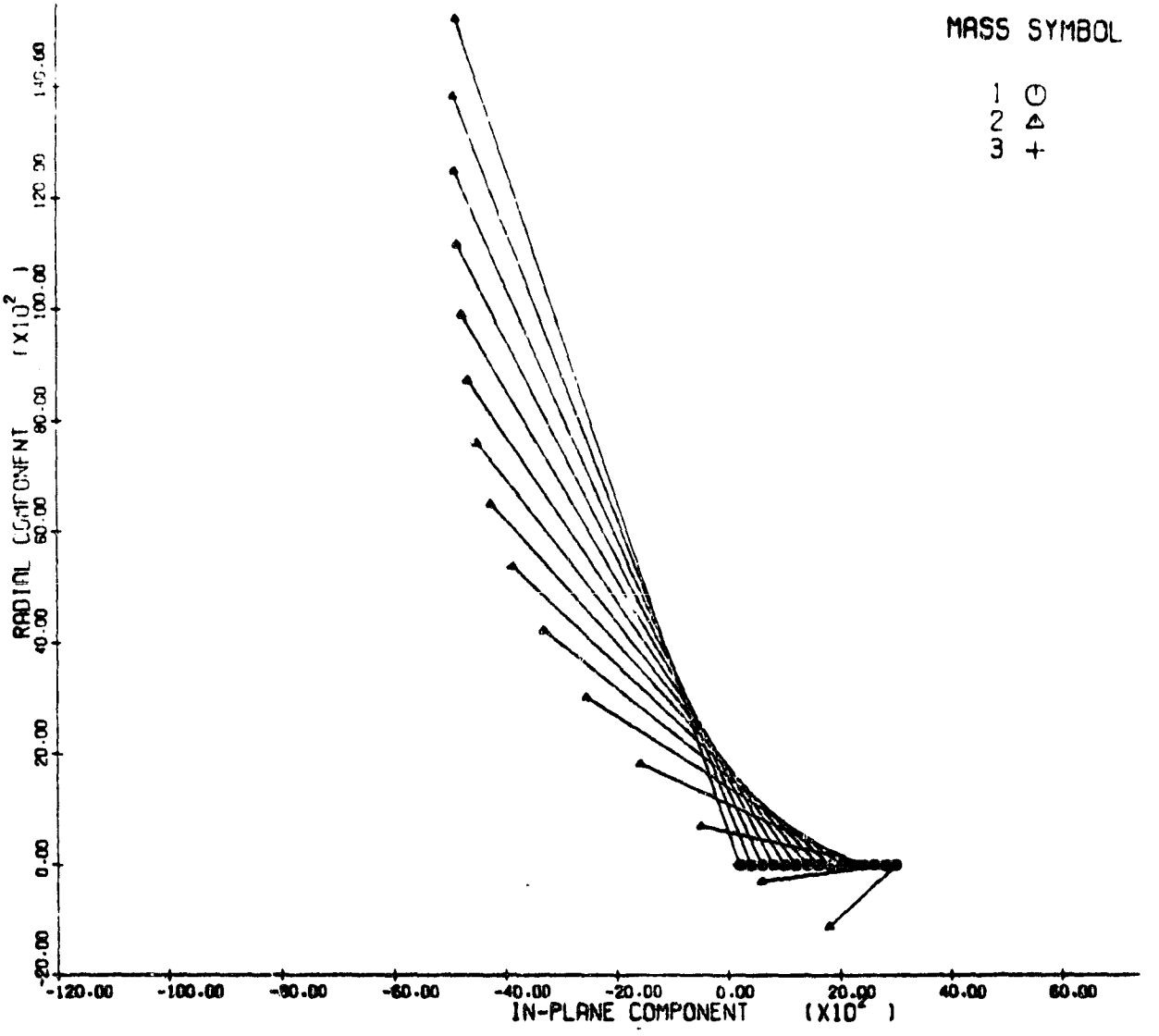

(c)

Figure 5(c). Last 15 seconds of a payload climbing the tether to an upper launching platform. The motion of the upper platform is shown relative to the payload climbing the wire - in-plane vs. radial behavior.

(a)

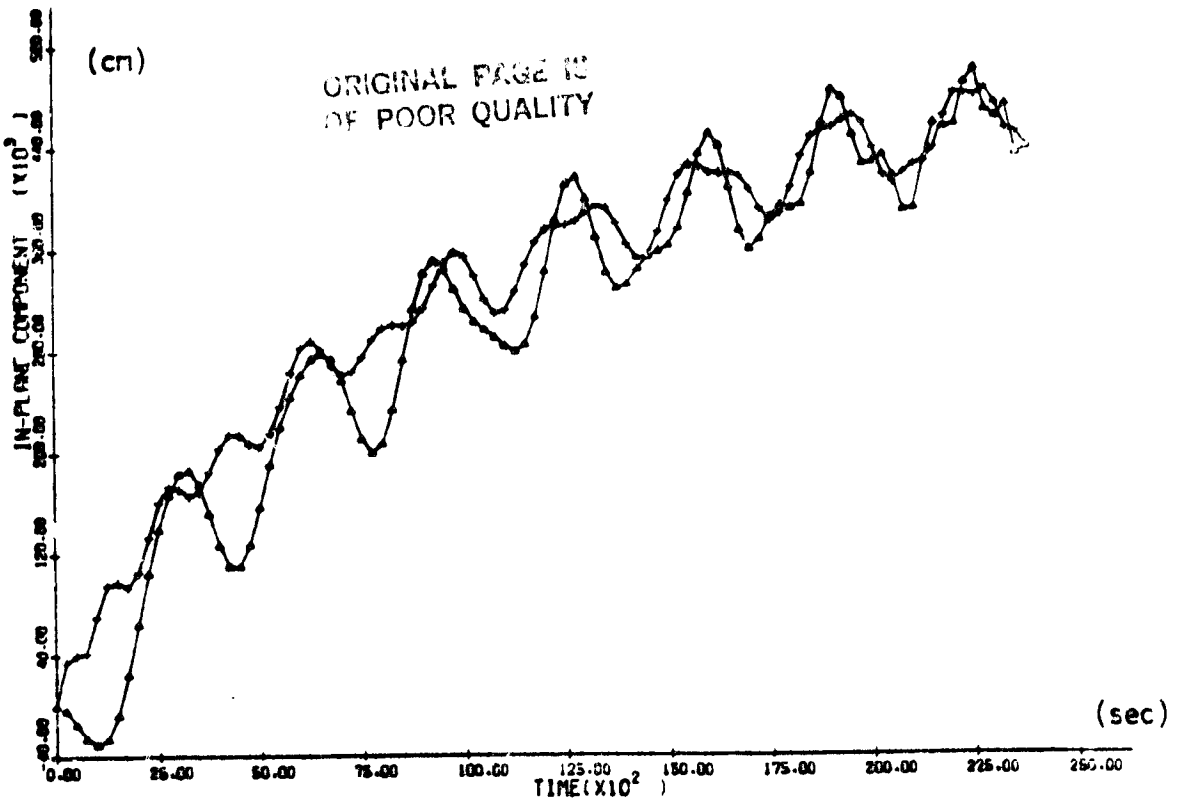

(b)

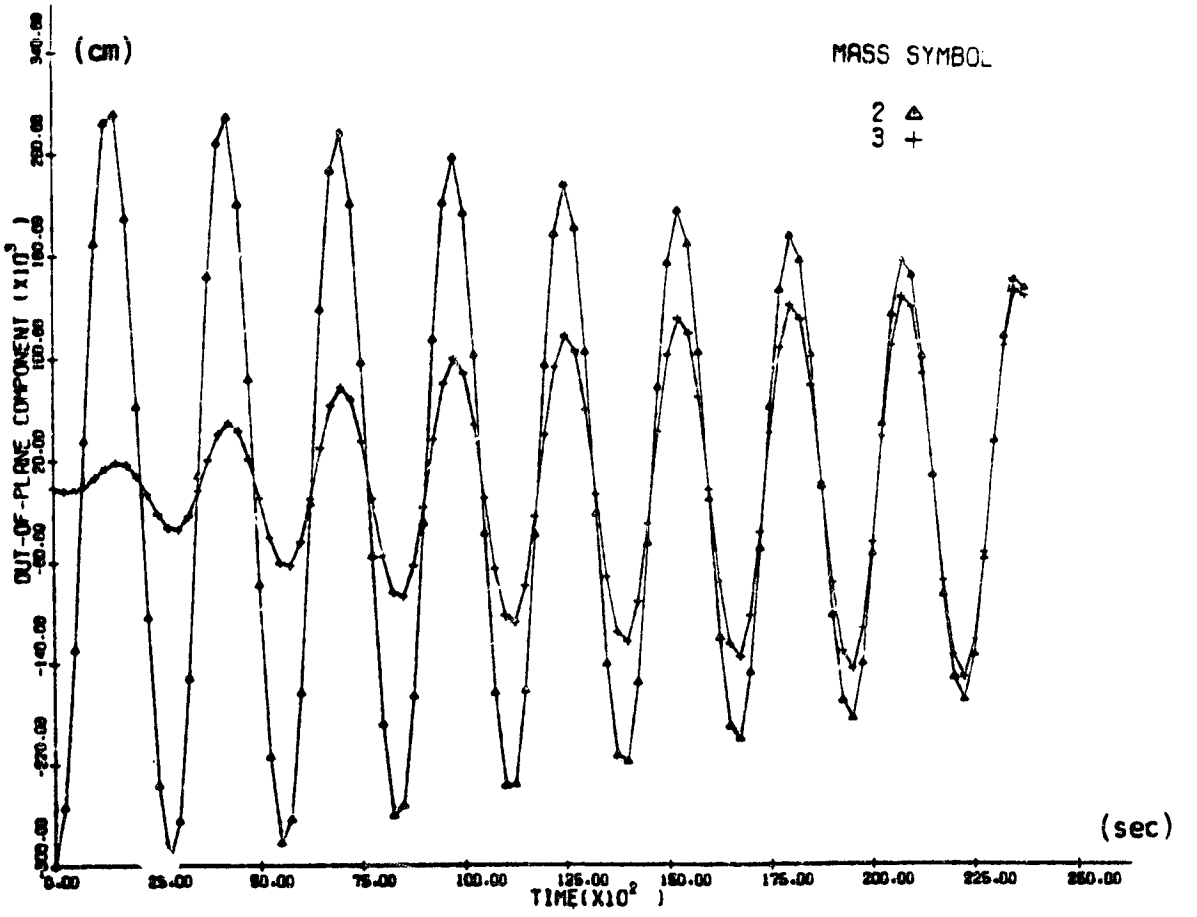

Figure 6 . Payload climbing the tether to an upper launching platform with an initial out-of-plane displacement. Part a) is the in-plane, part b) the out-of-plane, part c) the in-plane vs. radial, and part d) the out-of-plane vs. radial.

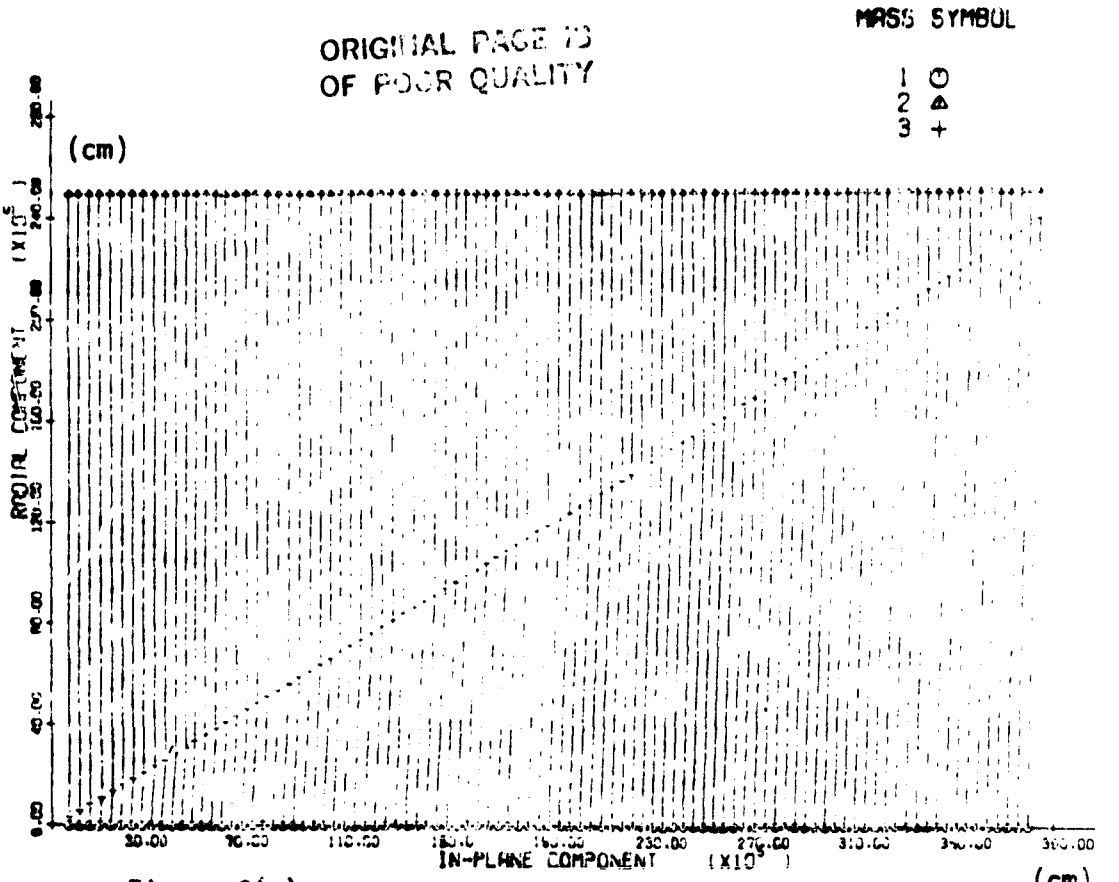

Figure 6(c).

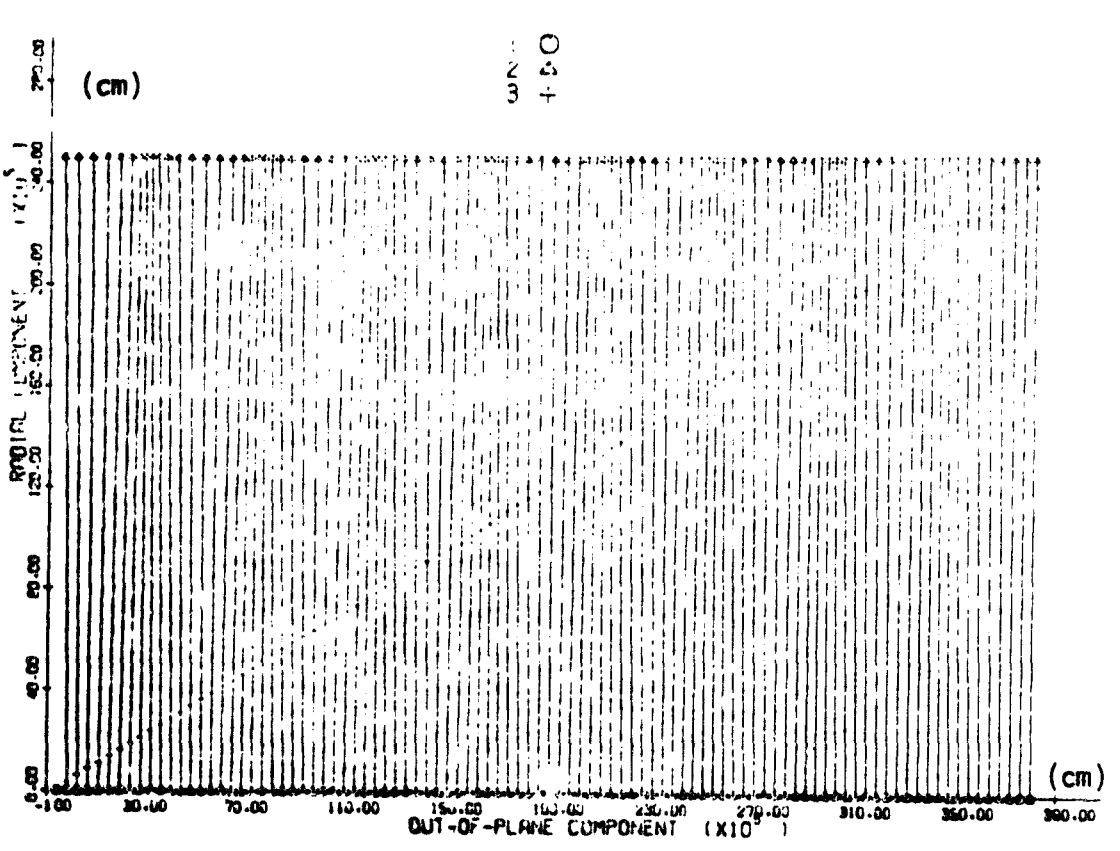

Figure 6(d).

coriolis forces in the in-plane component. Transverse oscillations could be produced in the out-of-plane component by having the payload out of line along the wire. The run was continued another 1070 seconds with output every 10 seconds. At the last output point which is 4.7 seconds from the end of the ascent, the platform is 20 meters above the payload in the radial direction, and 42 meters displaced in the in-plane direction. The behavior seems essentially the same as in the previous run with no out-of-plane displacement.

In conclusion, the simulations of payload transport along the wire using the SKYHOOK program indicate that the process is quite stable. The radial motion along the wire introduces coriolis forces that produce transverse oscillations in the in-plane, but not the out-of-plane direction. In the case of a heavy payload approaching the end of the wire at high velocity, unstable behavior would result in the last few seconds. A slowdown phase is obviously required. Additional simulations would be needed to develop an appropriate procedure and determine if the rate needs special control at the end to prevent the buildup of oscillations duirng the final approach.

4.0 Simulation of a Payload Launch Using an Orbiting Tether Facility

The M.I.T. section of the Final Report for this contract (Appendix A) describes on page 29 a numerical example of the Snuttle launching a payload using an orbiting tether facility. The Shuttle docks with the tether platform, transfers the payload, deploys the tether, releases the payload, retrieves the tether part way such that when the tether system is released its center of gravity will be back at its original altitude, and then undocks from the tether system at apogee. After undocking the tether system continues the retrieval to the original state. The M.I.T. calculations assume the center of gravity of the system remains constant during reeling

processes and neglects the effect of librations that are generated during the reeling. Simulations have been done using the SKYHOOK program to see the influence of these effects neglected in the theoretical calculations.

The deployment subroutine in the SKYHOOK program uses equations and parameters given on page 9 of NASA TM-X-64963, "A tether tension control law for tethered subsatellites deployed along local vertical." The commanded length is given by the table on page 10 of the report. The parameters on page 9 are computed for a specific subsatellite mass and orbital angular velocity, and the table of commanded lengths is for a specific tether length and deployment sequence. The table of commanded lengths has the undesirable quality of being discontinuous. In order to run the case described above the deployment subroutine has been rewritten in a more general form patterned after the retrieval subroutine. The parameters have been rewritten to use the actual masses and orbital angular velocity. Instead of using a table, the commanded length is computed as a fraction f of the actual length. For retrieval a value of .93 for f gives a slow stable retrieval. For deployment, f is greater than unity. It should be possible for f to be substantially greater than unity since deployment is an inherently stable operation in contrast to retrieval which must be done carefully in order to make sure there is no residual angular momentum that will cause the subsatellite to wrap around the Shuttle during the final stages of the approach to the Shuttle.

The SKYHOOK program has an input parameter the ejection velocity to be used on deployment. This ejection velocity may be large without introducing instabilities. In this way it is possible to quickly arrive at a sufficient distance from the Shuttle to obtain an adequate gravity gradient force for maintaining tension during the rest of the deployment. During

the initial phase the kinetic energy of ejection can be used to maintain tension. This tension will eventually use up the initial kinetic energy, but by then there is sufficient gravity gradient to continue the deployment under positive tension. The tension control law uses the reel motor to simulate a visco-elastic tether tuned to the libration frequency of the tether system. The viscous part of the control law provides the tension needed during the initial phases of the deployment. Test runs have been done with different ejection velocities to determine a suitable value for running the simulations of the launch sequence studied at M.I.T. One undesirable aspect of the dynamics is that the control law ends up slightly retrieving the system after the initial kinetic energy has been exhausted. In one test run, a wire mass point had just been deployed and the slight retrieval caused the wire length to fall slightly below the natural length of the wire segment. Since the program is not set up to eliminate mass points during deployment, there was loss of tension, and the tension control law was unable to operate properly. In lieu of pursuing a solution to this problem, which would be beyond the scope of this study, the M.I.T. case has been run without tether dynamics, integrating only the motion of the two end masses. More study of the deployment process is necessary to useful optimize the process.

In order to run the deployment, two sets of initial conditions need to be computed. The program uses only the state vector for the Shuttle initially. The DUMBBELL program is set up to compute initial conditions for two or more masses. By making some changes in the program to avoid singularities, it was possible to run the program with zero tether length to get the initial conditions for the Shuttle. The parameters of the system when fully deployed must be given for the other masses. Appendix A gives equations for computing the parameters of the system at each stage

of the operation. Since the SKYHOOK runs have no tether mass included, the parameters had to be recomputed with M_T set to zero. The equation for 1/L on page 27 of Appendix A is singular for M_T equal to zero. The equation has been rederived without M_T to get a non-singular expression. The first parameter needed to compute initial conditions for the deployment phase is the value of x, which becomes 21.18 km with no tether mass. This places the Shuttle at 378.82 km after the deployment is completed with the upper mass at 478.82 km. A tether diameter of .5 cm is sufficient to withstand the tension load, assuming a break strength of 2.7×10^{10} dynes/cm^2 and a safety factor of 4. Equilibrium parameters for this phase have been computed using the DUMBBELL program and used to do the deployment run with SKYHOOK.

The deployment run has been done using an ejection velocity of 5 meters/second. Figure 7 shows the results during the first 2000 seconds at 100 second intervals. Part a) is the tension vs. time, and part b) is the radial vs. in-plane configuration. Figure 7b uses a new plotting package recently developed in which the direction of motion has been reconciled with the order in which the configurations are plotted. Successive configurations have always been plotted to the right, but in the previous plotting package, the Shuttle motion was to the left. For this and all future plots, the direction of motion of the Shuttle is to the right. This change was implemented by reversing the sign of the horizontal (in-plane) component of each individual configuration. This is equivalent to looking at the orbit from the other side so that the direction of motion is reversed. In part a) the tension is initially high because of the damping term in the control law. The control law halts the outward motion of the subsatellite after about 500 seconds and there is a slight retrieval during the next few hundred seconds as seen in Figure 7b. The deployment then resumes again.

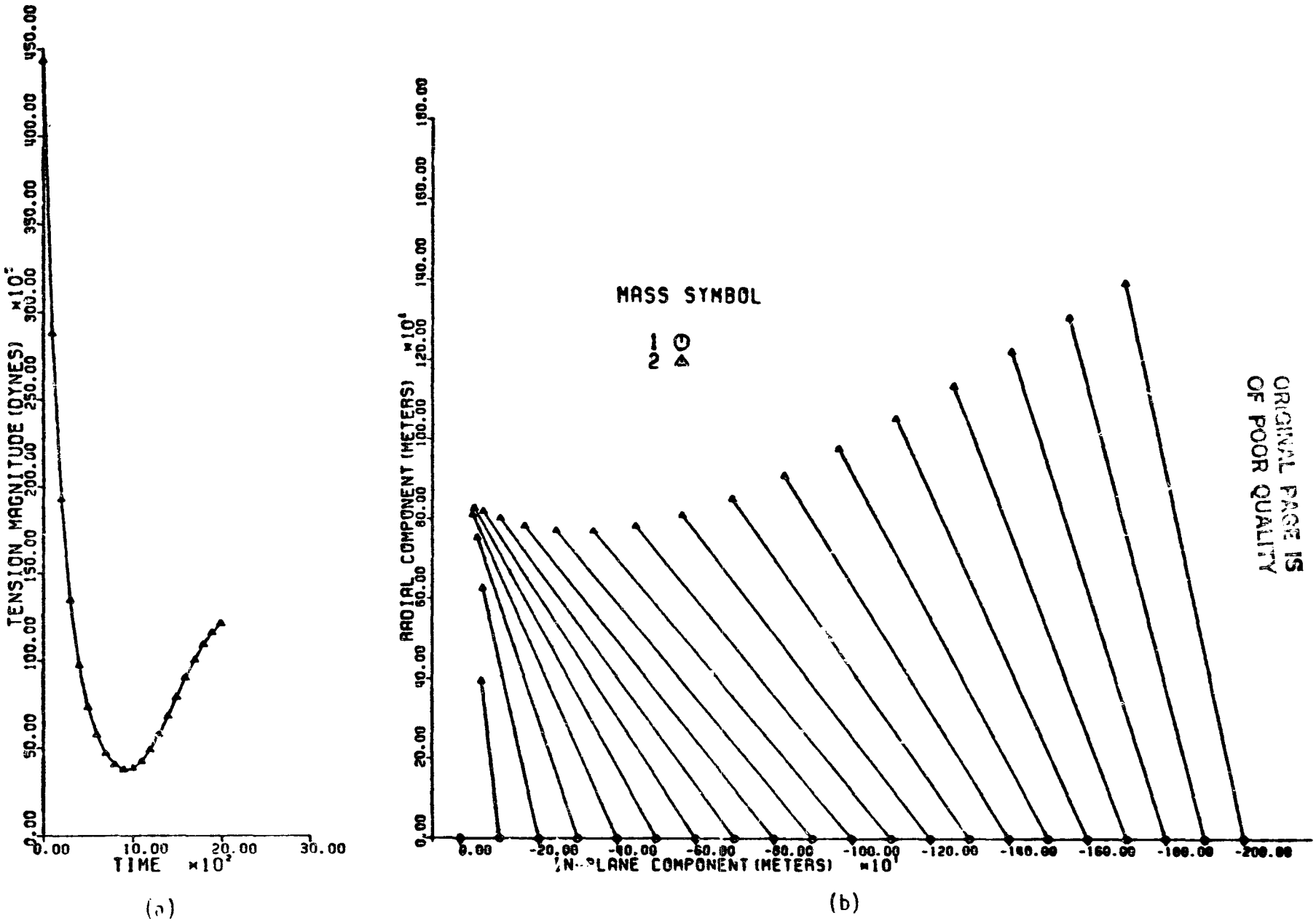

Figure 7. First 2000 seconds of the deployment. Part a) is the tension vs. time, and part b) is the radial vs. in-plane configuration.

One of the parameters of particular interest in this case being studied is the orbital altitude. This information is not contained in the standard SKYHOOK output. It can be obtained from the state vector printed at each output point. For convenience in restarting runs at a particular output point, a special version of subroutine DMPZ is used which writes the state vectors on a separate output file. A small program then reads this file to find the time requested and formats the state vector for input to a new SKYHOOK run. This formatting program has been modified for this study to also compute the radius vector and the magnitude of the velocity from the state vector. The altitude is computed by subtracting the earth radius, and then plotted along with the velocity using the printer page as a graph.

Figure 8 shows a condensed plot of the Shuttle altitude H1, payload altitude H2, Shuttle velocity V1, and payload velocity V2 during the deployment. During the first 1300 seconds which is roughly one quarter of an orbit, the Shuttle altitude increases from its initial value of 400.00 km to about 400.75 km. The altitude of the Shuttle should, of course, decrease during deployment. The initial increase in altitude is the result of a slight eccentricity in the orbit introduced by the ejection velocity of 5 m/sec. This gives the center of mass of the system a radial velocity of about 1.06 m/sec which should result in an altitude variation of about .94 km. Figure 8a shows the orbital eccentricity during the first revolution superimposed on the decrease in altitude resulting from the deployment. This eccentricity complicates the interpretation of the results. It could be eliminated by giving the Shuttle the reaction velocity that it would actually acquire during ejection of a payload.

Figure 9 shows the in-plane vs. radial behavior for the full deployment run. The deployment is completed at about 1800 seconds. In the SKYHOOK program, the tension at the Shuttle is computed from the control law during

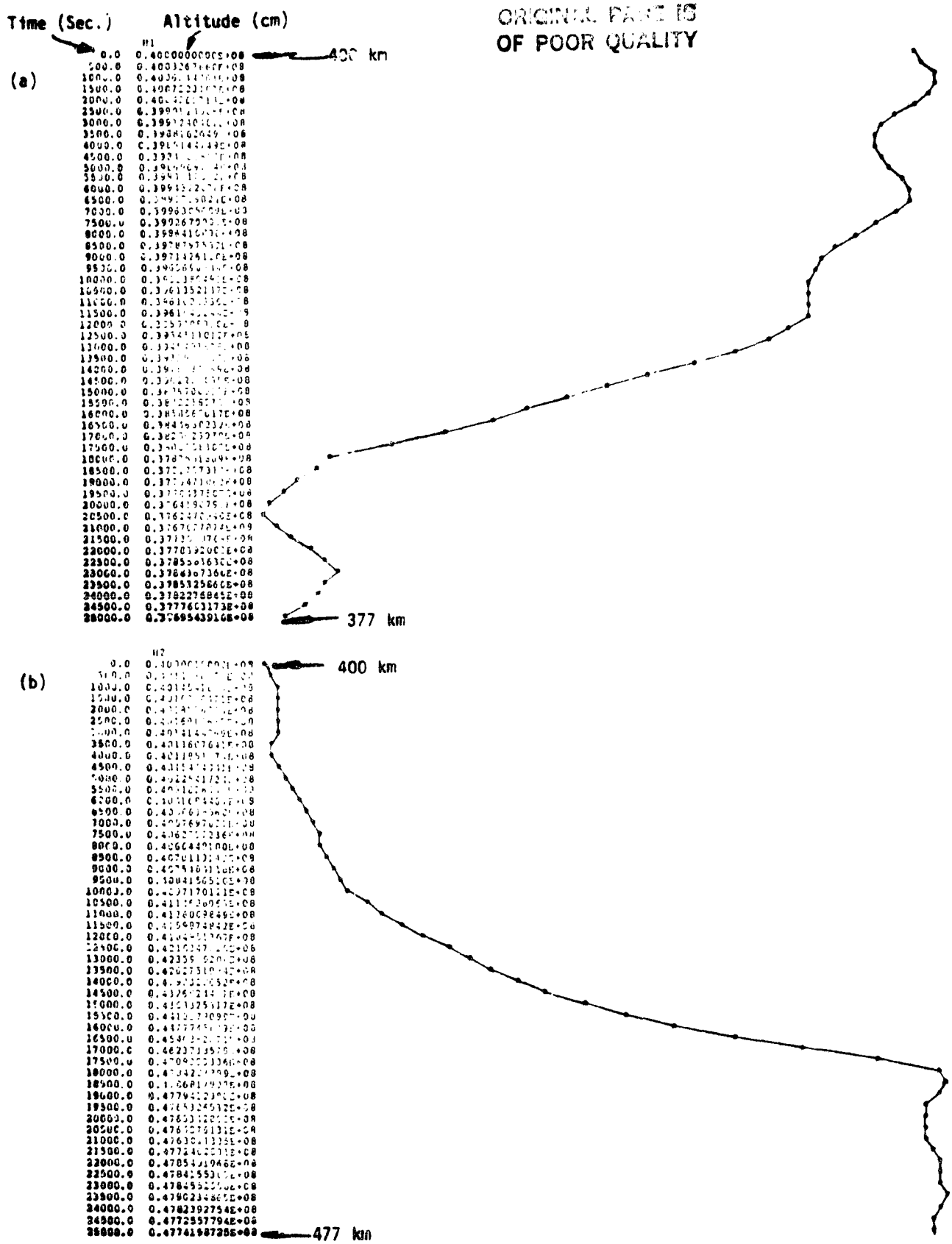

Figure 8. Altitude H (cm) and velocity V (cm/sec) of the Shuttle (mass 1) and subsatellite (mass 2) plotted at 500 second intervals during the deployment phase. The period from 18000 to 25000 seconds is a steady state integration after completion of the deployment. a) Shuttle altitude vs. time, b) subsatellite altitude vs. time; c) (next page) shuttle velocity vs. time, d) subsatellite velocity vs. time.

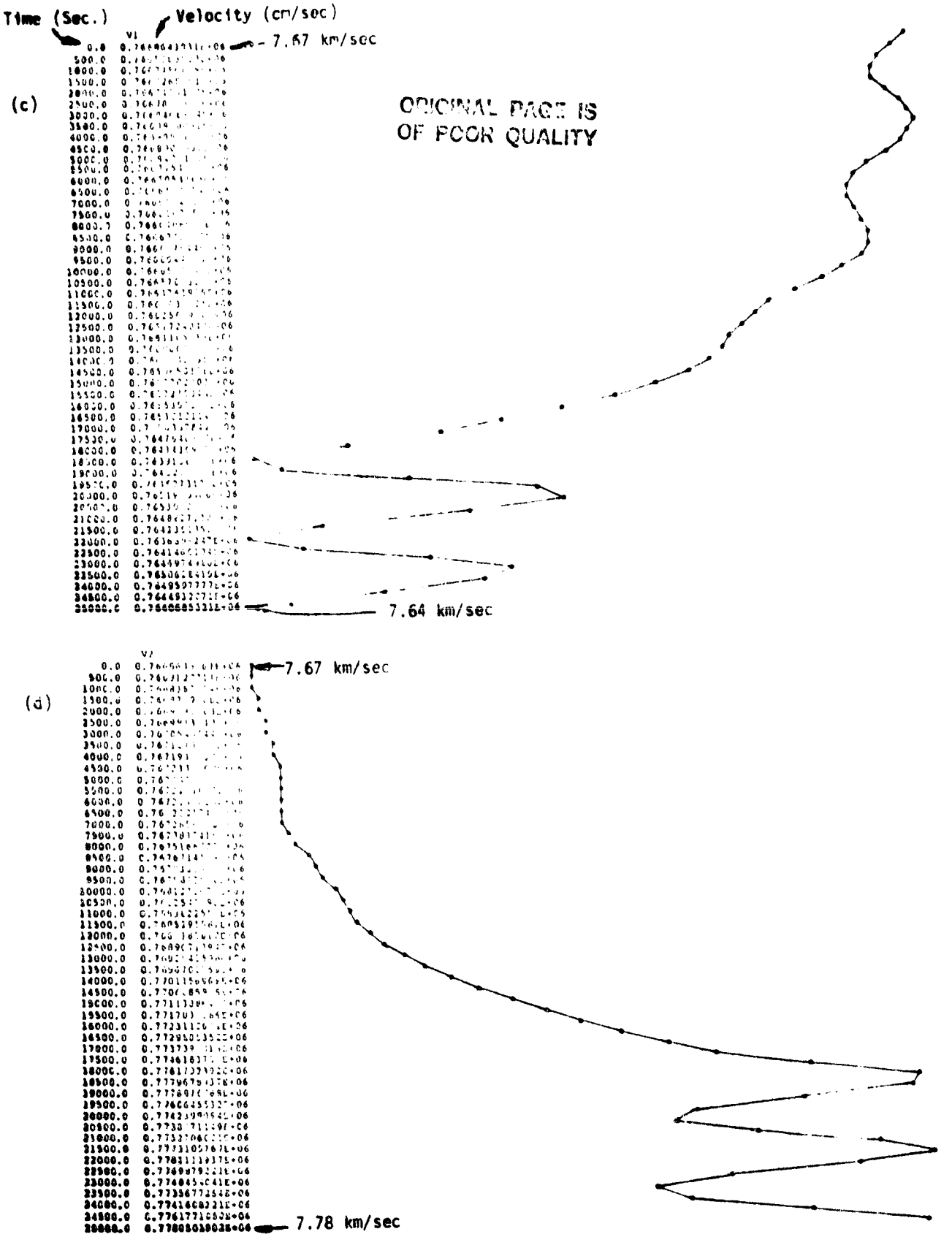

Figure 8. (Cont.) c) Shuttle velocity vs. time, d) subsatellite velocity vs. time.

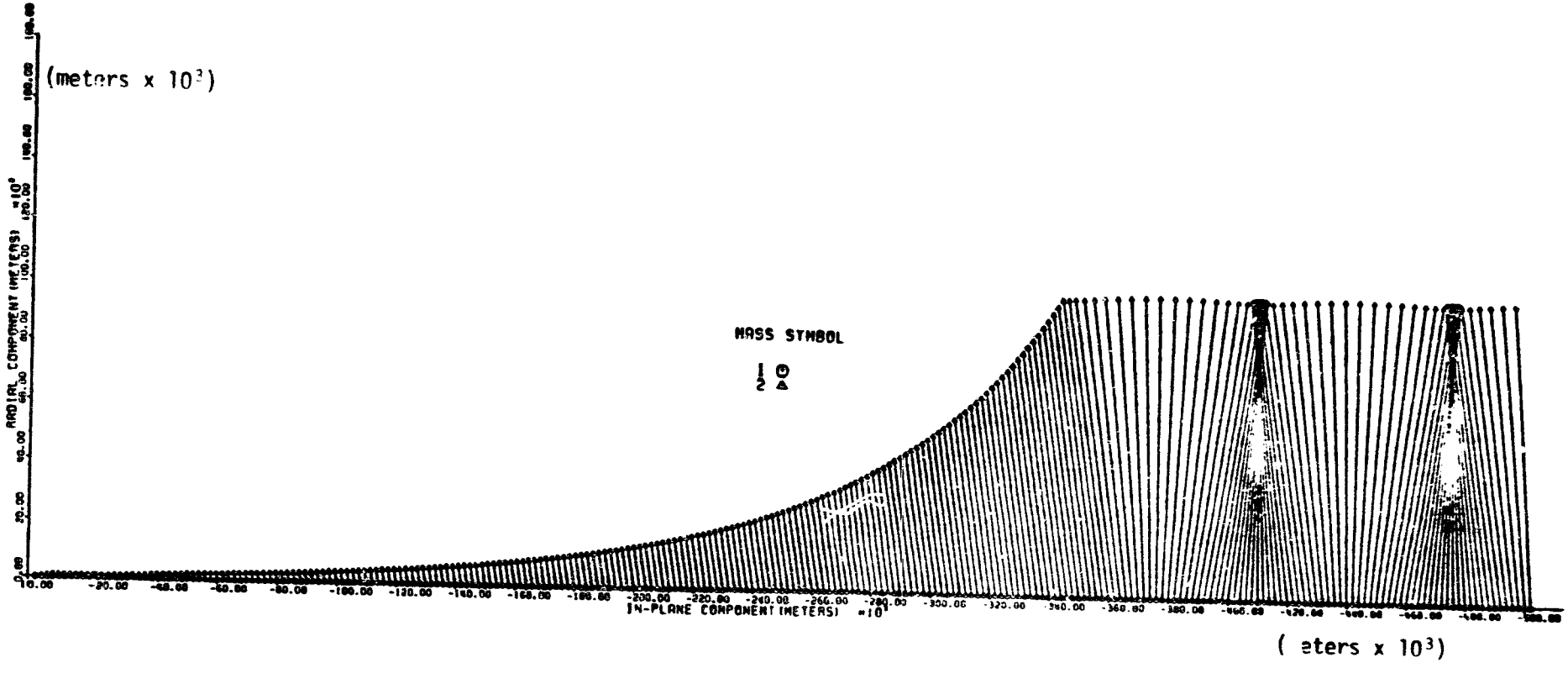

Figure 9. Radial vs. in-plane configuration for the deployment and steady state phase just after deployment.

deployment. When the tether reaches its full deployed length, the program switches to the steady state mode of integration where the tension is computed from the tether elasticity and damping. In this run, the damping parameter has been set to the value required for critical damping of the longitudinal oscillations of the subsatellite at the end of the tether. In this way, the momentum of the subsatellite is arrested without recoil at the end of the deployment. Although the tether itself has little internal damping, the reel motor could simulate a damper if operated under an appropriate control law. At the end of the deployment, the in-plane displacement of the tether is about 15 km to the rear, which is an angle of about 8.6 degrees. After completion of the deployment, the system librates as seen at the end of Figure 9. The libration could be avoided by introducing a control law that terminates the deployment with a slow-down phase where the deployment rate is controlled so that the wire returns to the vertical position without overshoot.

The SKYHOOK program terminates the deployment phase at the first output point where the tether length exceeds the natural wire length given on output. The natural length is then recomputed based on the actual length and tension at the output point. In this case, the computed natural length used after completion of the deployment was 100.105 km. At the equilibrium tension of .6939 x 10^9 dynes, the actual length of the tether is 100.6 km. Since the system is librating, the tension varies from about .592 to .836 x 10^9 dynes and the length from 100.54 to 100.71 km. The altitude of the Shuttle varies from 376.2 to 378.8 km and the altitude of the payload from 476.3 to 479.0 km. The computed altitudes of the Shuttle and payload fully deployed were 378.8 and 478.8 respectively. Comparison of the computed and actual altitudes is complicated by the fact that the deployed tether length is .6 km too long, the orbit has an eccentricity causing an altitude fluctuation of about .94 km, and the system is librating with an amplitude that

can cause an altitude fluctuation at the ends of about one km. The maximum altitude of the system is about equal to the theoretically computed value, but the average altitude seems to be on the order of one km lower. It might be useful to do a more careful analysis of deployment, retrieval, and librations to study possible interactions with the orbital dynamics of the center of mass. The output from the SKYHOOK program contains the information necessary to compute the work done by the reel motor, the gravitational potential, the kinetic energy of the center of mass, and about the center of mass. The orbital angular momentum can also be studied.

In order to see the effects of libration, the rest of the study is divided into two cases. In the first case, the payload was released during the forward swing of the tether at the point where the tether is vertical and has its maximum forward velocity. In the second case the payload is released on a backward swing. The orbit of the payload after release requires no numerical integration and can be calculated from the state vector at release. The orbital parameters of interest are the semi-major axis a and the eccentricity e. The semi-major axis is given by

$$a = 1/(2/r - v^2/GM)$$

and the eccentricity is given by

$$e = \sqrt{1 - r^2 v_t^2/GMa}$$

where v_t is the tangential velocity. The program for plotting the radius vector r and the magnitude of the velocity v has been modified to compute the tangential velocity from the state vector and calculate a and e at the time requested on input. The apogee and perigee are given by a + ae and a - ae.

The state vector at 18800 seconds has been used to calculate the orbit of the payload released on a forward swing. The payload goes into an orbit with a perigee of 478.4 km and a apogee of 1075.0 km. For the

backward swing the state vector at 20400 seconds has been used. The payload orbit in this case has a perigee of 476.7 km and an apogee of 896.1 km. The apogee is almost 180 km higher when the payload is released on the forward swing.

The state vectors at 18800 seconds and at 20400 seconds have been used as the initial conditions for the second stage of the operation which is retrieval of the subsatellite until the center of gravity of the tether system is at the original altitude of 400 km at apogee. With the tether mass included, the tether should be retrieved to a length of 50.56 km. Without the tether mass, using the formula

$$1/L = M_L\ (M_{LP} + M_{UP})\ (M_{SH} + M_{LP})/(M_{TOT}M_{UP}M_{SH})$$

the system should be retrieved to a length of 47.068 km (the terms in the equation are as defined on page 24 of Appendix A. Figure 10 shows the results of two retrieval runs. Parts a) and b) are the tension and in-plane vs. radial plots after release on the forward swing. Parts c) and d) are the tension and in-plane vs. radial plots after release on a backward swing. The case for the forward swing was run for 7400 seconds until the tether was retrieved to a length of 39.17 km. The case for the backward swing was run for 7600 seconds to a tether length of 39.38 km. Interpolating in the plots of tether length vs. time to obtain the point where the tether is 47.068 km long gives 5970 seconds for the forward case and 6028 seconds for the backward case. In Figures 10b and 10d we see that the initial librations have been damped out and the tether is being retrieved at a steady angle which brings the subsatellite slightly ahead of the Shuttle. An appropriate control law could return the tether to the vertical before ending the retrieval if this were desirable.

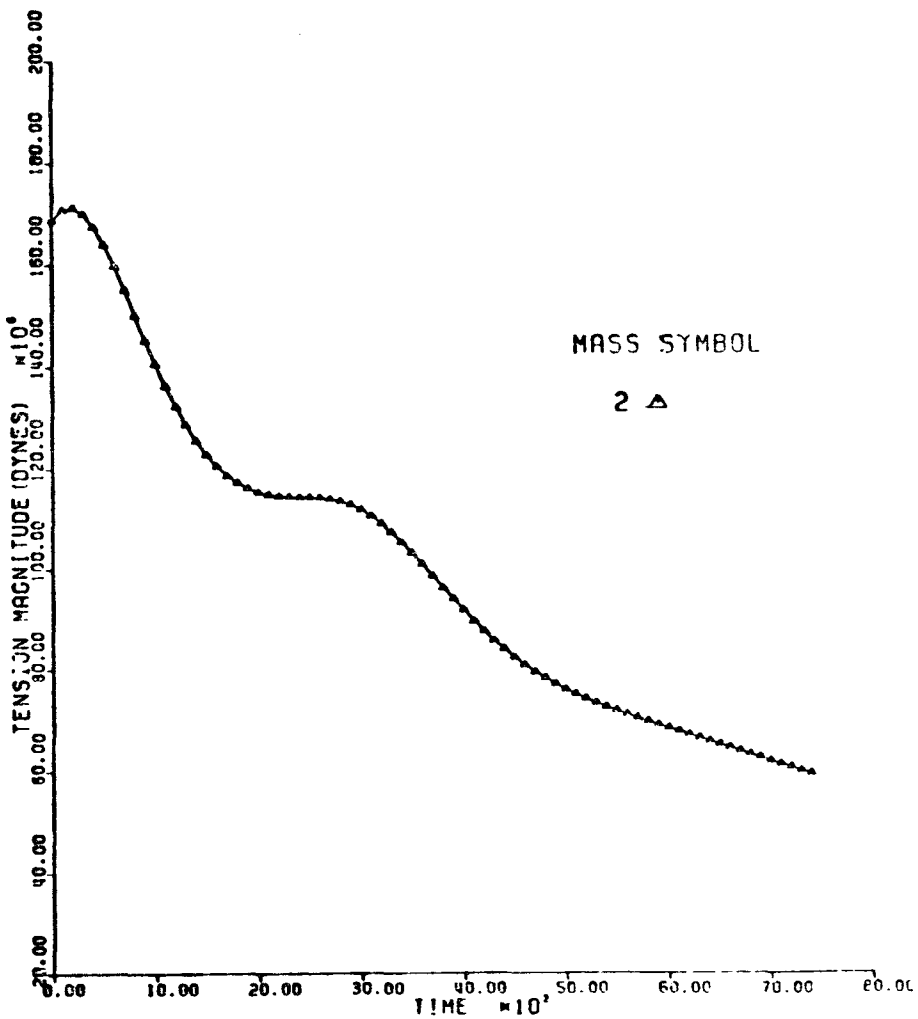

(a)

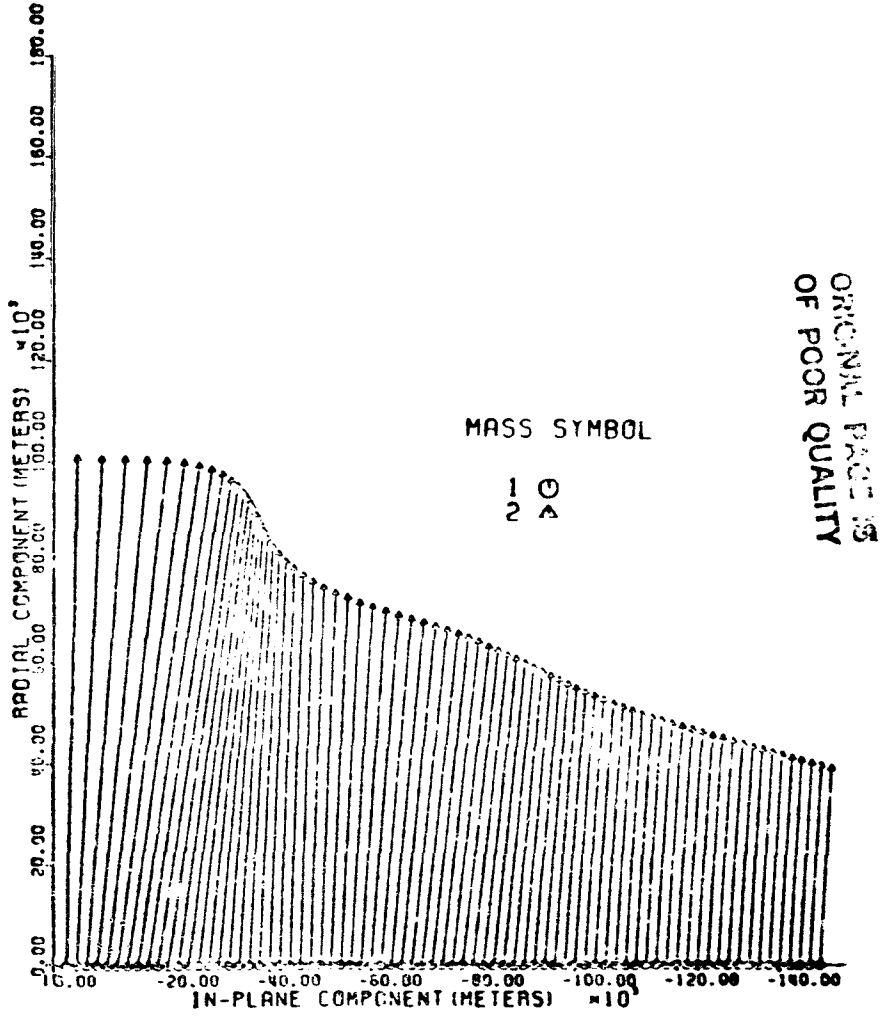

(b)

Figure 10. Tension vs. time and radial vs. in-plane configuration during partial retrevial. Parts a) and b) are after payload release on the forward swing; parts c) and d) (next page) are after release on the backward swing.

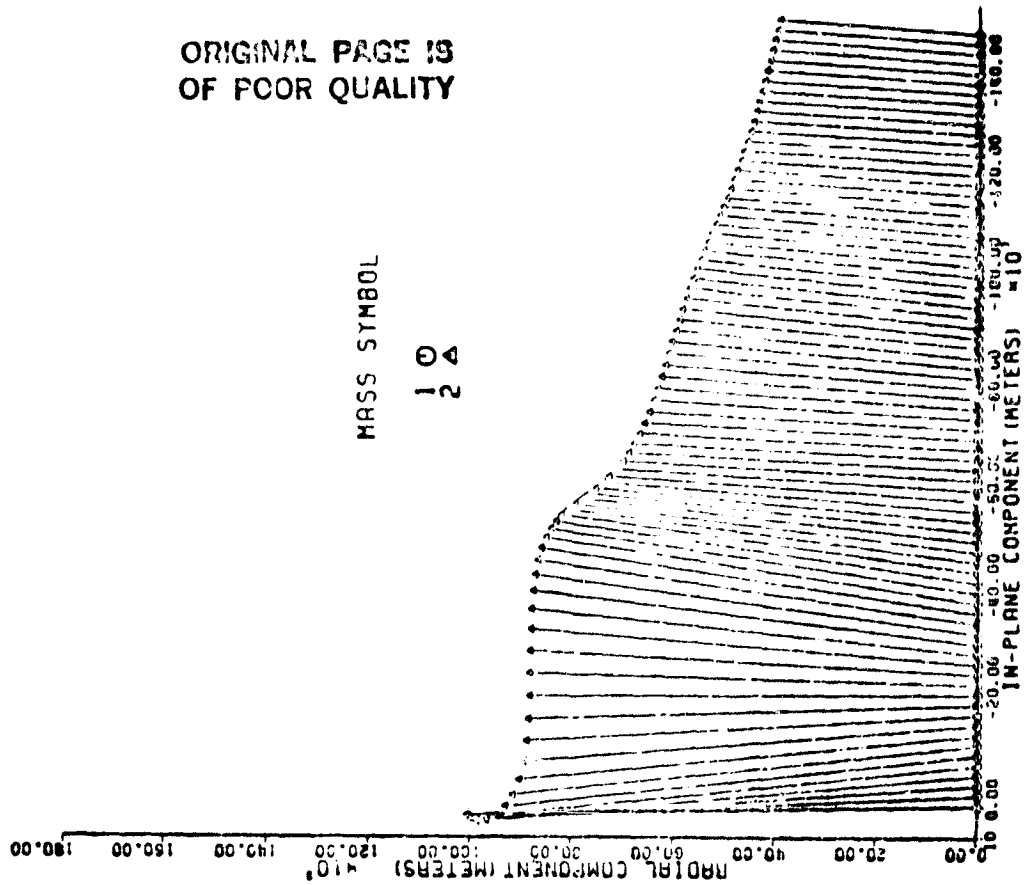

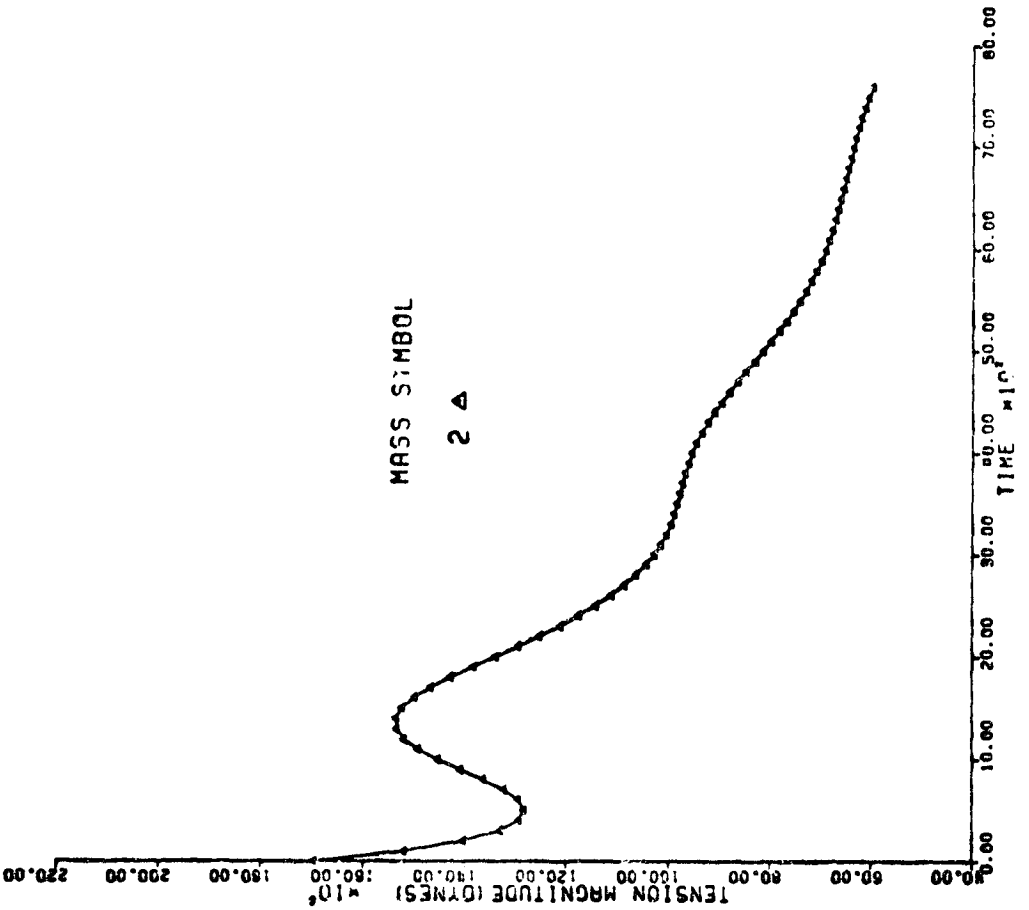

Figure 10. (Cont.) Behavior after payload release on the backward swing.

The SKYHOOK runs have been done with output every 100 seconds. In order to obtain the state vector where the tether length is 47.068 km it is necessary to interpolate in the output. The program described earlier for reading the output state vectors and formatting them for input has been modified to interpolate between the output points. As a check, the tether length is also computed for the interpolated state vector. The interpolated state vectors at these times have been used as input to the third stage of the processing which is steady state integration from the end of the retrieval to the next apogee passage where the Shuttle undocks with the tether system. In order to determine the orbit of the tether system after undocking from the Shuttle the program for reading the state vectors has been modified to read the masses of the upper and lower pallets, and compute the state vector for the center of gravity of the tether system. This state vector is then used to calculate the post release semi-major axis and eccentricity of the orbit of the tether system.

The first runs done in the steady state phase were unsatisfactory because of the linear interpolation used to obtain the initial conditions from the output of the retrieval phase. Since both the position and velocity are rotating vectors, the linear interpolation results in a systematic shortening of the magnitude of the radius vector and velocity, which makes the orbits too low. The perigee is reduced by approximately 7 times the error in the radius vector which was about 10 km in one of the cases. The interpolation has been modified by retaining the same linear interpolation for the direction of the state vectors but obtaining the magnitude of the vectors by linear interpolation between the magnitudes of the output position and velocity vectors. This method should give much better results particularly for a circular or low eccentricity orbit. For each of the two cases (payload release on the forward and backward swings) the orbit of the center of mass

of the tether system after undocking at apogee has been calculated analytically from the state vector at apogee. The final retrieval run to put the tether into its original condition has been omitted since it does not appear to be essential judging from analysis of the runs up to this point.

An assumption inherent in the theoretical formulas used to calculate the state of the system at various stages is that the center of mass of the system does not change significantly during deployment and retrieval. In a long system, there is a difference between the center of mass and the "orbital center" of the system defined as the point where the gravitational and centrifugal accelerations are equal. For this case, the orbital center of the whole system fully deployed is at 399.756 km when the center of mass is at 400 km. That is there is a difference of almost 1/4 km between the two centers of the system. The angular velocity before deployment in a circular orbit at 400 km is .001131402 rad/sec. When deployed with the center of mass at 400 km in a circular orbit the angular velocity is .001131463 rad/sec. The program for computing the orbit of the center of mass has been tested on a short equilibrium run in the fully deployed state. The program computed an apogee of 401.46 km and perigee of 400.00 km. The distance from the apogee to the orbital center at 399.757 km is 1.70 km which is 7 times the distance of .243 km between the center of mass and the orbital center. Since it is the orbital center of the system that orbits the same as a free particle, it has been decided to use the orbital center rather than the center of mass as a reference point for studying the motion of the center of the system. The position of the orbital center of the system $\bar{r}$ is given by the expression

$$r = [\Sigma m_i r_i / (\Sigma m_i / r_i^2)]^{1/3}$$

where the r's are measured from the center of the earth. The program has been modified to compute the state vector at the orbital center and derive the orbital parameters of that state vector.

In order to study the behavior of the center of the system as a function of time, two additional plots giving the altitude and velocity of the orbital center have been added to the program that reads the output state vectors. Figure 11 shows the plots for the deployment phase of the operation. The orbital eccentricity resulting in fluctuations of about .93 km shows clearly at the beginning of the run. There is a decrease in mean altitude at the end of the run to about 398.5 km. The decrease in altitude is larger than can be attributed to the difference between the center of mass and the orbital center. The decrease of 1.5 km is on the order of other minor effects and has not been studied to understand the underlying reasons. An approach for studying the problem is discussed earlier in this report. Plots of the altitude of the center of mass have been done for the other phases also. Since the other phases are all less than two orbits it is difficult to determine a mean altitude from the plots. Orbital elements have been computed at the beginning and end of each run for the orbital center. In addition, the elements for the tether system and the Shuttle have been calculated from the state vector at the time the Shuttle undocks at apogee.

Table 1 gives the apogee, perigee and semi-major axis (SMA) in km for the times of interest in all the SKYHOOK runs. Run 1 is the deployment of the system out to 100.6 km. Run 2 is the retrieval to 47.068 km after releasing the payload at 18800 seconds on a forward swing of the tether. Run 3 is the retrieval after release on a backward swing at 20400 seconds. Run 4 is a steady state integration starting from the state vector after 5970 seconds of retrieval in run 2. Run 5 is a steady state integration using

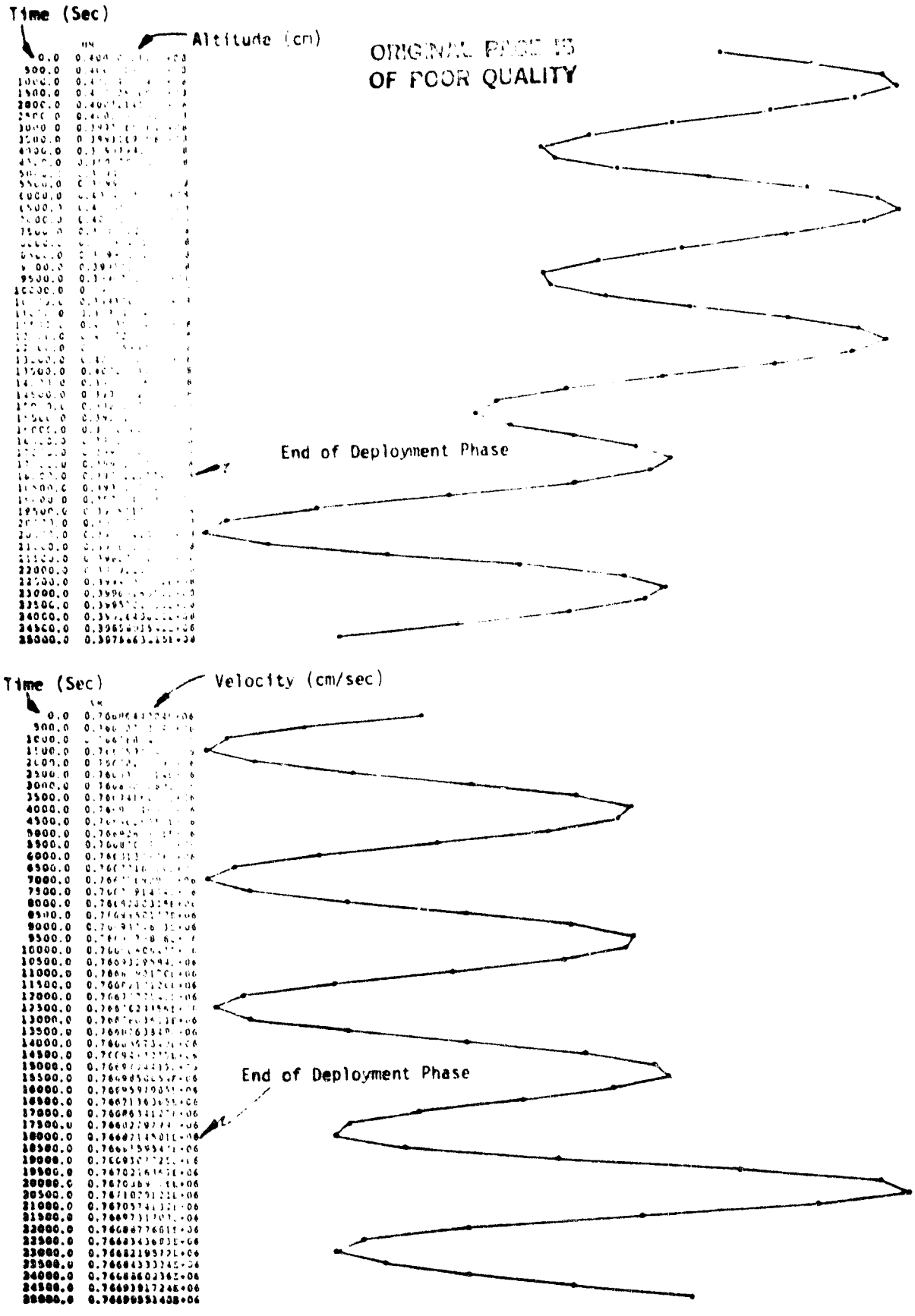

Figure 11. Altitude (cm) and velocity (cm/sec) of the orbital center during the deployment phase and steady state integration just after completion of deployment.

Table 1

Line	Run	Time	Masses	Apogee	Perigee	SMA
1	1	0	86+23.109	400.9365	399.0645	400.0005
2	1	18800	86+23.109	399.5803	396.9313	398.2608
3	1	18800	19.109	1075.0220	478.4437	776.7329
4	1	20400	86+23.109	400.2854	397.2581	398.7717
5	1	20400	19.109	896.1484	476.7392	686.4438
6	2	0	86 + 4	382.1875	265.7070	323.9473
7	2	5970	86 + 4	382.5229	266.0826	324.3028
8	3	0	86 + 4	380.6198	301.6923	341.1561
9	3	6206	86 + 4	380.9478	301.8230	341.3854
10	4	0	86 + 4	382.5229	266.0826	324.3028
11	4	5100	86 + 4	382.5223	266.0773	324.2998
12	4	5100	6 + 4	404.6969	379.3752	392.0361
13	4	5100	80	380.3441	251.5480	315.9460
14	5	0	86 + 4	380.9478	301.8230	341.3854
15	5	4050	86 + 4	380.8854	301.8820	341.3837
16	5	4050	6 + 4	419.8848	396.5458	408.2153
17	5	4850	80	378.7827	287.4962	333.1395

Apogee, perigee, and semi-major axis at various stages of the launch sequence. The values are for the orbital centers of the masses listed in the fourth column, namely the Shuttle (80 tons), lower pallet (6 tons), upper pallet (4 tons), upper pallet plus payload (23.109 tons), Shuttle plus lower pallet (86 tons), and payload (19.109 tons). Run 1 is the deployment, runs 2 and 3 are partial retrieval after release on the forward and backward swings respectively, and runs 4 and 5 are steady state runs from the end of the retrieval in runs 2 and 3 respectively to the next apogee passage.

as input the state vector after 6.06 seconds of retrieval in run 3. In run 1, the lower mass is 86 tons and the upper is 23.109. In the other runs, the lower mass is 86 tons and the upper is 4 tons. For runs 4 and 5 the state vector for the orbital center of the tether system alone has been computed at the time of undocking. The mass of the lower pallet is 6 tons and the upper is 4 tons. Finally, the state vector for the Shuttle (80 tons) at the apogee of runs 4 and 5 has been used to get the orbit of the Shuttle after undocking from the tether system. The masses listed in the Table indicate which configuration is being computed.

Line 1 in Table 1 is the orbit at the beginning of the deployment. The computed eccentricity agrees with the plots of altitude in Figure 11. Lines 2 to 5 are the orbital parameters at the time of payload release on the forward (18800 sec) and backward (20400 sec) swings. The average semi-major axis of lines 2 and 4 is 398.5 km indicating a drop of 1.5 km during deployment. This agrees with the results seen in the plots of the orbital altitude vs. time. The semi-major axis of the orbital center is about .5 km higher on the backward swing (line 4) than on the forward swing (line 2). Lines 6 and 7 give the orbital parameters at the beginning and end of the partial retrieval after release on the forward swing at 18800 sec. The semi-major axis has increased by .36 km during the retrieval. Lines 8 and 9 are the corresponding results for retrieval after release on a backward swing. The increase in altitude here is .23 km. The semi-major axis is about 17.1 km lower in run 2 than in run 3 as a result of the greater energy given to the payload by releasing on the forward swing. Lines 10 and 11 give the orbital parameters at the beginning and end of the steady state run from the end of retrieval to tether system release at apogee for the case of payload release on the forward swing. The semi-major axis is nearly constant. Line 12 is the subsequent orbit of the

tether system after undocking, and line 13 is the final orbit of the Shuttle. Lines 14 through 17 give the corresponding information for the case of payload release on a backward swing of the tether. Lines 14 and 15 show no change in semi-major axis. The average semi-major axis of the tether system after undocking obtained from lines 12 and 16 is 400.1 km. This is within .1 km of the theoretically calculated altitude of 400 km. The orbit of the tether system is 8 km higher than predicted for the case of payload release on a forward swing and 8 km lower on the backward swing. The tether system orbits are eccentric by 12.7 and 11.7 km for the forward and backward cases respectively. The average perigee of the Shuttle after undocking from the tether obtained from lines 13 and 17 is 269.5 km. This agrees within .1 km with the theoretically calculated value of 269.4 km. The final Shuttle perigee is 18 km lower or higher depending on whether the payload is released on the forward or backward swing.

In conclusion, the simulations done with the SKYHOOK program give good agreement with the theoretically calculated results from the M.I.T. study and indicate the order of magnitude of the perturbing effect of librations not considered in the theoretical study. The results indicate some altitude changes during reeling operations, and fluctuations within the libration cycle. These effects are about an order of magnitude smaller than the impact of releasing the payload on the forward or backward swing.

Appendix A

The Use of Tethers for Payload Orbital Transfer

Final Report on Subcontract SV1-52006

Submitted to the Smithsonian Astrophysical Observatory

by the Space Systems Laboratory of the

Massachusetts Institute of Technology

Prepared by

Manuel Martinez-Sanchez

March 22, 1982

Table of Contents

1. Introduction

Rocket propulsion is a well established method for moving payloads in space, and has thus far enjoyed a virtual monopoly in such applications. This preeminence is likely to continue for the foreseeable future, but with the advent of new and more flexible tools for access to space, such as the Space Shuttle, and with the constant struggle for more payload per unit cost, we are likely to witness the development of alternatives and supplements that will achieve the same mission with less mass (and cost) expenditure. Planetary gravity assist can be regarded as one such alternative, in practical use today; other concepts, such as geomagnetic propulsion, interplanetary ramjets, etc., have been proposed as future developments.

In this report, we explore a relatively simple concept for enhancing interorbital transfer capabilities. It is well known that in an extended orbiting body only certain points (those on the Earth-centered circle through the body's orbital center) are in centrifugal-gravitational equilibrium. Other points in the body undergo a net resultant force (the gravity gradient force), which, for elongated bodies, tends to align them along the local vertical. Thus, if a satellite is joined to a larger spacecraft in circular orbit by means of a long, lightweight cable (tether), its equilibrium position would be directly above or directly below that spacecraft, along the local vertical. A certain point (close to the system center of mass), intermediate between satellite and spacecraft, would be in true orbital equilibrium, while the two end masses would be pulling on the tether. If the masses of the two bodies are m_1 and m_2, the cable length

is L and the orbital angular velocity is Ω, the cable tension is

$$F = 3\Omega^2 L m_{12} \quad ; \quad m_{12} = \frac{m_1 m_2}{m_1 + m_2} \quad \text{(reduced mass)}$$

which can be recognized as the local weight of a body of mass m_{12} (close to the smaller of the two masses), times a factor $3L/R_{ORBIT}$. This force arises because the linear velocity of the (outer) mass is (greater) than that required for orbital equilibrium at its location. Therefore, if the cable is cut, the upper body will enter an elliptical orbit whose perigee is at the initial altitude of that body in the compound structure; simultaneously, the lower body enters another elliptical orbit, this one with its apogee at the initial altitude of this body.

We can now imagine the lower body to be either an orbiting Space Shuttle or an orbiting space platform, and the upper body to be a relatively light satellite; if the tether is long, the satellite will go into a high elliptical orbit, while the platform will enter an orbit with a slightly lowered perigee. If we want the system to be reuseable, some thrust must be applied to the platform to raise it to its original orbit. We will see in what follows that the total impulse required to do this is at least equal to that which would be required to place the satellite in its high ultimate orbit using thrust instead of the tether. However, and this is the crucial point of the system, the platform can be raised using high specific impulse, low thrust, electric rockets in the period between missions, while in each mission the satellite is inserted in its orbit in a rapid, quasi-impulsive manner by the tether.

Alternatively, in the case where the Shuttle is the lower spacecraft, we may choose to reenter after releasing the payload, with no need to reestablish the orbit. Some operational complications arise in this case, as will be discussed in the text, but the maneuver is feasible within certain limits. The net effect in either case can be a large overall propellant savings in the upper stage, or, equivalently, the ability to transfer significantly larger payloads with a given amount of propellant.

In the present study we have identified and assessed a variety of ways to implement these concepts. Given the limited scope of the effort, the study has been restricted to conceptualizing each system, performing first order orbital calculations to determine payload gains, and, at least for a few of the most attractive systems, carrying out conceptual designs that allow estimates of mass and power to be made. In addition, detailed tether dynamical studies were made for one case where apparently no prior work existed (see Appendix 4) , and very limited cost estimations were made for some of the systems in order to gain insight on return-on-investment times.

For the purposes of this final report we have chosen to present the material in what seems to be the most logical order, namely, from the simpler and most clearly feasible systems to those whose implementation offers difficulties, but which, by the same token, offer the greatest potential promise in terms of performance. This is not the order in which the work evolved chronologically, and some unevenness of detail may be unavoidable as a consequence.

For the sake of clarity, we present here a brief description of each of the systems studied, with some comments on their salient features. A

detailed discussion of each of them is to be found in the body of the report:

(a) Tethers as Shuttle facilities. The simplest implementation of the tether concept is when the tether system is permanently attached to the Shuttle and is flown into and out of space in each mission. Clearly, this displaces some Shuttle payload, and its utility must be restricted. We found, however, that for high energy Shuttle missions, such as polar orbits, where payload is not limited by structural considerations, the Shuttle flight envelope can be appreciably extended by a short, rewindable on-board tether. For 28.5° orbits, no advantage was found using tethers.

(b) Space-based, low mass tether systems. Another promising system is one where the tether and its associated hardware are left in space after each reuse. For tether lengths not exceeding some 100-150 Km, depending on payload, the lower mass can be provided by the Shuttle itself, docked to the rewinding end of the tether. Payloads are brought up by the Shuttle, each attached to its Orbital Transfer Vehicle; they are mounted on the tether end, the tether is deployed and the payload is released, after which the OTV fires to place the payload in its transfer orbit. The Shuttle now enters a lower elliptical orbit, but not low enough to force reentry; the tether is partially rewound and released at a condition such that, after autonomous completion of rewinding, it is back in its original orbit. The Shuttle now reenters.

For the lengths indicated for this and the previous system, the tether mass is fairly small, and winding-unwinding operations, using rate controls that have been studied elsewhere (Ref. 1.1), should present little problem. Payload increases of some 13% are indicated for a Centaur OTV used from LEO to GEO with a 100 Km tether. Deep space missions can also be significantly enhanced.

(c) Platform-based intermediate tether systems. Higher performance can be obtained with longer tethers. At this point, however, a lower platform more massive than one empty Shuttle becomes necessary to prevent reentry after release of the payload. Orbiting space stations of the kind envisioned for the 1990's are natural candidates. Now, the platform orbit must be restored by application of low level, long duration, high specific impulse thrust. This, in turn, establishes fairly high requirements for electrical power on the space station, which may become the factor limiting the achievable tether length. In addition, the tether itself becomes too massive to be conveniently rewound after each mission; an alternative concept that was evolved consists of a "ferry" or elevator which travels the length of the tether (up to some 250-300 Km) to deliver the payload-OTV combination and return. The dynamics of this travelling ferry was studied in some detail, and no real problems were encountered, although, as in other systems, climbing rate must be carefully controlled. For Centaur transfers from LEO to GEO, a 250 Km tether of this sort allows some 38% payload increase, but requires about 400 Kw of electrical power in the space station (for orbit recovery in 14 days).

(d) Large-scale tether systems for LEO-GEO transfer. We also studied more ambitious systems involving two permanent tethers, one in LEO (radially out) and one in GEO (radially in). The payload-OTV is released by the lower tether and a first impulse is applied by the OTV to enter a Hohmann orbit. At its apogee, a second impulse matches speed with the lower end of the GEO tether, and, after capture by it, the payload travels along the tether to GEO orbit. By proper choice of parameters, the rendezvous can be attempted again after an integer number of orbits. This system can in principle be pushed to the limit where no propulsion is needed on the payload, if the

initial LEO orbit is equatorial; however, this requires tethers with lengths of the order of 1200 Km in LEO and 10,000 Km in GEO, and of great mass. Intermediate solutions are possible using nonzero impulses in LEO and GEO; for instance, a 430 Km LEO tether (weighing 7.5 times the OTV mass) and a 5900 Km GEO tether (of mass 10 times that of the OTV) can be combined to obtain a factor of 2.8 in payload capacity for a Centaur vehicle.

Ref. 1.1 Charles C. Rupp, NASA TM x-64963 "A tether tension control law for tethered subsatellites deployed along the local vertical."

2. Tethers as Shuttle Facilities

Use of a tether system as a permanent facility of the Shuttle does not appear justified for missions that fall within the operational envelope of the orbiter with its integral OMS tanks. This is because, even though the tether allows deployment of the payload from a lower Shuttle orbit (typically an elliptic one), the payload cannot be increased due to other constraints, such as payload bay structural integrity and c.g. location. The only savings are then in the use of less OMS fuel, but these cannot balance the loss of revenue from the payload displaced by the tether itself. An example is shown in Table 2.1: a 47 Km tether allows payload to be placed in a 500/500 Km orbit from a Shuttle in a 185/453 Km orbit, with an OMS fuel savings of $33,000. However, the mass and length of the tether facility displaces payload worth $2.80 M. Similar results are shown for a polar orbit.

There are some possible scenarios where a Shuttle based tether could be cost-effective. These refer to low Earth orbits high enough (particularly for polar orbits) that payload is limited by OMS fuel capacity, including extension kits. A trade-off study is next presented to determine how far the operating envelope can be extended by a permanent Shuttle tether.

If the OMS fuel extension kits are not available to the Space Transportation System, then the relevant comparison is between the basic Shuttle with only the integral OMS tanks and the Shuttle with the on-board tether system. The advantages of the tether system are then apparent, resulting in a flight envelope comparable to that afforded by the fuel kits.

TABLE 2.1

COST TO LOW ENERGY MISSION**

	Space Telescope	Polar Orbit
	Orbit 500Km/28.8°	1000 Km/97°
Weight of Payload (kg)	11,000	3,000
Length of Payload (m)	13.1	9.0
Diameter of Payload (m)	4.26	
Cost to current Shuttle ($M)	20.20	23.07
Cost to Shuttle + Orbiter based tether system ($M)	23.00	29.8
Lost revenue from displaced payload ($M)	-2.80	-6.73
OMS fuel savings ($M)	(0.033)	(0.083)
Benefit of using tether system ($M)	-2.77	-6.647

**

1) Cost per Shuttle flight = $27.3 at ETR

$46.9 at WTR

2) Elliptic Shuttle orbit + tether transfer perigee altitude = 185 km

Calculation of the Shuttle Mission Envelope with an On-Board Tether System.

We adopt as a prototype mission one where payload is to be delivered to a circular orbit by releasing it from a tether which is attached to a reeling device carried on board the Shuttle, and which is subsequently retrieved by it. The Shuttle itself flies an elliptic orbit with its apogee lower than the payload orbit (by an amount equal to the tether length). It is injected into this orbit by a velocity increment applied by the OMS at some point in a standard 185 Km circular parking orbit. After release of the payload, the Shuttle enters a new elliptic orbit with perigee lower than the original 185 Km, and then de-orbits by application of an additional ΔV (such as to give a theoretical perigee of 0 Km). For calculations, one further OMS firing of 30.5 m/sec (106.7 m/sec for WTR launch) is assumed for insertion of the loaded Shuttle into the parking orbit, and a 12.8 m/sec ΔV reserve is assumed.

An example launch sequence (for an intended payload orbit of 600 Km altitude and 28.5° inclination) is shown in Table 2.2.

Starting from the parking orbit at radius R_p (equal to the perigee length of the transfer orbit), the Shuttle enters the transfer orbit of apogee R_A by an OMS firing having a ΔV of

$$\Delta V_{insertion} = \sqrt{\frac{\mu}{R_p}} \left(\sqrt{\frac{2R_A}{R_A + R_p}} - 1 \right) \tag{1}$$

The angular velocity at apogee can be expressed as V_A/R_A, and must be equal to that in a circular orbit at the final payload radius $R_f = R_A + L_T$, where L_T is the tether length. This gives

$$\frac{\mu}{R_A^3} \frac{2R_p}{R_A + R_p} = \sqrt{\frac{\mu}{R_f^3}} \tag{2}$$

which can be rewritten as

$$\frac{2R_p}{R_f + R_p - L_T} = \frac{(R_f - L_T)^3}{R_f^3} \tag{3}$$

This equation is to be solved for the tether length L_T in terms of the parking orbit radius and the final orbital radius. $\Delta V_{ins.}$ then follows from Eq. (1), using $R_A = R_f - L_T$.

Table 2.2. Typical sequence of mission events

STS/on-board tether system

From ETR to 28.5° 600 km circular orbit

Event	delta-V(OMS) m/sec	Resultant h_a/h_p, km
Shuttle insertion	30.5	185/185
Injection burn	100.4	534.3/185
Payload release orbit		600/600
Shuttle after P.L. release		516.2/68.8
Shuttle deorbit	55.1	516.2/0

(note: delta-V reserve = 12.8 m/sec)

The tension T in the tether is constant if its own mass can be ignored relative to the satellite mass. If we further assume that the satellite mass is small compared to that of the Shuttle (a conservative assumption), and that the tension at perigee can be estimated as if the orbit were circular with $R = R_p$, we can write (Ref. 2.1)

$$T = M_L \frac{V_p^2}{R_p} \lambda \left(\frac{3}{1+\lambda} + \frac{\lambda}{1+\lambda} \right)^2 \qquad (4)$$

where M_L is the payload mass and $\lambda = L_T/R_p$.

For a Kevlar Aramid cable of 0.9 mm diameter the mass is m = 0.59 Kg/Km, and the minimum break strength is $T_{Br.} = 90$ Kg = 882 Nt.* Allowing a safetv factor f_s ($f_s = 5$ was used in calculations), the number of strands is $\frac{T.f_s}{T_{Br}}$, and the tether mass is

$$M_T = \frac{T.f_s m}{T_{Br}} L_T \qquad (5)$$

The mass of the reeling and other devices is expected to be proportional to the tether mass. Based on Ref.(2.1), we estimate for the total tether system

$$M_{Ts} = 4.7\ M_T \qquad (6)$$

Notice that, to this approximation, M_{Ts} is proportional to M_L, the

---

Ref. 2.1 NASA CR-132780, Appendix D, p. 222.

---

*Note that somewhat different values of the working stress have been used in other sections of this report. The value used in each case has been clearly identified, however. For a discussion of the uncertainties in an estimate of this parameter, see Appendix 1.

payload mass; the quantity

$$m_{Ts} = \frac{M_{Ts}}{M_L} \tag{7}$$

is therefore a function of the orbital parameters, but not of M_L .

The mass of the orbiter at ME burnout is

$$M_o = M_{oe} + M_L + M_{Ts} + M_p \tag{8}$$

where M_{oe} is the empty mass and M_p the mass of OMS fuel carried (either that in the integral OMS, or including an integer number of OMS kits as well). The fuel required for insertion into the parking orbit plus injection into the transfer orbit (total velocity increment = ΔV_1) is $M_o(1-\mu_1)$ where

$$\mu_1 = e^{-\Delta V_1/gI_{sp}} \tag{9}$$

The mass after releasing the payload is then $M_o\mu_1 - M_L$, and after the deorbiting burn (ΔV_2), the mass is

$$(M_o\mu_1 - M_L)\,\mu_2 \quad , \quad \text{with}$$

$$\mu_2 = e^{-\Delta V_2/gI_{sp}} \tag{10}$$

This mass is to be equated to $M_{oe} + M_{Ts}$, since, by assumption, all the OMS fuel has been used up:

$$[(M_{oe} + M_L + M_{Ts} + M_p)\mu_1 - M_L]\mu_2 = M_{oe} + M_{Ts} \tag{11}$$

and using $M_{Ts} = M_L\, m_{Ts}$,

$$M_L = \frac{M_p \mu_1 \mu_2 - M_{oe}(1 - \mu_1 \mu_2)}{m_{TS}(1 - \mu_1 \mu_2) + \mu_2(1 - \mu_1)} \qquad (12)$$

This equation allows calculation of the maximum payload capability of a Shuttle-tether system combination for a given payload orbit and a given OMS option. An additional limitation was used, namely, that the sum of the payload, tether system and OMS kits should not exceed 29500 Kg, the full load capability of the Orbiter.

The results of these calculations are displayed in Fig. 2.1 (for ETR launch into a 28.5° inclination orbit) and Fig. 2.2 (for WTR launch into a 104° orbit). The basic Shuttle envelopes shown for reference were calculated from the same basic equations, modified to allow variable "parking orbit" altitudes and no tether.

Fig. 2.1 shows that the combination Integral-OMS-plus-tether has substantially more payload capacity than the basic Integral OMS Shuttle for a 28.5° orbit; it allows,for instance, 21 Ton payloads to a 700 Km orbit without any extension kit. The same is true when OMS kits are added to both systems (without and with tether). When we consider the envelope of the curves for the tether system with varying numbers of extension fuel kits, we find that it does not exceed the corresponding envelope without tethers. Thus, if extension kits were available, the usefulness of the on-board tether would be marginal.

For the polar orbit case, Fig. 2.2 shows the same, and even more pronounced, gains in payload-altitude performance for polar orbits. In fact, even the envelope is now extended; i.e., certain missions which are simply not accessible to the Shuttle with any number of extension

kits now become feasible. This is the case for orbits between 500 and 700 Km, for which payload extension of some 2 tons become possible using the integral OMS tanks plus a tether system. An example of the use of this extended capacity would be the possibility of placing the 11 ton Space Telescope in a 600 Km polar orbit. Similarly, while no payload can be delivered by the Shuttle to orbits higher than 960 Km (even with two extra fuel kits), the tether system with one single kit allows some 4.4 tons to be placed in 1000 Km orbit (2 tons with the tether and no kit).

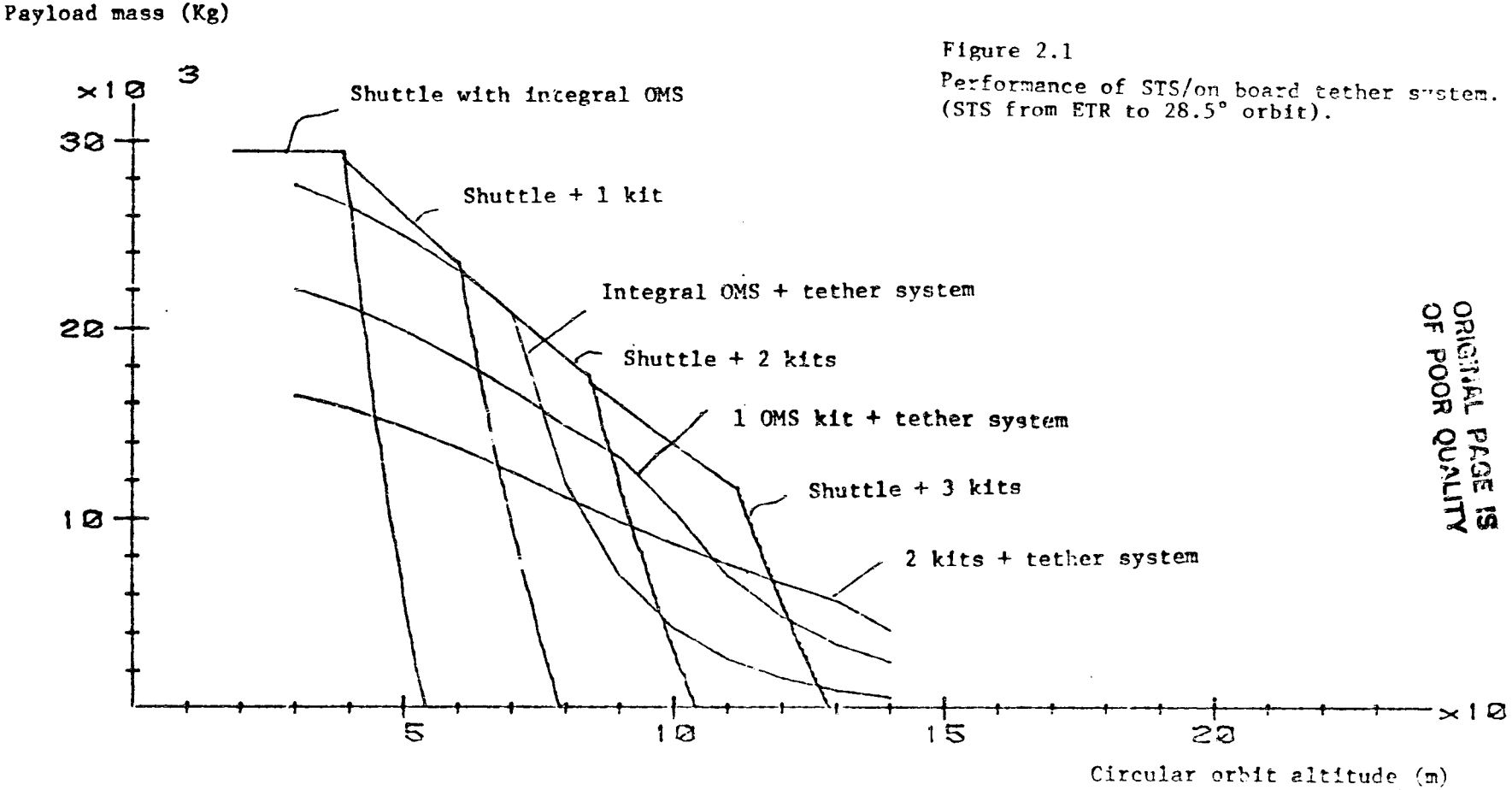

Figure 2.1
Performance of STS/on board tether system.
(STS from ETR to 28.5° orbit).

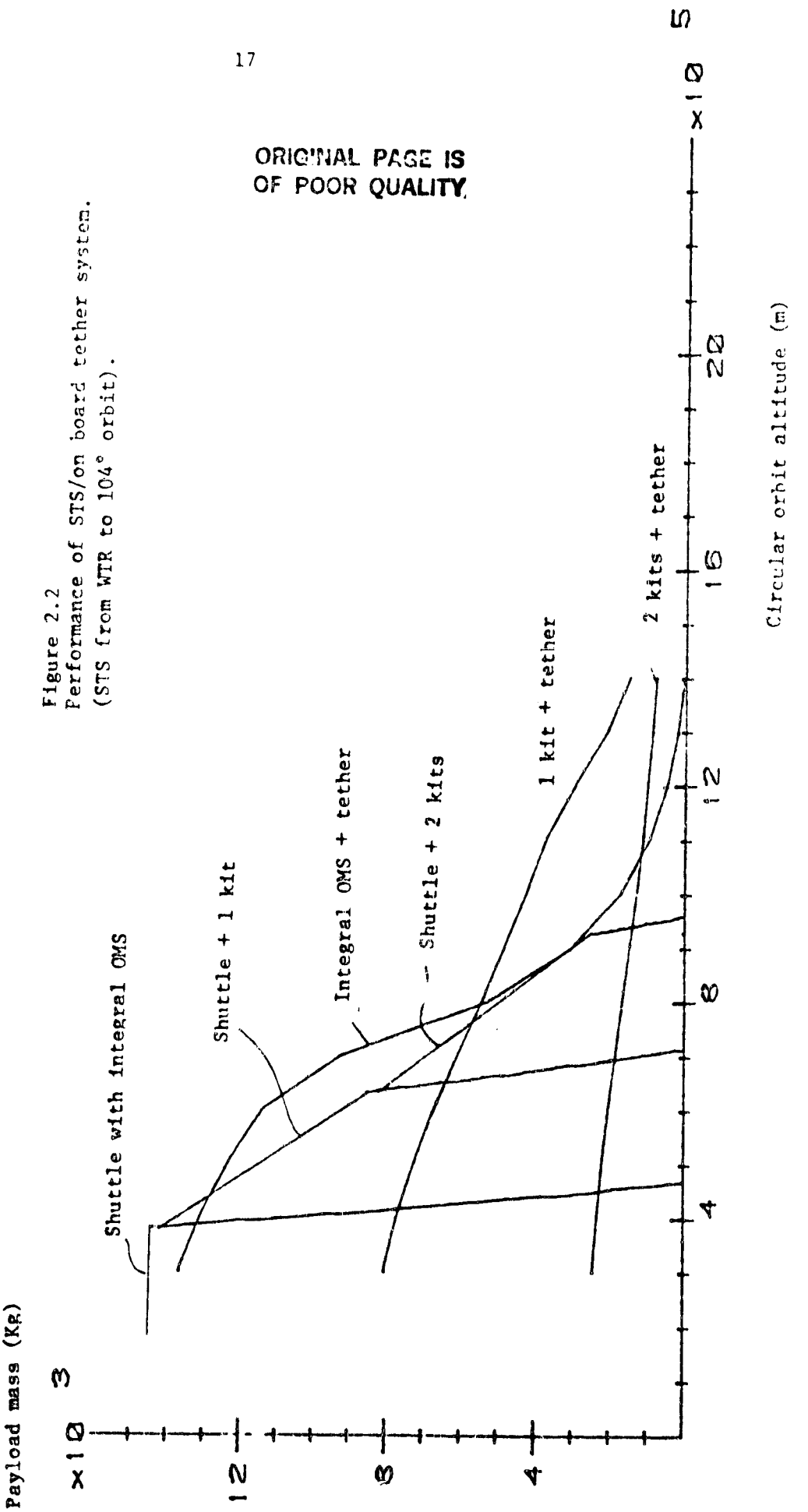

Figure 2.2
Performance of STS/on board tether system.
(STS from WTR to 104° orbit).

3. Space-Based, Low Mass Tether System.

Preliminary Considerations.

The concept of leaving the tether in orbit for reuse was introduced early in our study, and validated by simple orbital dynamics calculations, which showed marked increases in payload capability both for orbit transfers and for deep space missions. In these initial calculations, the reaction mass attached to the tether base was assumed large for simplicity, and no account was taken of tether mass (although the tether length was restricted to less than 400 Km to keep its mass within reasonable limits, see Appendix 1).

Table 3.1 shows some results of these calculations, assuming a two-stage IUS vehicle is attached to the payload and used for the initial and circularization firings in a LEO-GEO transfer. The tether is attached to a massive LEO base. Payload increases of roughly 20% per 100 Km of tether are predicted.

Similar results for deep space missions are shown in Table 3.2, this time in conjunction with a Centaur vehicle. The value of $c_3 = 80$ Km^2/sec^2 is typical of direct Galileo orbits, and, as shown, an 8% payload increase is predicted per 100 Km tether length. For other excess hyperbolic velocities, the results are given in Fig. 3.1.

3.1 System description.

While these calculations clearly show the desirability of such tether systems, they ignore the complications due to the finite mass of the lower platform. In particular, these can be important if this platform is simply the Space Shuttle, plus possibly a lighter station at the lower tether end.

Table 3.1

PAYLOAD BENEFIT FOR GEOSYNCHRONOUS ORBIT TRANSFER*

Tether length (km)	Payload Weight (kg)	Payload increase (%)
0	2465	
100	3122	18
200	3675	39
300	4326	63
400	5100	93

*Calculation conditions:

1. SHUTTLE + Two stage IUS

Stage	1	2
Isp(sec)	291.9	289.7
f stru.	.946	.933
WT prop.(kg)	9707	(2722)

2. Parking orbit: 300/300 km

3. Tether system dock with shuttle in parking orbit.

Table 3.2

PAYLOAD BENEFIT FOR SOLAR SYSTEM EXPLORATION**

C3 (km2/sec2)	Tether length (km)	Injected mass (kg)	Increase (%)
15	0	7693	
	100	8253	7.2
	200	8857	15
	300	9511	23.6
400	400	10219	32.8
80	0	2246	
	100	2413	7.4
	200	2589	15.2
	300	2771	25.3
	400	2963	31.9

** Calculation conditions:

1. SHUTTLE + CENTAUR

   Isp = 444 sec

   WT of propellant = 13608 kg

   Dry WT = 1827 kg

2. Parking orbit: 300/300 km

3. Tether system dock with shuttle in parking orbit.

4. $C_3 = V^2 - \frac{2\mu_e}{r}$

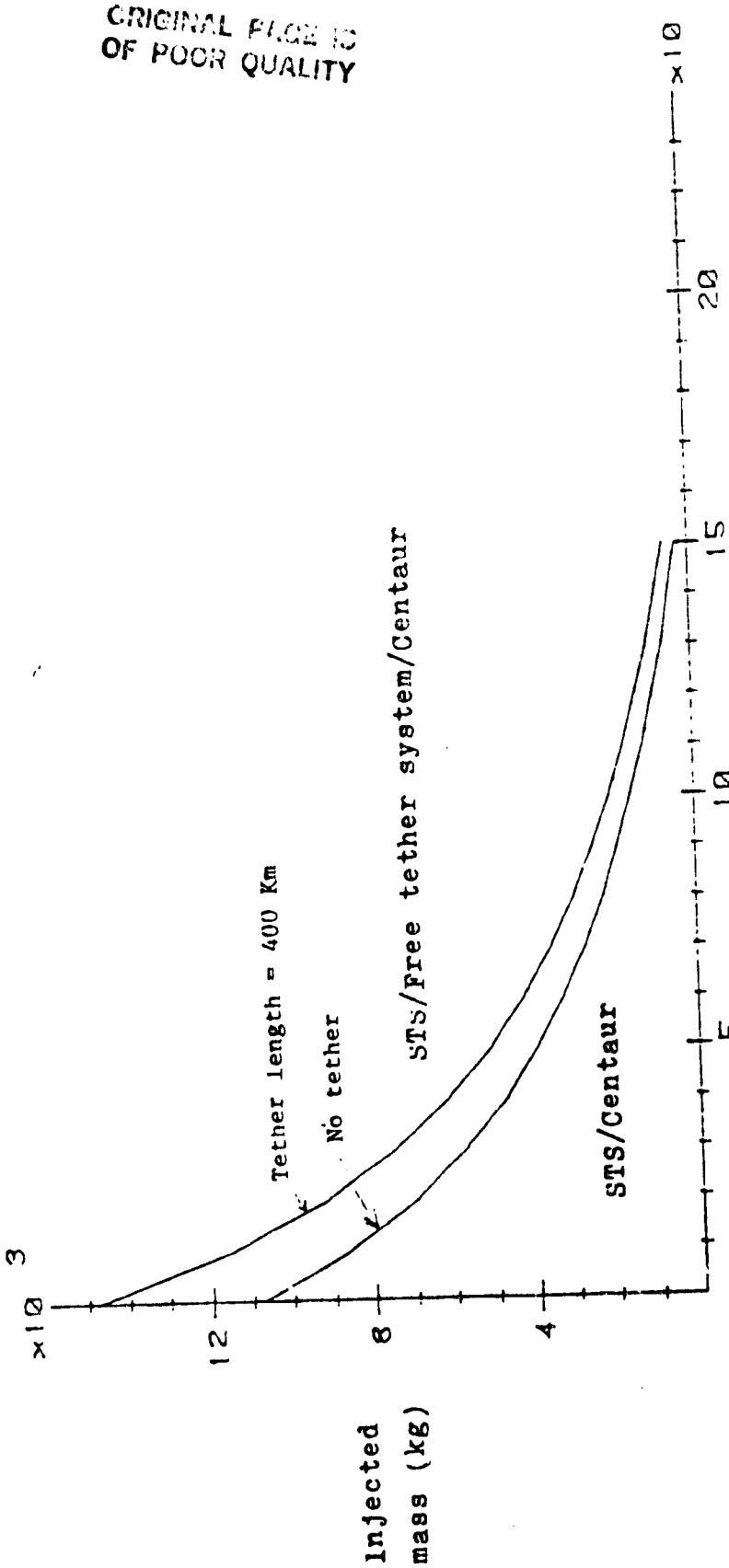

Figure 3.1 STS/Free tether system enhances launch capability.

This combination is quite attractive in that it reduces to a minimum the needs for elaborate and costly space platforms, and is therefore amenable to an early implementation. In the remainder of this section we describe and analyze a reuseable, low mass tether system for use in conjunction with the present Space Transportation System.

3.2 Space-based, low mass tether systems for orbital transfer assist.

The core of this system is a pair of relatively light space platforms connected by a tether of up to about 100/200 Km length. The lower platform can be quite similar to the pallets used as Airborne Support Equipment (ASE) for mating the IUS rocket vehicle to the Shuttle payload bay. It would be designed to house the wind/unwind mechanism and controls, to house the fully wound tether during initial launch and between missions, and to dock and interface with the Shuttle for subsequent missions.

The second, or upper platform, has as its mission to receive the OTV/payload package from each loaded Shuttle after its docking with the lower platform, to hold this package during tether unwinding, and to release it after stabilization at the fully extended position. Due to the low gravity gradient forces involved in this system, this upper pallet can be considerably lighter than the aforementioned ASE.

After releasing the OTV, the tether would be rewound in stages as discussed below, and the whole system would be left in orbit for reuse. Since its total mass is of the order of 15 Tons, the system can be delivered by one single initial Shuttle flight. Its reuseability is in principle only limited by tether wear.

Following is a step-by-step description of the typical mission for this system:

Stage 0: Shuttle flight delivers tether system to orbit (between 300-400 Km). System consists of a lower pallet, designed to dock with subsequent Shuttles and to wind-unwind the tether, a length of tether (100-200 Km, depending on payload), and an upper pallet, or teleoperator, designed to hold the OTV and payload.

Stage 1: Later, another Shuttle flight docks with tether system. OTV + payload is transferred to upper pallet. Tether is unwound slowly, at controlled rate. After stabilization, OTV is released.

Stage 2: OTV fires, places payload on transfer ellipse. At GEO, OTV circularizes.

Stage 3: Shuttle, docked to pallet and with extended tether enters an elliptic orbit, with perigee above sensible atmosphere. While in this configuration, tether is partially rewound, until its c.g. coincides at apogee with original c.g. altitude.

Stage 4: Shuttle releases (at one apogee passage) tether system, which stays in original circular orbit. After release, pallet completes tether rewinding. Shuttle itself goes into slightly modified elliptic orbit, from which it reenters as desired. Tether system is ready for reuse.

3.3 Performance analysis.

Nomenclature:

L = tether length

M_L = mass of OTV + payload

M_{up} = mass of upper pallet

M_T = mass of tether

M_{Lp} = mass of lower pallet

M_{SH} = mass of lower platform (Shuttle)

M_{tot} = sum of these

R_{LEO} = radius of orbit for autonomous tether system. After Shuttle docking and tether deployment, R_{LEO} is the orbit radius for the overall c.g.

G = Overall c.g. before OTV release

G' = Overall c.g. after OTV release

x = distance from Shuttle to G

x' = distance from Shuttle to G' before partial rewinding

$\tilde{x}'$ = distance from Shuttle to G' after partial rewinding

$\tilde{x}_{TS}$ = distance from Shuttle to tether system c.g. after partial rewinding

Before payload release (but after tether deployment), the overal c.g. (G) is at a distance x from the Shuttle-mated lower pallet:

$$x = \frac{M_L + M_{up} + M_T/2}{M_{TOT}} L$$

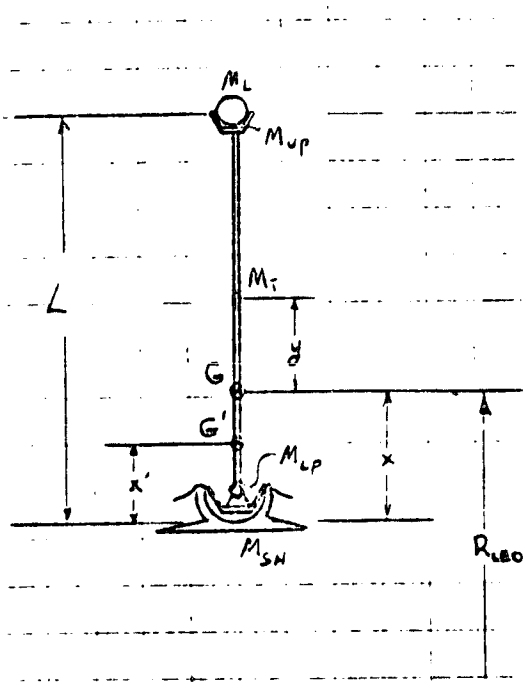

$$M_{TOT} = M_{SH} + M_{L_p} + M_T + M_{up} + M_L$$

After M_L separates, the new c.g. (G') is at

$$x' = \frac{M_{up} + M_T/2}{M_{TOT} - M_L} L$$

Point G' now enters an elliptic orbit with apogee

$$R_a = R_{LEO} - (x - x')$$

and apogee velocity

$$v_a = \sqrt{\frac{\mu}{R_{LEO}^3}} [R_{LEO} - (x - x')]$$

Using

$$v_a^2 = \frac{\mu}{R_a} \frac{2R_p}{R_a + R_p}$$, and expanding

to 1st order in $(x-x')/R_{LEO}$, we find from the above

$$R_p \approx R_{LEO} - 7(x - x')$$

Next, we slowly rewind, while G' stays in the same elliptic orbit. When the new tether length is ℓ, the distance between G' and the Shuttle is

$$\tilde{x}' = \frac{M_{up} + \tilde{M}_T/2}{M_{TOT} - M_L}\,\ell$$

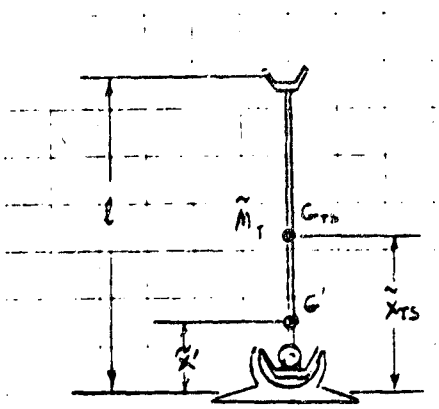

where $\tilde{M}_T = M_T\,\ell/L$

and $\tilde{M}_{LP} = M_{LP} + (1 - \frac{\ell}{L})\,M_T$

so that $\tilde{M}_T + \tilde{M}_{LP} = M_T + M_{LP}$

Also, the distance to the c.g. (G_{TS}) of the tether system alone is

$$\tilde{x}_{TS} = \frac{M_{up} + \tilde{M}_T/2}{M_{LP} + M_T + \tilde{M}_{up}}\,\ell$$

The orbital eccentricity $e = \frac{R_a - R_p}{R_a + R_p} \simeq 6\,\frac{x - x'}{R_{LEO}}$ forces in-plane oscillations of the tether at the orbital frequency and with amplitude e. It can be shown readily that their effect is of second order in $\frac{x - x'}{R_{LEO}}$, and will not be included in this analysis (although they should be assessed in a more careful study).

The forward speed of G_{TS} at apogee is therefore

$$v_{GTS} \simeq v_a + (\tilde{x}_{TS} - \tilde{x}')\,\frac{v_a}{R_a}$$

We want to stop rewinding and release the OTV at apogee when v_{GTS} coincides with the orbital speed at the location of G_{TS}, i.e., at

$$R_{GTS} = R_{G'} + \tilde{x}_{TS} - \tilde{x}' = R_{LEO} + \tilde{x}_{TS} - \tilde{x}' - x + x'$$

This leads to the condition

$$\sqrt{\frac{\mu}{R_{LEO} + \tilde{x}_{TS} - x + x' - \tilde{x}'}} = \sqrt{\frac{\mu}{R_{LEO}^3}}\,[R_{LEO} - (x - x')] + \sqrt{\frac{\mu}{R_{LEO}^3}}\,(\tilde{x}_{TS} - \tilde{x}')$$

or, after expansion and simplification,

$$\tilde{x}_{TS} - \tilde{x}' = x - x'$$

In words, the c.g. of the tether system alone must be made to coincide with the original overall c.g. If this condition is satisfied at the instant the Shuttle detaches from the partially rewound tether system, the latter (its c.g.) will remain in the original circular orbit. Final rewinding after this time will not affect this result, and so the fully retracted tether system is ready for reuse.

Using the formulas derived for x, x', $\tilde{x}_{TS}$ and $\tilde{x}'$, we can now calculate the required partial rewinding length:

$$-\frac{M_{up} + \frac{M_T}{2}\frac{\ell}{L}}{M_{TOT} - M_L - M_{SH}}\,\ell - \frac{M_{up} + \frac{M_T}{2}\frac{\ell}{L}}{M_{TOT} - M_L}\,\ell = \frac{M_L + M_{up} + M_T/2}{M_{TOT}}\,L - \frac{M_{up} + M_T/2}{M_{TOT} - M_L}\,L$$

or, after simplification

$$\frac{\ell}{L} = -\frac{M_{up}}{M_T} + \sqrt{\left(\frac{M_{up}}{M_T}\right)^2 + 2\,\frac{M_L}{M_{TOT}}\,\frac{M_{TS}}{M_T}\,\frac{M_{SH} + M_{LP} + M_T/2}{M_{SH}}}$$

where $M_{TS} = M_{LP} + M_T + M_{up}$ (tether system mass).

After releasing the tether system, the Shuttle itself enters a new elliptic orbit with apogee at

$$R_a = R_{C'} - \tilde{x}' = R_{LEO} - x + x' - \tilde{x}'$$

with apogee velocity

$$v_a = -\sqrt{\frac{\mu}{R^3_{LEO}}}\ R_a$$

Hence its new perigee is at

$$R_{p,SH} = R_{LEO} - 7(x - x' + \tilde{x}')$$

This may in some cases be actually higher than the altitude of the Shuttle in the first perigee passage after payload release, but before any rewinding. Thus, one should also check this altitude.

$$h_{MIN,SH.} = R_{p,C'} - x' - R_E = h_{LEO} - 7x + 6x'$$

Numerical Example.

Consider the case where the system is orbited at $R_{LEO} = R_E + 400$ Km, the tether length is 100 Km and the loaded Centaur mass is 19,109 Kg. Of this mass. 5009 Kg are payload.

For these conditions the tether mass is (See Appendix 1).

$$M_T = 0.140 \times 19{,}109 = 2675 \text{ Kg}$$

We find for this example ΔV_p = 2235 m/sec , ΔV_a = 1448 m/sec .

Using the Centaur data M_p = 10870 Kg, M_s = 3230 Kg, I_{sp} = 444 sec, the payload mass then is

$$M_{pay} = 4935 \text{ Kg}$$

and the loaded OTV mass is

$$M_L = 18{,}992 \text{ Kg}$$

These are indeed close to the assumed values. For comparison, if the tether were not used, one would need ΔV_a = 2398 m/sec, ΔV_p = 1456 m/sec, giving M_{pay} = 4356 Kg. Thus, the tether system allows a 13.3% increase in payload to GEO.

The same calculation was repeated for L = 150 Km, M_L = 19,412 Kg of which 5312 Kg are payload), M_T = 0.711 M_L = 6910 Kg and, on account of the higher tether mass to be rewound and stored, M_{LP} = 13,000 Kg. The results are now

M_{TOTAL} = 123,322 Kg	M_{TS} = 23,910 Kg
x = 32.68 Km	x' = 10.76 Km
ℓ = 105.76 Km	$\tilde{M}_T$ = 4,892 Kg
$\tilde{x}'$ = 6.56 Km	$\tilde{x}_{TS}$ = 28.51 Km
$h_{MIN,SH}$ = 235.8 Km	$h_{SH,P}$ = 200.6 Km

Thus, 150 Km is still feasible with a full Centaur payload, allowing a payload increase of 20.5% over the unassisted Centaur. However, the tether system is now bulky and heavy enough that rewinding operations may begin to be cumbersome.

3.5 Estimation of Pallet Masses for the 100 Km Case.

From the masses and c.g. locations of the previous examples, the tether tension can be calculated. After payload release, but before significant rewinding, we find

$$F = 980 \text{ Nt}$$

whereas immediately after Shuttle detachment,

$$F = 530 \text{ Nt}$$

A rewinding velocity of 1 m/sec is assumed. This should cause librations of no more than 2-4° amplitude, provided appropriate damping and terminal tension control is exerted, and implies some 14 hrs. for each of the two rewinding phases (under Shuttle power and own power respectively).

With these data, the power required on board the lower pallet for the autonomous rewinding phase is 530 watt. Allowing for mechanical losses and some maneuvering margin, a 1 Kw power supply is adequate. This can be provided in a variety of ways; perhaps the most compact for this application would be a H_2-O_2 fuel cell similar to those in the Shuttle itself. The mass and volume of cryogenic fuel needed is minimal, and the length of time when cryogenics must be stored on the pallet is only the duration of the rewinding phase. The mass of the 1 Kw fuel cell can be about 10 Kg, plus about 5 Kg for reactants and tankage.

The rewinding motor itself must also be on the lower pallet. It must also be used as a generator to absorb the mechanical power generated during the deployment of the tether with the OTV and payload at its end. Since

this operation is done while the pallet is mated to the Shuttle, the generated power (about 5 KW peak), can be used to supplement the Shuttle's own power supply, or can be radiated from a resistor bank. Allowing for losses, an 8 KW DC motor-generator seems adequate; at a conservative 25 Kg/KW, this implies a mass of 200 Kg, to which we should add another 200 Kg for gearing to the low RPM required.

Additional mass items for the lower pallet include the reel drum and supporting structure. The volume of the fully rewound tether is about 2.1 m^3; an aluminum drum 1.2 m. long with a core diameter of 0.4 m and end plates of 1.6 m, using 2 cm Al. thickness has a mass of 200 Kg. A similar mass can be assumed for the drum supports.

The main structure of the pallet itself, including its Shuttle interfaces, can conservatively be likened to the Airborne Support Equipment for the IUS vehicle, which has a mass of 4160 Kg. After adding the items just discussed (power, motor-generator, reel and reel support), the lower pallet mass comes to 4975 Kg. Thus, even allowing for 10% growth, the 6000 Kg used in the calculations seems conservative. Regarding the upper pallet, its main features may again be likened to those of the ASE, except that, since launch loads need not be absorbed (only the approximately 1/20 g gravity gradient force), it must be possible to lighten its structure considerably. Some attitude control propulsion should be added, mainly for control of rotation about the tether line and of out-of-plane oscillations; no estimate of these needs is available, but it is unlikely that the required thrusters and fuel would exceed 500 Kg. Altogether, the figure of 400 Kg for the upper pallet appears reasonable.

3.6 Estimated Economic Performance.

It is clear that a detailed assessment of the economies of adopting the scheme under discussion would require a much more thorough design and systems study. However, some preliminary considerations can be advanced at this point.

First, the initial development and deployment of the tether system requires some up-front investment. Since only a medium level of technology is involved, an R & D and procurement cost of $40 M can be estimated. To this we must add the initial launch cost; assuming the Shuttle flight can be shared, the 13,000 Kg tether system would displace cargo revenue of about $18 M.

Let c_0 be the cost per Kg for transportation to LEO ($1000/Kg for the Shuttle) and C_{otv} the procurement cost of the OTV (estimated at $50 M for the Centaur). Let also M_{OTV}, $M_{pay,0}$ and M_{pay} be the OTV mass, payload mass with no tether used and payload mass with the tether system.

Then, the costs per Kg of payload to GEO without and with tether are

$$c_{w/o} = c_o \left(1 + \frac{M_{OTV}}{M_{pay,o}}\right) + \frac{C_{OTV}}{M_{pay,o}}$$

$$c_w = c_o \left(1 + \frac{M_{OTV}}{M_{pay}}\right) + \frac{C_{OTV}}{M_{pay}}$$

The cost saved per flight due to the extra payload allowed by the tether is then

$$(c_{w/o} - c_w)\, M_{pay} = (c_o M_{OTV} + C_{OTV})\left(\frac{M_{pay}}{M_{pay,o}} - 1\right)$$

and, denoting by $C_{cap.}$ the initial capital investment, the number of flights required to pay back that investment is

$$N = \frac{C_{cap}}{(c_o M_{OTV} + C_{OTV})\left(\frac{M_{pay}}{M_{pay,o}} - 1\right)}$$

Using $C_{cap} = 40 + 18 = 50$ M\$, $c_o = \$1000/Kg$, $M_{OTV} = 15{,}000$ Kg, $C_{OTV} = \$50$ M and a 13.3% payload increase, we find

$$N = 6.9$$

which indicates a very rapid payback, and justifies ignoring discounting considerations at this stage. Other issues that need a deeper examination are the possible increase in mission support costs due to the added complexity of the transfer maneuver, and the impact of this maneuver on the overall Shuttle flight costs. Some compensation may occur due to the reduced deorbiting ΔV needed after the tether release.

4. Platform-Based Intermediate Tether Systems

4.1 Introduction

As shown in Appendix 1, the mass of a tether with a given mass at its end increases about quadratically with the tether length up to some 250 Km, after which, even with an optimally tapered cross-section, the mass increases much faster. The numerical examples of Sec. 3 showed that, for payloads consisting of a fully loaded OTV of the Centaur or IUS type, a free-flying, re-windable tether that uses the Shuttle as reaction mass, is limited to about 150 Km in length. Beyond this length, a larger reaction mass is necessary, with a means of restoring its orbit after a launch, and rewinding becomes undesirable. In this section we consider systems of this type, anchored to an orbiting Space Station. Insertion of payloads into a LEO-GEO transfer orbit is the mission studied in detail; however, other missions may be possible for a Space Station-based permanent tether facility, including capture and release of higher near-Earth satellites for inspection and repair.

4.2 Tether-Assisted Insertion into GEO Transfer Orbit

The system to be considered can be summarized as follows:

a) A Low Earth Orbit space station is assumed to have a radial outward tether deployed as a permanent facility. It must also have some electric thrusting capability (over and above that required for drag make-up).

b) This tether is restricted to lengths below 300 km, in order to keep the tether mass from becoming dominant for its own tension. This length also provides a reasonable extrapolation of already planned tether technology (~100 km).

c) Payloads (attached to an OTV vehicle, such as Centaur or IUS) are delivered by Shuttle flights to the space station, and are attached to a sliding "ferry" for transportation to the other end of the tether. The ferry must have a braking system, a radiator for disposing of the brake heat, controls for speed and some power generation capacity for return.

d) After release from the tether end, the OTV engines are fired to supplement the velocity up to that required for insertion in a Hohmann ellipse leading to GEO altitude. Circularization in GEO is made with a second OTV firing.

Let L be the tether length, M'_{PL} the mass of the combination space platform--deployed tether and R_{LEO} the orbital radius of the platform before payload deployment. After deployment, the payload is at a radius $R_p = R_{LEO} + L \frac{M'_{PL}}{M'_{PL} + m}$, where m is the mass of payload, OTV and ferry, while the platform sinks to $R_{PL} = R_{LEO} - L \frac{m}{M'_{PL} + m}$. The velocity of the payload just after release is $\sqrt{\frac{\mu}{R_{LEO}}} \frac{R_p}{R_{LEO}}$ and after adding a perigee impulse ΔV_p, it becomes the perigee velocity of the transfer ellipse, with apogee at R_{GEO}, namely

$$\sqrt{\frac{\mu}{R_p} \frac{2R_{GEO}}{R_p + R_{GEO}}} .$$

Thus

$$\Delta V_p = \sqrt{\frac{\mu}{R_p} \frac{2R_{GEO}}{R_p + R_{GEO}}} - \sqrt{\frac{\mu}{R_{LEO}} \frac{R_p}{R_{LEO}}}$$

or, in dimensionless form,

$$\frac{\Delta V_p}{V_{C,\,LEO}} = \sqrt{\frac{2\rho}{f\,(f + \rho)}} - f \qquad (1)$$

where $v_{C,LEO} = \sqrt{\frac{\mu}{R_{LEO}}}$, $\rho = \frac{R_{GEO}}{R_{LEO}}$, and $f = 1 + \frac{\lambda}{1+\nu}$, with $\lambda = \frac{L}{R_{LEO}}$, $\nu = \frac{m}{M'_{PL}}$

The usual expression for the Hohmann transfer is recovered for $f = 1$. At the apogee, the circularization impulse must be

$$\Delta V_a = v_{C,GEO} - \sqrt{\frac{\mu}{R_{GEO}} \frac{2R_p}{R_p + R_{GEO}}}, \text{ where } v_{C,GEO} = \sqrt{\frac{\mu}{R_{GEO}}}$$

or

$$\frac{\Delta V_a}{v_{C,GEO}} = 1 - \sqrt{\frac{2f}{f + \rho}} \tag{2}$$

The platform mass must be large enough to prevent too low a platform perigee after release; as shown in Section 3, this perigee is at

$$R_{P,PL} = \frac{(1 - \frac{\lambda\nu}{1+\nu})^4}{2 - (1 - \frac{\lambda\nu}{1+\nu})^3} R_{LEO} \simeq (1 - 7 \frac{\lambda\nu}{1+\nu}) R_{LEO} \tag{3}$$

An example of calculations for this system is shown in Table 4.1. The space station is taken to be in a 400 km orbit (R_{LEO} = 6770 km), while R_{GEO} = 42200 km. The values of ν_{MAX} shown are those that would give a 250 km platform perigee; a reduction by 1/1.5 is assumed for safety, and is given as the ν adopted (heavier platform). The tether mass is calculated for tapered Kevlar Aramid (ρ = 1.44 g/cm^3, $\sigma = 1.397 \times 10^9$ NT/m^2, safety factor = 4). The payloads and initial OTV loaded masses are for an assumed Centaur vehicle (structural mass = 3230 kg, propellant mass = 10870 kg, exhaust velocity = 4355 m/sec). No orbital plane change was

considered. As the table shows, there is a 20% gain in payload for a 150 km tether, and a 38% gain for a 250 km tether. The mass of the wire itself varies from 0.14 to 1.27 of the maximum end mass. Since this mass is of the order of 25 ton in this example, the maximum tether mass (for 250 km) is about 32 ton. The platform mass varies from 5.3 to 14.7 times the end mass (as a minimum); i.e., from 130 to 370 ton; presumably, this would include the empty Shuttle attached to it. All these figures are reasonable, and appear to be within the scale of the contemplated Space Operations Center, or expansions of it.

Tether length (km)	0	100	150	200	250	
$\lambda = L/R_{LEO}$	0	0.01477	0.02216	0.02954	0.03693	
ω_{MAX}	0	0.273	0.167	0.120	0.0937	
ω(adopted)	0	0.182	0.111	0.080	0.0625	
M(Tether)/m	0	0.140	0.356	0.711	1.269	
M(Platf. only)/m	-	5.35	8.65	11.79	14.73	
f	1	1.0125	1.0199	1.02735	1.03476	
ΔV_p (m/sec)	2398	2233	2133	2035	1938	
ΔV_a (m/sec)	1456	1447	1442	1437	1432	
ΔV_{TOT} (m/sec)	3854	3680	3575	3472	3370	
M_L (kg)	4409	5009	5312	5684	6076	Centaur
M_0 (loaded OTV) (kg)	18,509	19,109	19,412	19,784	20,176	OTV

Table 4.1 Performance of tether-assisted LEO-GEO system.
R_{LEO} = 400 + 6370 km.

4.3 The Platform Propulsion System.

The climbout of the ferry would lower the platform c.g., and the release of the payload/OTV would send the platform into an elliptic orbit with perigee well above the atmosphere. A propulsion system is required on board the platform to restore its orbit before the next launch. The thrust can be applied either after or during the ferry excursion.

Mercury bombardment ion engines have been developed to the point where confident performance and mass estimations can be made. Byers (Ref.4.1) presented a methodology based on extrapolations from existing thrusters which can serve as the basis for our analysis. Specific impulses (I_{sp}) from below 2000 sec to over 4000 sec are possible by adjustment of voltages. Very low values of I_{sp} lead to high propellant resupply rates, as well as to low efficiency of the thrusters. On the other hand, very high I_{sp} implies high power requirements, with attendant mass increases. We present next a study to determine the appropriate specific impulse for our application.

The input power to a battery of ion engines operating at exhaust velocity c, with propulsive efficiency η_p and thrust F is

$$P = Fc/2\eta_p \tag{4}$$

and in terms of the velocity increment ΔV to be imparted to a mass M in a time t_b ,

$$P = Mc\Delta V/2\eta_p t_b \tag{5}$$

In Appendix 3, an expression (Eq. (28) of that Appendix) is derived for the ΔV required to re-establish the orbit of a space station at R_{LEO} after release of a payload from the end of a tether line of length L:

$$\Delta V = 2.352\, v_c \left(\frac{L}{R_{LEO}}\right)\left(\frac{m'}{M_{Total}}\right) \tag{6}$$

where m' is the mass released (OTV + payload), L is the tether length, and v_c is the circular velocity in LEO. If the engines operate after payload release, the mass to be accelerated is $M = M_{TOT} - m'$. Also, Eq. (5) gives the average power during orbit recovery, but, as shown in Appendix 3, the thrust must be applied in a modulated fashion,

$$F = F_0 \left(1 - \frac{3}{2}\cos\theta\right) \tag{7}$$

where θ is orbital azimuth from perigee. This leads to a ratio

$$\frac{P_{max}}{\langle P \rangle} = \frac{|F|_{max}}{\langle |F| \rangle} = \frac{5/2}{1.176} \tag{8}$$

Therefore the peak power required is

$$P_{max} = \frac{5}{2}\frac{c}{\eta_p}\, m' \left(1 - \frac{m'}{M_{TOT}}\right)\left(\frac{L}{R_{LEO}}\right)\frac{v_c}{t_b} \tag{9}$$

Some modification is needed if platform thrust is also applied during the ferry climbout phase, but since $\frac{m'}{M_{TOT}}$ is typically ~ 0.1, the impact on P_{max} is minimal. Notice the small sensitivity of P_{max} to $M_{platform}$, and the proportionality with tether length.

The amount of propellant (M_{H_g}) used follows from Eq. (6):

$$M_{H_g} = \frac{M\Delta V}{c} = 2.352\ m'\left(1 - \frac{m'}{M_{TOT}}\right)\left(\frac{L}{R_{LEO}}\right)\frac{v_c}{c} \tag{10}$$

The propulsive efficiency of ion engines increases as the specific impulse at which they operate is increased.

In general one can write

$$\eta_p = \frac{\eta_{cD}}{1 + \left(\frac{2eV_{LOSS}}{m_i c^2}\right)} \tag{11}$$

where η_{cD} is the power conditioning and distribution efficiency, V_{LOSS} is the thruster power loss per ampere beam current and e and m_i are the ion charge and mass respectively. From the detailed analysis of Byers (Ref.4.1) one can use for existing and near term mercury ion engines at 0.95 propellant utilization fraction the values

$$\eta_{c_D} = 0.752 \quad , \quad V_{LOSS} = 133 \text{ Volts}$$

this gives

$$\eta_p = \frac{0.752}{1 + 1.282\times10^8/c^2} \tag{12}$$

(an almost equally good fit can be obtained for the more physical value V_{LOSS} = 150 Volts if η_{c_D} is raised to 0.765).

The cost per mission includes some components that are sensitive to the choice of exit velocity c for the ion engines. These are

(a) A recurring cost $c_{H_g} M_{H_g}$, where C_{H_g} is the cost of mercury per Kg (in orbit)

(b) Non-recurring costs, mainly the cost $C_{p_s} M_{p_s}$ of the power system, where $M_{p_s} = \alpha P_{max}$ and α is the specific mass of the power system (Kg/watt). Other non-recurring costs that may depend on c are those associated with the ion engine hardware; higher specific impulse implies smaller fuel tanks and other fuel-related components, but larger power conditioning and power-related components. Overall, Ref. 4.1 concludes that the engine system mass is insensitive to specific impulse, so we omit this from our discussion.

We are thus led to choose the engine specific impulse c/g by minimizing the partial cost

$$\phi = c_{H_g} M_{H_g} + \frac{C_{ps}}{N} \alpha P_{max} \tag{13}$$

where N is the number of reuses of the power system. Using Eqs. (9), (10) and (11) this can be rewritten as

$$\phi = 1.063 \frac{\alpha C_{ps}}{N t_b \eta_c} \left(c + \frac{c_\ell^2 + c_\alpha^2}{c}\right) \tag{14}$$

where

$$c_\ell^2 = \frac{2e V_{LOSS}}{m_i} \tag{15}$$

$$c_\alpha^2 = \frac{1}{1.063} \frac{c_{Hg}}{c_{ps}} N \frac{t_b \eta_c}{\alpha} \tag{16}$$

Differentiation gives

$$c_{OPT} = \sqrt{c_\ell^2 + c_\alpha^2} \tag{17}$$

i.e., $c_{OPT} \simeq c_\ell$ for no reusability, but $c_{OP} \sim \sqrt{N}$ for many reuses.

An estimate of the cost of a multi-hundred Kw solar array can be obtained from Ref.4.2, where detailed design and costing is performed for several types of arrays in the 400-600 Kw power range. The lowest cost (for low concentration ratio GaAs cells) was found to be 326 $/Avg.Watt, of which about 90 $/Watt corresponds to launch costs. The array specific mass was also found to be about 10 Kg/Kw(BOL). For an assumed ratio of average to BOL power of 0.85, this leads to 27,700 $/Kg array cost (7630 $/Kg for launch).

The high array launch cost just mentioned is related to the special arrangements for pressurized Shuttle bay stowage and self-deployment. By comparison, supply of mercury propellant to the space station is likely to be a simple operation: we assume a cost of mercury in orbit of $c_{Hg} = 2000$ $/Kw (including a comparatively minor allowance for purchase price).

The power system specific mass α includes not only the array itself, but also other components, such as gimbals, regulators and battery system for eclipses. For the first two items we follow Ref.4.3 and assume the following masses:

Gimballing system	**4 Kg/Kw**
Regulators	**5 Kg/Kw**

For the batteries, we assume $Ni-H_2$ type, with energy density 17 watt hr/Kg and charge-discharge efficiency of 0.77 (Ref. 4.3). The total energy storage needed can be calculated using the thrust profile of Eq. (7) if the eclipse time is specified. The worst case for shadowing occurs when the sun lies in the orbital plane, and gives a shadow time

$$t_{sh} = 2\sqrt{\frac{R^3_{LEO}}{\mu}} \sin^{-1}\left(\frac{R_E}{R_{LEO}}\right) \tag{18}$$

where R_E is the Earth radius.

An additional consideration to be made pertains to the relative location of the eclipse zone and the orbital perigee; this is important, since, according to Eq. (7), the perigee power demand is only 1/5 of the peak demand (at apogee). Apogee for the perturbed platform orbit occurs at the location of payload release, and one can in principle place it at orbital noon to minimize energy storage. Since the fuel cost of moving the payload within a GEO orbit is small, it seems reasonable to assume such a release strategy. With this assumption, the mean power demand during eclipse is given by

$$\frac{\langle P_{sh}\rangle}{P_{max}} = \frac{2}{\theta_{sh}} \int_0^{\theta_{sh}/2} \frac{|2-3\cos\theta|}{5} d\theta = \frac{2}{5} + \frac{0.2216 - 0.6\, R_E/R_{LEO}}{\sin^{-1}\left(\frac{R_E}{R_{LEO}}\right)} \tag{19}$$

where $\theta_{sh} = 2 \sin^{-1} R_E/R_{LEO}$ is the orbital arc in shadow. A similar calculation can be made for the capacity excess during the sunlit phase of an orbit for an array dimensioned for peak power.

Some results of these calculations are shown in Table 4.2.

Table 4.2

Orbit altitude (Km)	100	200	300	400	500	600
Max. Shadow time (minutes)	38.37	37.26	36.56	36.08	35.73	35.46
$\langle P_{sh} \rangle / P_{max}$	0.1353	0.1279	0.1232	0.1201	0.1181	0.1166
$\frac{\text{Ideal storage req'd}}{P_{max}}$ (Kwh/Kw)	0.08652	0.07943	0.07507	0.07222	0.07033	0.06891
$\frac{\text{Excess capacity during sunlight}}{\text{storage required}}$	2.423	3.009	3.516	3.976	4.402	4.799

The last row of Table 4.2 shows that no extra array area is required for battery charging. The storage required is only weakly dependent on orbital altitude. Using the value 0.07222 (for 400 Km orbits), and including a battery efficiency of 0.77, the battery mass needed is

$$\frac{\text{Battery mass}}{\text{Peak power}} = \frac{0.07222 \times 1000 \text{(Watt hr/Kw)}}{0.77 \times 17 \quad \text{(Watt hr/Kg)}} = 5.52 \text{ Kg/Kw}$$

Thus, including the array, gimballing, regulators and battery system, we arrive at a power source specific mass

$$\alpha = \frac{(10 + 4)}{0.85} + 5 + 5.5 = 27.0 \text{ Kg/(Kw to engines)} \qquad (20)$$

where the factor of 0.85 accounts for the extra BOL array area required to accommodate cell degradation.

For the case where the Centaur OTV is used, the mass released is of the order of 20,000 Kg (See Sec. 3), varying slightly with LEO altitude and tether length. For power estimation purposes, the ratio m/M_{TOT} will be assumed to be 0.06; this is compatible with a safe platform perigee height, and in any case, is an insensitive parameter (Eqs. (9), (10)). Finally, we choose a total ion engine firing time of 14 days; as we will see below, this is about twice the ferry roundtrip time adopted in this study, and should therefore set the maximum mission frequency for the tether system.

With these parameters, Eqs. (17), (9) and (10) read

$$c_{OPT} = \sqrt{1.282\times10^{8} + 2.289\times10^{6}\ N}$$

$$P_{MAX}^{(BOL)} = \frac{3.854\times10^{-2}}{0.85}\ \frac{c}{\eta_p}\ v_c\ \left(\frac{L}{R_{LEO}}\right)$$

$$M_{H_g} = 44200\ \frac{L}{R_{LEO}}\ \frac{v_c}{c}$$

Table 4.3 shows calculated results for a 250 Km tether

N		1	10	30	100	300
c_{OPT}(m/sec)		11,420	12,290	14,030	18,900	28,550
$(I_{sp})_{OPT}$(sec)		1,166	1,254	1,432	1,928	2,913
at c_{OPT}	η_p	0.380	0.407	0.455	0.5533	0.6498
	P_{max}(KW) (EOL/BOL)	331/389	332.3/390.9	338.8/398.6	345.5/441.8	483/568.2
	M_{H_g} (Kg/mission)	1,095	1,018	891.9	662.2	438.4

Table 4.3 Optimized propulsion system parameters as a function of number of reuses, for a 250 Km tether and a 400 Km LEO orbit.

and a 400 Km platform orbit. These results are insensitive to orbital height, while P_{MAX} and M_{H_g} scale in proportion to tether length. As shown, the range of specific impulses from 1500 to 3000 sec is optimum, depending on reusability. The tradeoff between power and propellant mass is apparent from the last two rows of Table 4.3.

If we adopt I_{sp} = 2000 sec (optimum for about 115 reuses), Byers' analysis (Ref. 4.1) can be rather directly applied. The accelerating voltage and net voltage (including the decel electrode) are 2000 and 443 Volts respectively. The individual thruster diameter was selected at 50 cm. The results are summarized in Table 4.4 (for a 250 Km tether).

Table 4.4 Platform propulsion system characteristics

Type	Hg ion bombardment	
Diameter per thruster	50 cm	
Specific impulse	2000 sec	
Thrusting time	14 days	
Thrust per unit	0.546 Nt	
Thrust power per unit (including distribution losses)	9.56 Kw	
No. of thrusters required	41 (+ 4 extras)	
Mercury mass per mission	632 Kg	
Solar array power (EOL/BOL)	384.2/452 Kw	
Thrust system mass (thrusters, thermal control, power supplies, interface module structure, etc.)		5464 Kg
Solar array mass		4520 Kg
Solar array gimballing mass		1808 Kg
Solar array regulators mass		2260 Kg
Battery system mass		2113 Kg
Total propulsion related mass		16,165 Kg

4.4 The Ferry Drive System.

In this section we calculate the required power generation and power dissipation capacities of the ferry vehicle that transports the payload and OTV to the end of the tether line.

Let m be the outbound travelling mass, made up of the OTV, the payload and the returnable ferry

$$m = m' + M_F \qquad (21)$$

where $m' = M_{OTV} + M_{LOAD}$ and M_F = ferry mass. When the ferry is at a distance y from the lower platform, its distance from the (moving) overall center of mass is $y - y_{cg} = (1 - \nu)\, y - \nu_T L$, where

$$\nu = \frac{m}{M_p + m + M_T} \quad , \quad \nu_T = \frac{M_T}{M_p + m + M_T} \quad , \quad \nu_p = \frac{M_p}{M_p + m + M_T} \qquad (22)$$

and M_p and M_T are the lower and upper platform masses respectively. Hence, the mechanical power being generated when the upward velocity is $\frac{dy}{dt}$ is

$$P_{up} = 3\Omega^2 m \left(\frac{dy}{dt}\right)[(1 - \nu)y - \nu_T L] \qquad (23)$$

Notice $P_{up} < 0$ when $y < \frac{\nu_T}{1-\nu} L$; i.e., external power must be supplied to reach this point (at which time the ferry is at the overall c.g.). For $y > \frac{\nu_T}{1-\nu} L$, power is being generated.

A similar expression applies for the return trip, when the travelling mass is the ferry alone:

$$P_{down} = \Omega^2 M_F \left(\frac{dy}{dt}\right)\left[(1 - \nu^F) y - \nu_T^F L\right] \qquad (24)$$

where ν^F and ν_T^F are analogous to ν, ν_T, but with M_F replacing m. Here, since $\frac{dy}{dt} < 0$, P_{down} is negative (external power needed) whenever $y > \frac{\nu_T^F}{1-\nu^F}$, i.e., most of the time.

The first question arising is the disposition of the mechanical power available during most of the ascent phase; this power can be conveniently and controllably converted to electrical form by driving a DC motor-generator in the generator mode from the (non-sliding) guiding pulleys which engage the tether line. Three options will be considered here:

(a) Storage of enough energy for the return trip, radiation of the remainder.

(b) Use of the generated energy to power ion engines on the ferry, thus contributing to the orbital recovery of the platform.

(c) Radiation of all the generated energy.

Regarding option (a), we notice that it would allow elimination of a separate power source for the return trip, such as a solar panel (supplemented by batteries for eclipse times). Thus, the option can be assessed by comparing the required battery mass needed to that of the displaced power supply.

For the power supply, if one is used, the BOL array power required, assuming 85% degradation at EOL, 75% DC motor efficiency, 77% battery

efficiency and 36.1 min. shadow time/56.4 min. sun time (400 Km orbit), must be

$$P_{sa,BOL} = \frac{P_{down,max}}{0.75}\left(\frac{1}{0.85} + \frac{36.1}{0.77 \times 56.4}\right) = 2.68\ P_{down,max} \tag{25}$$

The mass of this power system is then

$$M_{ps} = \alpha_{sa} P_{sa,BOL} + \frac{E_{Batt}}{\beta} \tag{26}$$

where, following Ref. 4.3, α_{sa} = 12 Kg/Kw (blanket) + 5 Kg/Kw (regulators) + 4 Kg/Kw (gimballing) = 21 Kg/Kw.

Also, E_{batt} is the energy to be stored in the batteries for the eclipse time, and β = 17 Watt h/Kg is the energy density of the assumed N_i-H_2 batteries, so that

$$\frac{E_{batt}}{\beta} = \frac{P_{down,max}}{0.75 \times 0.77} \times \frac{36.1}{60} \quad \frac{1}{0.017} = 61.3\ P_{down,max} \tag{27}$$

Altogether, then,

$$\frac{M_{Ps}}{P_{down,max}} = 118\ \text{Kg/Kw} \tag{28}$$

The mechanical energy needed for ferry return can be calculated by integration of Eq. (24). This leads to a battery mass estimate of

$$M_{batt} = \frac{3\Omega^2 L^2 M_F \left(\frac{1-\nu'}{2} - \nu_T'\right)}{0.77 \times 0.75\ \beta} \tag{29}$$

and comparing to Eq. (24),

$$\frac{M_{batt}}{P_{down,max}} = \frac{L}{v} \frac{1}{0.77 \times 0.75\ \beta} \quad \frac{\frac{1-\nu'}{2} - \nu_T'}{1-\nu'-\nu_T'} \tag{3}$$

For a constant velocity return, L/v is the return time. Using β = 17 Watth/Kg, $\nu' = 0.02$, $\nu_T' = 0.01$, we obtain

$$\frac{M_{batt}}{P_{down,max}} = 1.20\ t(days)\ (Kg/Kw) \tag{31}$$

Comparison of (28) and (31) shows clearly that, except for unreasonably fast returns, storage of power requires much more mass than direct generation via an on-board solar array system.

Regarding option (b) (propulsive use of power generated), a simple calculation will show that the contribution to the required ΔV for recovery of orbital platform is too small to be worth considering. The thrust that can be generated with a power P is $F = 2\eta_p P/c$. Also,

$$\Delta V = \frac{1}{M_{TOT}} \int_0^T F dt$$

Thus, using for the power $P = 0.75\ P_{down}$ and using Eq. (24), we obtain

$$\Delta V = 2.25\ \eta_p \nu' \frac{\Omega^2 L^2}{c} \left[\left(\frac{M_F}{m'} + \frac{1}{2} \right) \nu_p' - \frac{3}{2} \nu_T' \right] \tag{32}$$

For values of the variables comparable to those used in other parts of this report, this ΔV amounts to less than 1 m/sec. For comparison, typical required ΔV values for platform orbit recovery amount to 50-100 m/sec. Therefore, it does not seem advisable to include electric thrusters in the ferry for primary propulsion. On the other hand, one can expect a need for attitude control and out-of-plane libration control of the ferry; these

needs have not been quantified yet, but the ready availability of the brake electric power may make it attractive to perform these tasks with ion thrusters.

Following the above arguments, only option (c) (radiation of all (or most) of the brake power) remains. This would appear to pose no special problems, since the power is in electrical form and can be radiated from resistive loads whose design temperature can be quite high.

Consistent with this design concept, a solar array power supply is needed for the return trip, with a mass/power ratio of 113 Kg/Kw (Eq. (28)). The peak power needed depends directly on the mass of the ferry, which has not yet been determined precisely. For an OTV-payload combination of 20,000 Kg mass, a preliminary estimate is M_F = 3000 Kg (DC motor-generator, controls, guiding pulleys, OTV attachments, trussing). Following Eq. (24), for a tether length of 250 Km, and a ferry speed of 1 m/sec (return time - 2.89 days), this gives a peak mechanical power requirement of 5.6 Kw, and therefore a solar array-battery system mass of 670 Kg. This can be easily reduced, however, by operating the ferry at a lower speed near the end of the tether, where the gravity gradient force is largest.

4.5 Dynamics of the tether system during ferry transfer.

When the tether system is permanently deployed and payloads, with their orbital transfer vehicles, have to travel along the cable, new dynamic effects may arise which have not been dealt with in the literature. For instance, the ascent velocity v of a ferry of mass m gives rise to a backward Coriolis force $2m\Omega v$, which leads to oscillatory in-plane motion

of both, the ascending mass and the two end masses (the main platform below and a small terminal platform above). At least some of the modes of oscillation have the feature of a rapidly increasing frequency as the distance between two of the masses approaches zero; there is therefore the potential for a wrap-around type of instability when the ferry approaches the end of the tether. Similar effects can arise due to the tether elasticity, and here the risk is that of greatly enhanced tension due to dynamic effects.

Two lines of attack have been followed in this problem. On the one hand, an analytical theory with some simplifications was worked out, first for the in-plane oscillations (Appendix 4), and then for the stretch oscillations (Ref. 4.4). This separation of the problem into two individual problems is allowable because, due to the linearization used, the two types of motion decouple to the order retained. Independently, the same problem was treated at the Smithsonian Astrophysical Observatory (SAO) using numerical methods which bypass the need for many of the approximations used in the analysis; these SAO calculations will be reported separately.

Both studies reached very similar conclusions: for a tip mass of the order of 10% of the platform mass, enough tension exists in the tether to prevent instabilities and maintain oscillations within fairly small bounds for climbing speeds of the order of 1 m/sec. The only time when a divergence may occur is the terminal approach phase; and even there, careful speed control in that phase can ensure a smooth maneuver. The detailed analysis for the in-plane case is given in Appendix 4; a WKB approximation was used, together with an inner-outer matching process near each end of the climb.

References

4.1 Byers, D.C., "Characteristics of Primary Electric Propulsion Systems," AIAA paper 79-2041 (1979).

4.2 Woodcock, W.G., and Mann, J.A., "Multi-Hundred Kw Solar Arrays for Space." AIAA paper 80-9271 (1980).

4.3 "Space Operations Center, a Concept Analysis." A presentation by the Johnson Space Center (paper JSC-16277), Nov. 29, 1979.

4.4 Kolota, L., SM Thesis; to be submitted in March 1982 to the Department of Aeronautics/Astronautics, MIT.

5. Large-Scale Tether Systems for LEO-GEO Transfer.

The principal interest in orbital transfer relates to low-to-geosynchronous cases. We considered the possibility of performing such transfers without any transfer propulsion, or with small ΔV's at most. This requires a tether to be attached to a low Earth orbiting platform for release into the transfer ellipse, and another tether attached to a geosynchronous platform, to acquire the payload and circularize its orbit.

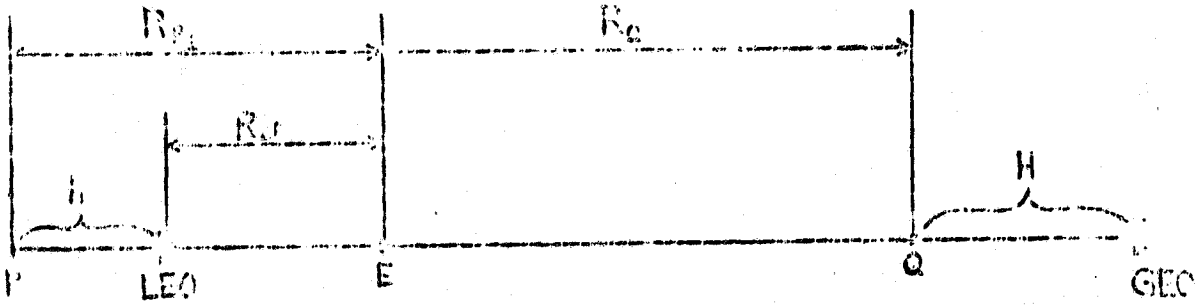

Figure 5.1. Geometry for a two-tether system.

The length H of the upper tether depends only upon the period P_2 chosen for the orbit of the payload (after application of an apogee velocity increment ΔV_Q . This is because two elements of that orbit are prescribed, namely, the semimajor axis (by the period) and the angular momentum (by the requirement that the angular velocity at apogee must equal that in the geosynchronous orbit). These conditions can be expressed as

$$P_2 = \frac{2\pi}{\sqrt{\mu_e}} \left(\frac{R_{P_2} + R_Q}{2}\right)^{3/2} \qquad (1)$$

(where R_{P_2} is the perigee of the orbit and μ_e the gravitational constant of Earth) and

$$V^2(\text{apogee}_2) = \mu_e \left(\frac{2}{R_\Omega} - \frac{2}{R_{P_2} + R_\Omega}\right) = V_{GS}^2 \left(\frac{R_\Omega}{R_{GS}}\right)^2 \qquad (2)$$

where the subscript GS refers to the geosynchronous orbit. Using $V_{GS}^2 = \mu_e/R_{GS}$, Eqs. (1) and (2) can be combined by elimination of R_{P_2}, to give

$$\frac{2\,(R_\Omega/R_{GS})}{2-(R_\Omega/R_{GS})^3} = \frac{2}{R_{GS}} \left(\frac{\sqrt{\mu_e}}{2\pi} P_2\right)^{2/3} \qquad (3)$$

which can be solved for R_Ω once P_2 is prescribed. The tether length follows then from

$$H = R_{GS} - R_\Omega \qquad (4)$$

and the perigee R_{P_2} from

$$R_{P_2} = \frac{R_\Omega^4}{2R_{GS}^3 - R_\Omega^3} \qquad (5)$$

The subscript 2 has been used so far to indicate conditions after application of ΔV_Q. For the ascent orbit (before ΔV_Q), the apogee velocity is

$$V(\text{apogee}_1) = V(\text{apogee}_2) - \Delta V_Q = V_{GS} \frac{R_Q}{R_{GS}} - \Delta V_Q \qquad (6)$$

and Eq. (2) can be modified to calculate the perigee R_{P_1} of this ascent orbit:

$$\mu_e \left(\frac{2}{R_Q} - \frac{2}{R_{P_1} + R_Q} \right) = \left(V_{GS} \frac{R_Q}{R_{GS}} - \Delta V_Q \right)^2 \qquad (7)$$

Once R_{P_1} is so determined, the velocity at perigee can be expressed (from conservation of angular momentum) as

$$V_{P_1} = \frac{R_Q}{R_{P_1}} V(\text{apo.}_1) = \frac{R_Q}{R_{P_1}} \left(V_{GS} \frac{R_Q}{R_{GS}} - \Delta V_Q \right) \qquad (8)$$

This velocity contains, in general, a propulsion-derived increment ΔV_P, applied at or immediately after release. The velocity of the end of the low-Earth tether is therefore

$$V_{\substack{\text{tether} \\ \text{end}}} = V_{P_1} - \Delta V_P \qquad (9)$$

and the orbital velocity $V_{C,LE}$ of the platform at R_{LE} (or, more precisely, of the orbital center of the tether payload system) is therefore

$$V_{C,LE} = \sqrt{\frac{\mu_e}{R_{LE}}} = (V_{P_1} - \Delta V_p) \frac{R_{LE}}{R_{P_1}} \tag{10}$$

from which R_{LE} can be calculated easily. Finally, the low-Earth tether length is

$$h = R_{P_1} - R_{LE} \tag{11}$$

Fig. 5.2 and Table 5.1 show calculated results for the case of $\Delta V_P = \Delta V_Q = 0$. If we impose the requirement that, in case of docking failure, the payload and the lower platform of the GEO tether should rendezvous again after an integer number of orbits, then the period P_2 (T in Fig. 5.2) must be a rational fraction m/n of a day (m, n integers). Thus, appropriate values of P_2 , for low m and n, are
1/3 day = 8 hr., 3/8 day = 9 hr., 2/5 day = 9.6 hr., 1/2 day = 12 hr.

As shown in Fig. 5.2, a period of 1/3 day implies an upper tether length of over 10,000 Km, and a lower tether length of about 1200 Km from a low Earth orbit at 1200 Km as well. Increasing the period to 1/2 day lowers the length of the upper tether to about 6000 Km, but it also requires the low Earth orbit to be at some 9000 Km altitude, with a 1600 Km tether.

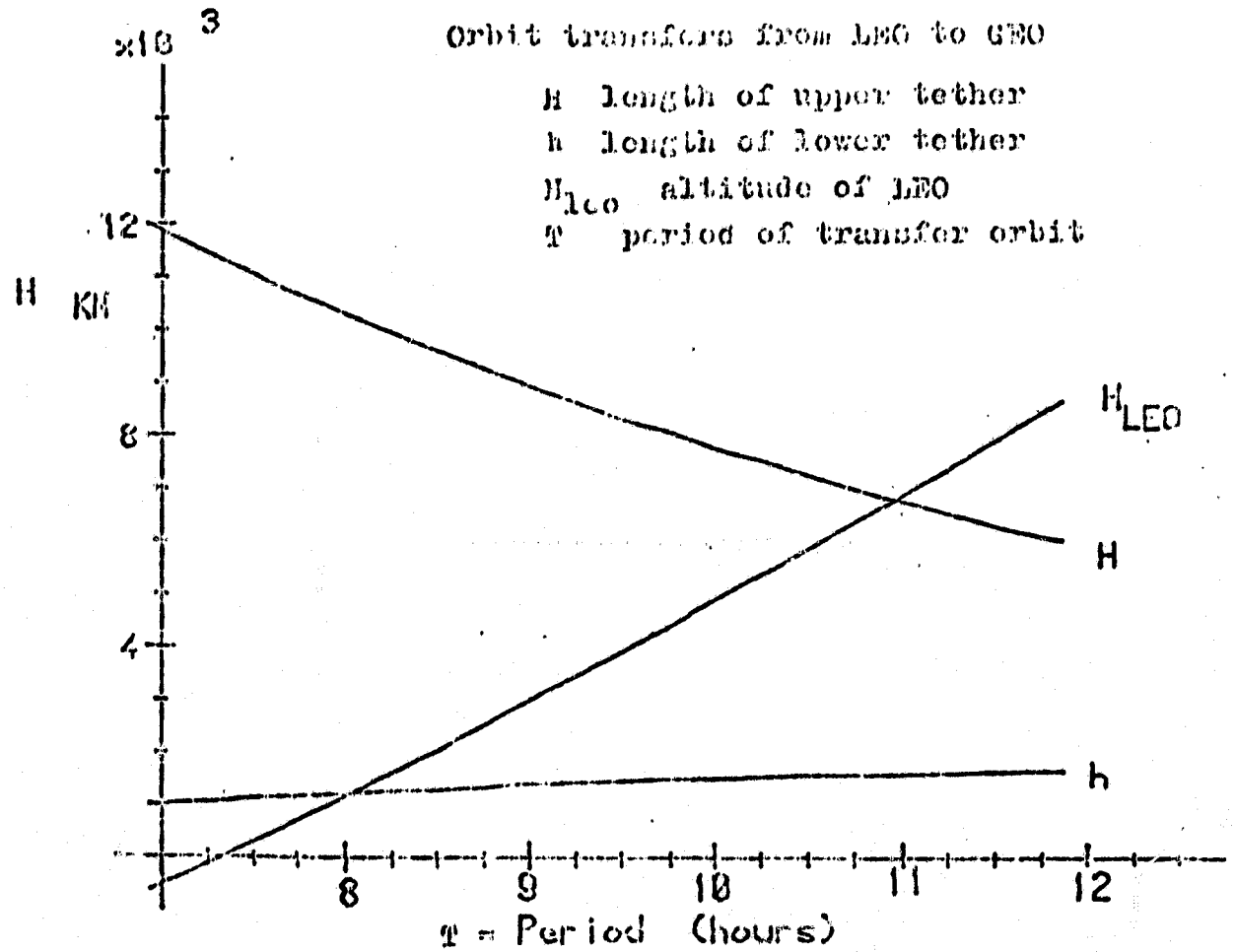

FIGURE 5.2. TWO-TETHER SYSTEM CHARACTERISTICS WITH $\Delta V_P = \Delta V_Q = 0$.

TABLE 5.1. TWO-IMPULSE SYSTEM CHARACTERISTICS WITH $\Delta V_P = \Delta V_Q = 0$.

H=	7600.000	T=	10.77674	H1=	1584.307	HLEO=	6402.393
H=	7750.000	T=	10.[illegible]514	H1=	1561.823	HLEO=	5900.947
H=	7500.000	T=	10.2[illegible]63	H1=	1537.997	HLEO=	5419.611
H=	7750.000	T=	10.04582	H1=	1513.000	HLEO=	4958.068
H=	8000.000	T=	9.817361	H1=	1486.986	HLEO=	4514.772
H=	8250.000	T=	9.595901	H1=	1460.100	HLEO=	4089.070
H=	8500.000	T=	9.381143	H1=	1432.474	HLEO=	3680.161
H=	8750.000	T=	9.172782	H1=	1404.236	HLEO=	3287.297
H=	9000.000	T=	8.970538	H1=	1375.486	HLEO=	2909.761
H=	9250.000	T=	8.774145	H1=	1346.331	HLEO=	2546.883
H=	9500.000	T=	8.583347	H1=	1316.864	HLEO=	2198.015
H=	9750.000	T=	8.397913	H1=	1287.168	HLEO=	1862.546
H=	10000.00	T=	8.217616	H1=	1257.319	HLEO=	1537.918
H=	10250.00	T=	8.042239	H1=	1227.390	HLEO=	1223.577
H=	10500.00	T=	7.871587	H1=	1197.443	HLEO=	931.0[illegible]
H=	10750.00	T=	7.705462	H1=	1167.537	HLEO=	643.7305
H=	11000.00	T=	7.543689	H1=	1137.726	HLEO=	367.2015
H=	11250.00	T=	7.386090	H1=	1108.060	HLEO=	101.2065
H=	11500.00	T=	7.232506	H1=	1078.576	HLEO=	-154.5057
H=	11750.00	T=	7.082776	H1=	1049.318	HLEO=	-401.4571
H=	12000.00	T=	6.936757	H1=	1020.325	HLEO=	-638.8290

NOTE: H1 is equivalent to h, which has previously been used.

The very long tethers required for this concept are, naturally quite heavy, and will have to be permanently deployed. There is a strong incentive to exploit the exponential dependence of mass on length by applying partial impulsive thrust at the ends of the transfer.

The tether mass calculation is contained in Appendix 1. It is of interest that the much longer GEO tether is of about the same mass.

The effect of introducing both perigee and apogee firings (ΔV_p and ΔV_Q respectively) was next investigated. The results for a wide range of parameters are listed in Tables 5.2 through 5.5. For the cases of the 1/3 and 1/2 day period, the results are also displayed graphically in Figs. 5.3 and 5.4. The effects are generally as follows:

(a) Increasing ΔV_p at constant period increases the altitude of LEO, and decreases the lower tether length, h.

(b) Increasing ΔV_Q at constant period decreases the altitude of LEO. For low ΔV_p, increases of ΔV_Q result in a shorter lower tether, but the reverse is true at high values of ΔV_p ($\gtrsim$ 800 m/sec).

(c) As discussed before, the length H of the upper tether is unaffected by either ΔV_p or ΔV_Q, but is reduced if the period is allowed to increase.

(d) For each transfer time and each value of ΔV_p, there is a maximum ΔV_Q for which the lower Earth orbit becomes too low (a limit of 200 Km was assumed here). Similarly, for each ΔV_Q, there is a minimum ΔV_p for the same reason.

(e) The length of the lower tether can be reduced to zero by increasing ΔV_p for each ΔV_Q. The effect of ΔV_Q on h is minor.

As an example of a combination which could be useful, we see in Fig. 4 that, from a 500 Km LE orbit, using a lower tether of length 390 Km and supplying a velocity increment $\Delta V_p = 1500 \frac{m}{sec}$ after release, a payload can be put into a transfer ellipse leading to capture by the lower end of a GEO tether of 5913 Km length, if an apogee velocity increment $\Delta V_Q = 725$ m/sec is applied prior to docking. If docking fails, another attempt can be made after one day (two orbits of the payload). Notice that for this lower tether length, its mass can be of the order of the payload mass.

Table 5.2. TRANSFER TO GEO BY TETHER, WITH ΔV's SUPPLIED BY PROPULSION

T = 1/3 day Upper Tether Length: H = 10,382 km

ΔV_P	ΔV_Q = 0	100	150	175	200	225	m/s
0	1218 / 1138	1142 / 297					
300	1035 / 1321	990 / 449					
600	841 / 1515	829 / 610					
900	633 / 1723	659 / 780	662 / 347				
1200	412 / 1944	477 / 962	500 / 510	508 / 295			
1500	175 / 2181	284 / 1155	325 / 685	343 / 460	359 / 242		
2000 m/s	* /	* /	9 / 1000	43 / 760	74 / 526	103 / 299	

KEY: Entries are: h(Km) / Altitude of LEO (Km) h = lower tether length X = LEO altitude < 200 km * = h negative

Table 5.3. TRANSFER TO GEO BY TETHER, WITH ΔV's SUPPLIED BY PROPULSION

T = 3/8 day Upper Tether Length = 8989 Km

ΔV_P \ ΔV_Q	0	100	200	300	325	340	350	375	400 m/s
0	1375 / 2920	1304 / 1879	1224 / 944						
300	1121 / 3176	1092 / 2091	1049 / 1119	996 / 246					
600	846 / 3450	866 / 2317	863 / 1305	843 / 299					
900	551 / [illegible]	624 / 2558	665 / 1503	681 / 561	682 / 341	682 / 212			
1200	233 / 4063	365 / 2817	454 / 1714	519 / 732	519 / 504	524 / 371	527 / 283		
1500	*	85 / 3096	228 / 1940	327 / 915	346 / 678	356 / 539	362 / 447	377 / 223	
2000	*	*	*	*	30 / 993	51 / 843	64 / 745	95 / 505	124 / 273

KEY: Entries are: h(Km) / Altitude of LEO (Km) X = LEO Altitude < 200 Km
* = h negative

Table 5.4. TRANSFER TO GEO BY TETHER, WITH ΔV's SUPPLIED BY PROPULSION

T = 2/5 day Upper Tether Length: Y = 8271 Km

ΔV_P \ ΔV_Q	0	100	200	300	400	425	450	475	490	m/s
0	1458 / 4047	1391 / 2875	1314 / 1826	1230 / 884						
300	1151 / 4353	1137 / 3129	1104 / 2036	1058 / 1057						
600	821 / 4634	865 / 3400	881 / 2259	875 / 1240	851 / 329					
900	464 / 5041	573 / 3692	642 / 2498	679 / 1435	692 / 488	692 / 268				
1200	76 / 5428	259 / 4007	387 / 2754	472 / 1643	523 / 657	532 / 428	539 / 265			
1500	*	*	111 / 3028	249 / 1866	343 / 837	361 / 598	377 / 365			
2000 m/s	*	*	*	*	17 / 1163	53 / 907	85 / 658	115 / 418	131 / 277	

KEY: Entries are h (km)/Altitude of LEO
h ≡ lower tether length

X = LEO altitude < 200 Km
* = h negative

Table 5.5. TRANSFER TO GEO FV TETHER, WITH ΔV's SUPPLIED BY PROPULSION

T = 1/2 day Upper Tether Length: L = 7513 Km

ΔV_p	ΔV_Q = 600	700	725	750	775	m/s
600	910 / 1203	877 / 257				
900	718 / 1396	722 / 412				
1200	512 / 1601	557 / 378	563 / 340			
1500	293 / 1820	331 / 753	397 / 505	411 / 267		
2000	*	62 / 1072	97 / 807	123 / 550	156 / 302	
m/s						

KEY: Entries are h(Km)/Altitude of LEO (Km) X = LEO altitude < 200 Km
* = h negative

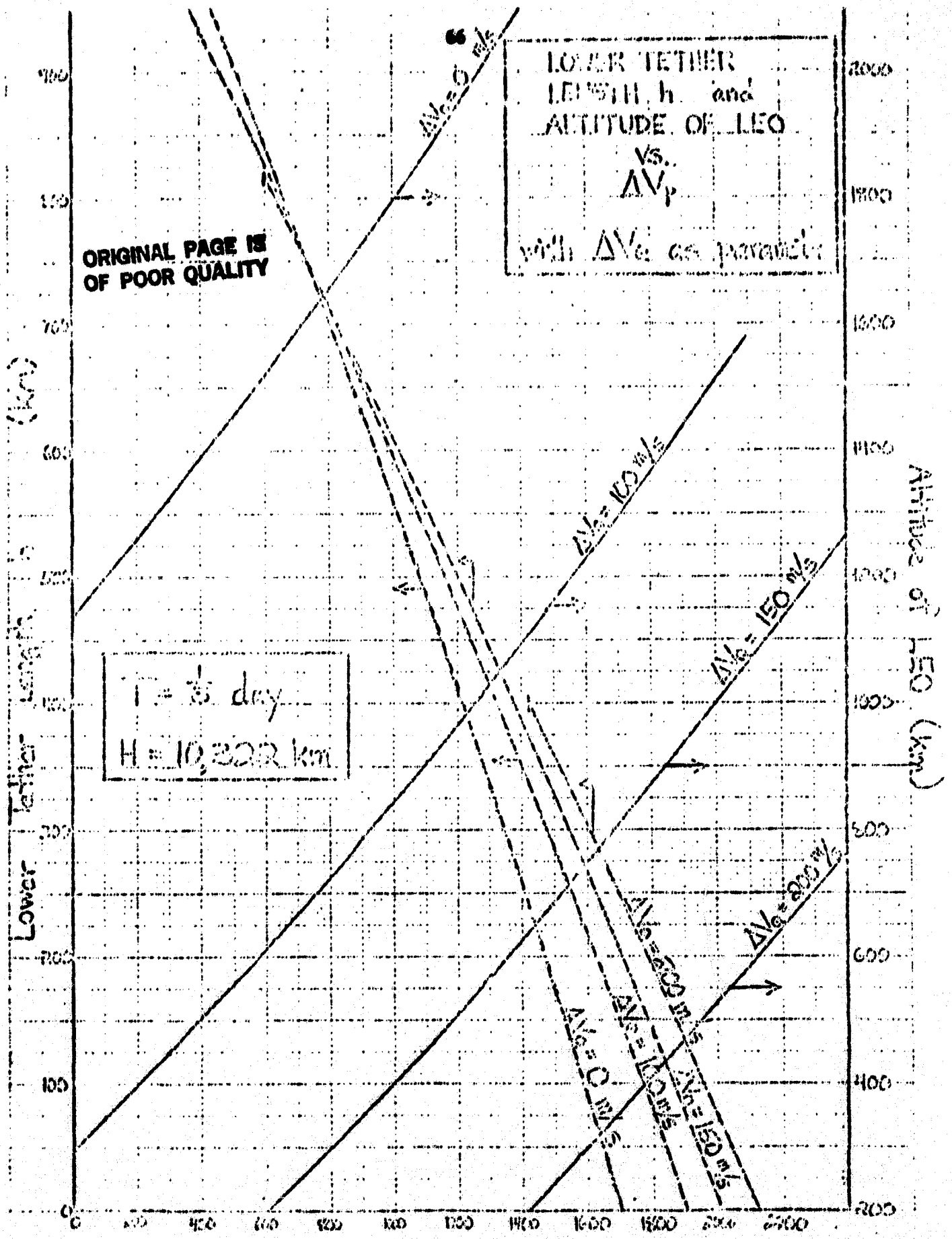
LOWER TETHER LENGTH h and ALTITUDE OF LEO VS. ΔV_p with ΔV_a as parameter
ORIGINAL PAGE IS OF POOR QUALITY
T = ½ day
H = 10,300 km
ΔV_a = 0 m/s
ΔV_a = 100 m/s
ΔV_a = 150 m/s
ΔV_a = 200 m/s
Lower Tether Length (km)
Altitude of LEO (km)
ΔV_p (at release) m/sec

Figure 5.3.

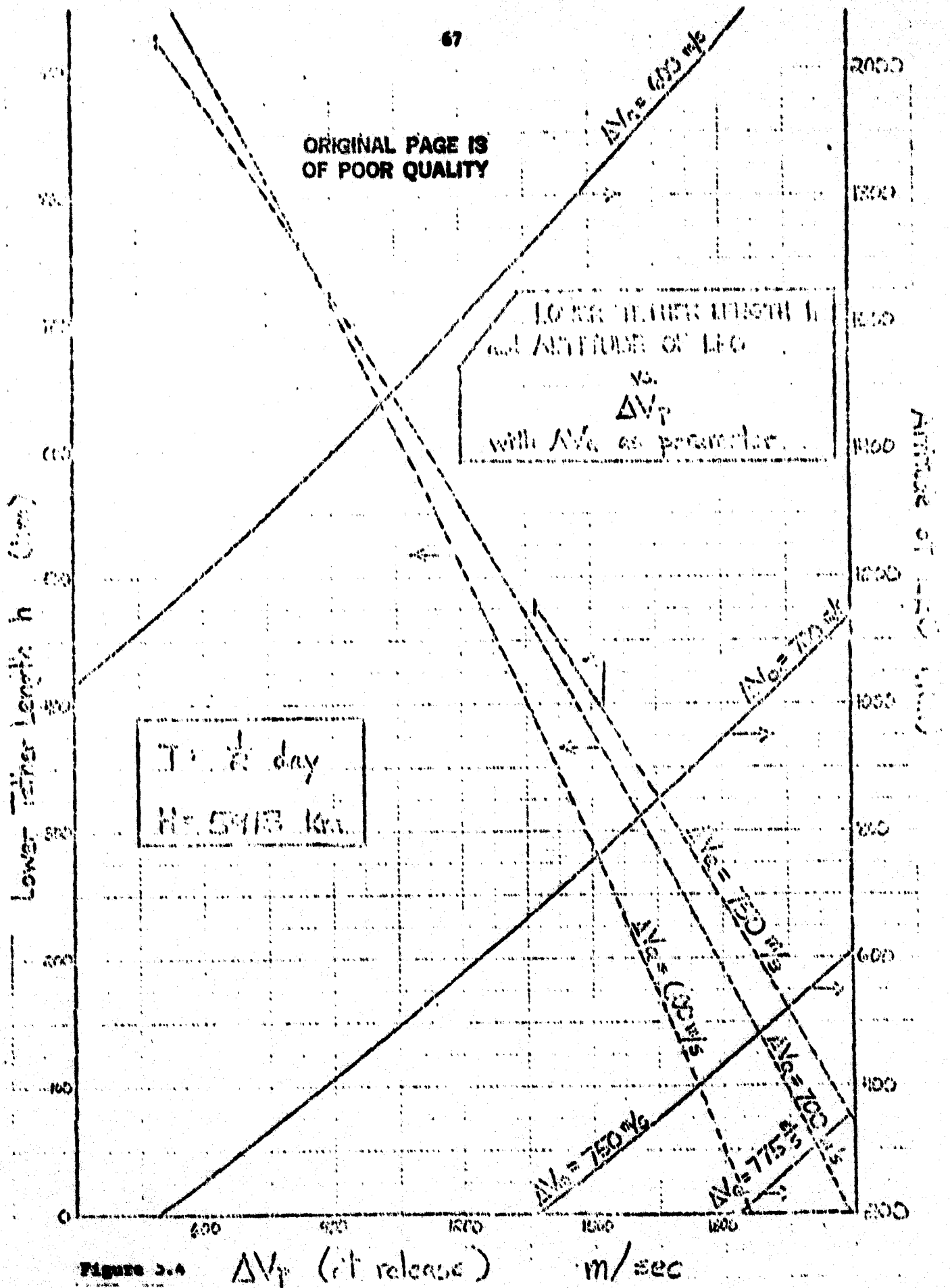

Figure 3.4

Orbital perturbations of the LEO platform

In the calculations so far we have implicitly assumed very heavy platforms both in LEO and in GEO. If the mass of the LEO platform is dominated by that of the Shuttle orbiter (docked to a light free-flying tether facility, the ratio $M_{platform}/M_{payload}$ may not be very large (8:1 for a 10 Tonne payload). The result may be an excessive lowering of the post-release Shuttle perigee. In this section we consider this effect, while still assuming a massive GEO platform.

The new geometrical arrangement for the lower tether is shown in Fig. 5.5. The orbital center is at R_c, given by (Ref.5.1)

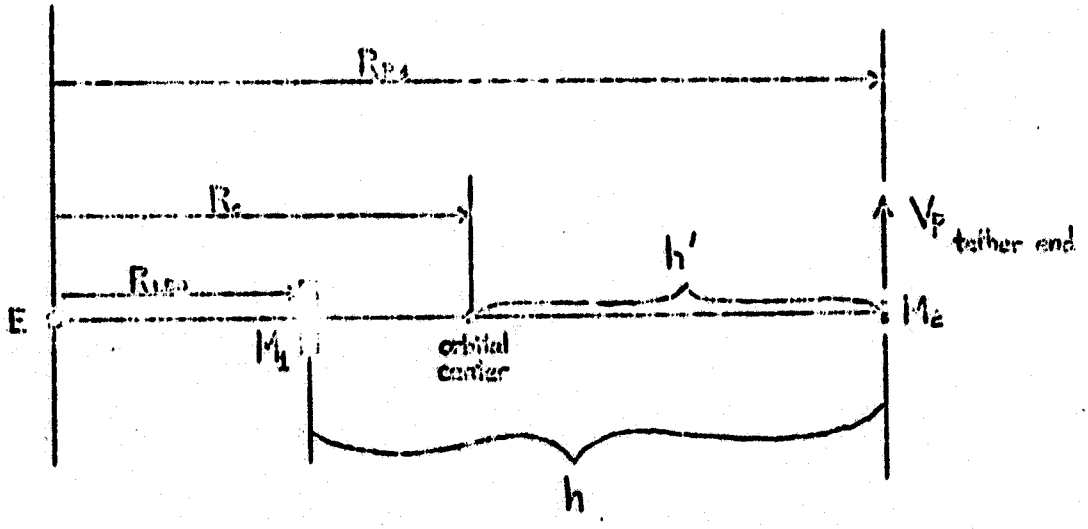

Figure 5.5. Geometry for a finite lower platform mass.

Ref.5.1. Study of Certain Launching Techniques Using Long Orbiting Tethers by Giuseppe Colombo. Final Report on grant NAG-8008, from the SAO to NASA, Feb. 1981.

$$R_c = \frac{\Sigma r_i m_i}{\Sigma m_i/r_i^2}^{1/3} \qquad (17)$$

and is located at a distance $h' = R_{p_1} - R_c$ from the transfer orbit perigee. Thus, h' replaces h and R_c replaces R_{LE} in our previous analysis (Eqs. (10), (11)). The new R_{LE} must be obtained from the explicit form of Eq. (17); for example, accounting only for two end masses M_1, M_2 (Fig. 5.5), we have

$$R_c = \frac{R_{LEO} M_1 + R_{p_1} M_2}{M_1/R^2_{LEO} + M/R^2_{p_1}}^{1/3} \qquad (18)$$

which can be solved for R_{LEO} .

The perigee of the post-release platform orbit can be calculated from Eq. (6) of Ref. 5.1, which for our case reads

$$S_2 = - R_{LEO} + 2/(2/R_{LEO} - R^2_{LEO}/R^3_c) \qquad (19)$$

The effect of this modification is to require a longer lower tether and to make high ΔV_Q values unfeasible (negative perigee). As an example, Tables 5.6 and 5.7 show a comparison (for 1/3 day period) of two cases, one with a massive LEO platform (M_1 = 5000 Tonne for M_2 = 10 Tonne). In the first case, where only a slight perturbation is introduced to the orbit, a tether length h = 998 Km can be used from a 521 Km orbit, which becomes a 521/511 orbit after release. Velocity increments ΔV_p= 300 m/sec. ΔV_Q = 100 m/sec are required. In the case with the light platform, the ΔV_Q = 100 is not allowable, and so, for ΔV_p= 300 m/sec, only ΔV_Q= 0 is possible. The result is a longer tether (1155 Km) and a higher orbit (1291/656).

TABLE 5.6. PLATFORM IN LEO

M1 = 5,000,000 kg (platform)

M2 = 10,000 kg (satellite)

P = 1/3 day H = 10,390 km

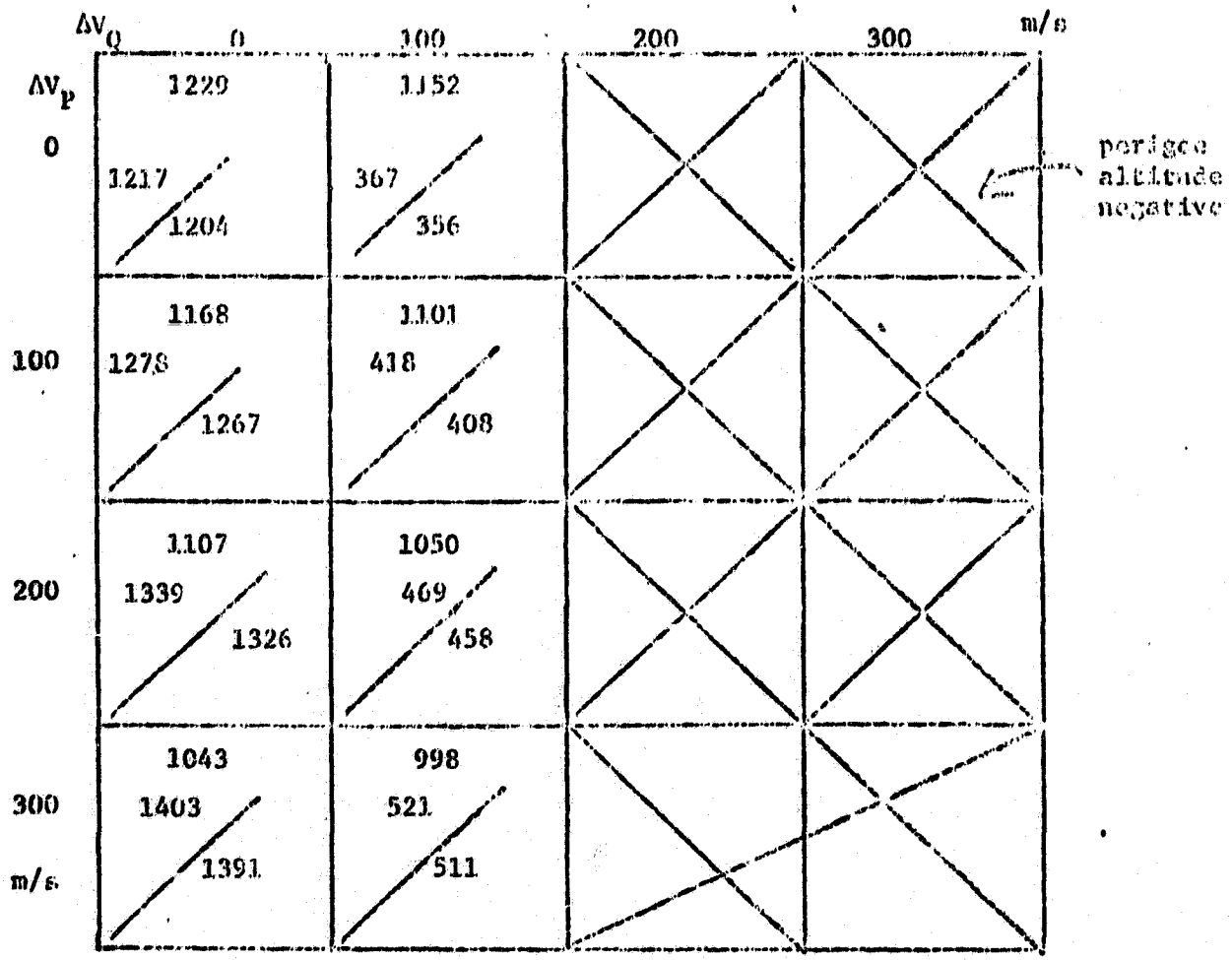

Entries are h in km

apogee altitude (km) / perigee altitude (km)

TABLE 5.7. SHUTTLE IN LEO

M1 = 80,000 kg (shuttle)

M2 = 10,000 kg (satellite)

P = 1/3 day H = 10,390 km

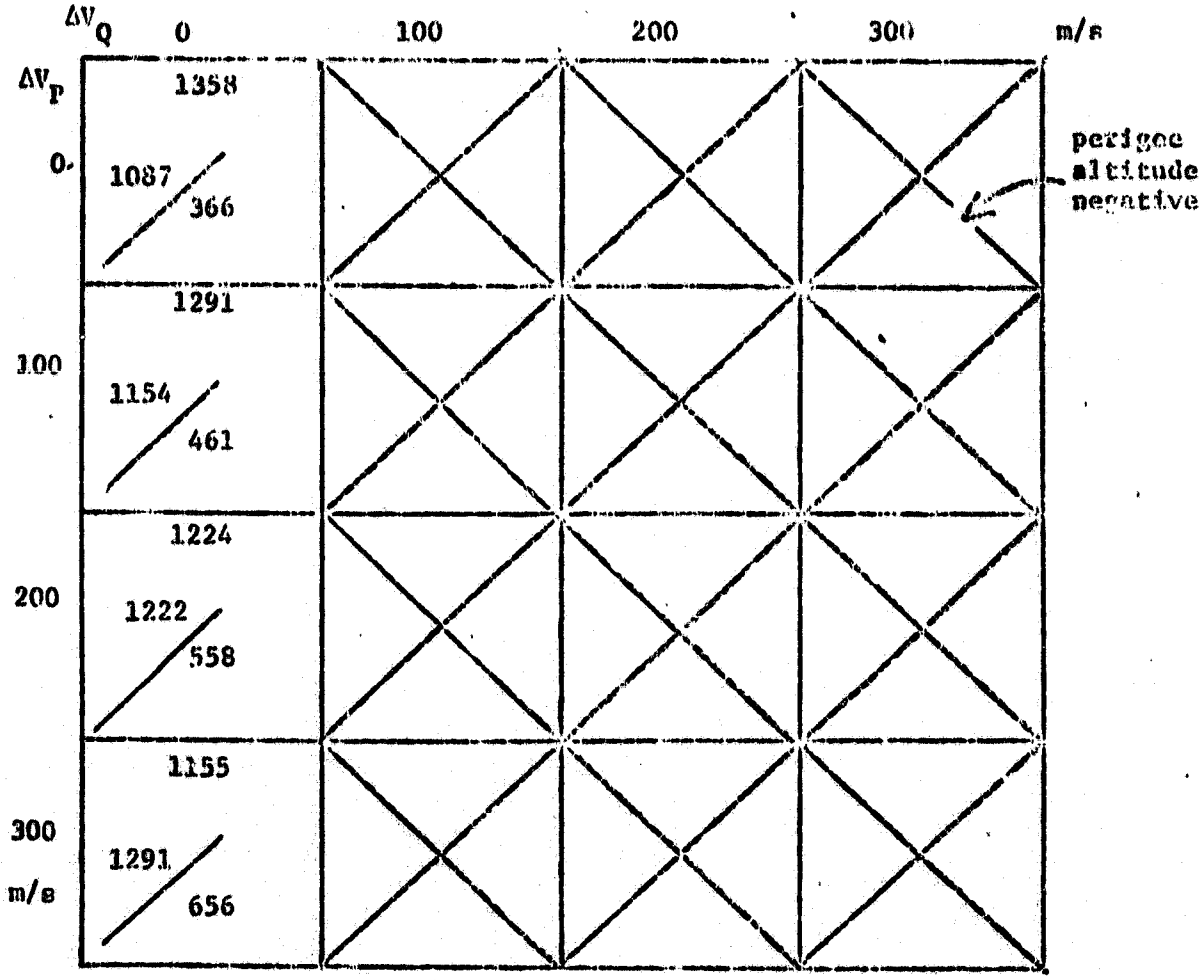

Entries are h in km
apogee altitude (km)
perigee altitude (km)

Appendix 1

Tether Properties and Tether Mass

1. Calculation of Tether Mass

For a radially deployed constant stress tether (stress = σ, density = ρ) the cross section A(r) must be maximum at the orbital center (approximately the c.g.) of the orbiting assembly. Let A_{max} be this maximum section and R_{LEO} the orbital radius out to the c.g. We can then easily find from statics that

$$A(r) = A_{max} \exp\left[\frac{\mu_e \rho}{\sigma}\left(\frac{3}{2R_{LEO}} - \frac{r^2}{2R_{LEO}^3} - \frac{1}{r}\right)\right] \tag{1}$$

Expanding and retaining only quadratic terms (or, alternatively, starting from a constant gravity gradient approximation),

$$A(r) \approx A_{max} \exp\left[-\frac{3}{2}\frac{\mu_e \rho}{\sigma R_{LEO}}\left(\frac{r-R_{LEO}}{R_{LEO}}\right)^2\right] \tag{2}$$

At the upper and lower end of the tether, the respective concentrated masses M_{TIP} and M_{PL} must be in force equilibrium between tether tension and gravity gradient force:

$$3\frac{\mu_e}{R_{LEO}^3} M_{tip}(L-x_{cg}) = \sigma A_{max} \exp\left[-\frac{3}{2}\frac{\mu_e \rho}{\sigma R_{LEO}}\left(\frac{L-x_{cg}}{R_{LEO}}\right)^2\right] \tag{3}$$

$$3\frac{\mu_e}{R_{LEO}^3} M_{PL}\, x_{cg} = \sigma A_{max} \exp\left[-\frac{3}{2}\frac{\mu_e \rho}{\sigma R_{LEO}}\left(\frac{x_{cg}}{R_{LEO}}\right)^2\right] \tag{4}$$

where L is the stretched tether length and x_{cg} is the distance from the lower platform to the overall c.g. of the system.

Equations (3) and (4) can be solved for A_{max} and x_{cg}. Unfortunately, except for limiting cases, this solution cannot be obtained in closed form. To facilitate discussion, let

$$\gamma = \frac{L}{R_{LEO}} \sqrt{\frac{3}{2}\frac{\mu_e \rho}{\sigma R_{LEO}}} \tag{5}$$

$$\nu = \frac{M_{tip}}{M_{PL}} \; ; \quad \xi = \frac{x_{cg}}{L} \tag{6a,b}$$

Then, by division of (3) by (4), and after simplification, one obtains an equation for ξ (c.g. position):

$$\nu\left(\frac{1}{\xi} - 1\right) = e^{-\gamma^2(1-2\xi)} \tag{7}$$

For short tethers ($\gamma << 1$), this has the approximate solution

$$\xi \simeq \frac{\nu}{1+\nu} \tag{8}$$

For other conditions, Table 1 lists values of ξ obtained from Eq. (7):

	ν=0	0.05	0.1	0.15	0.2
γ = 0	0	0.04761	0.09091	0.13043	0.16667
0.5	0	0.05869	0.10843	0.15150	0.18937
1	0	0.10011	0.16380	0.21097	0.24823
1.5	0	0.17652	0.24201	0.28396	0.31499
2	0	0.25775	0.31139	0.34371	0.36697
3	0	0.37446	0.39562	0.41393	0.42694
4	0	0.41687	0.43608	0.44732	0.45531

Table 1. Values of $\xi = \frac{x_{cg}}{L}$

The mass M_T of the tether can be obtained by integration of Eq. (2):

$$M_T = \rho A_{max} \int_{-x_{cg}}^{L-x_{cg}} \exp[-\gamma^2 (\frac{y}{L})^2] dy = \rho A_{max} \frac{\sqrt{\pi}}{2\gamma} [\mathrm{erf}(\gamma\xi) + \mathrm{erf}(\gamma(1-\xi))] \quad (8)$$

where $y = r - R_{LEO}$. The value of A_{max} is obtained from Eq. (3).

After some rearrangement, we obtain

$$\frac{M_T}{M_{tip}} = \sqrt{\pi}\, \gamma(1-\xi) e^{\gamma^2(1-\xi)^2} [\mathrm{erf}(\gamma\xi) + \mathrm{erf}(\gamma(1-\xi))] \quad (9)$$

For small γ (short tethers), Eq. (8) can be used approximatley for ξ, with the result

$$\frac{M_T}{M_{tip}} \simeq \sqrt{\pi}\, \frac{\gamma}{1+\nu} e^{(\frac{\gamma}{1+\nu})^2} [\mathrm{erf}(\frac{\gamma\nu}{1+\nu}) + \mathrm{erf}(\frac{\gamma}{1+\nu})] \quad (10)$$

$$\simeq 2 \frac{\gamma^2}{1+\nu} e^{(\frac{\gamma}{1+\nu})^2} \quad (11)$$

The last form, valid roughly when $\frac{\gamma}{1+\nu} < 0.3$, indicates a quadratic dependence of mass on length for short tethers, where the tip mass dominates clearly over the tether mass. When γ approaches unity, this changes to a much stronger exponential dependence, as the mass of the tether itself becomes dominant in determining its cross-section.

Table 2 lists values of M_T/M_{tip} for more general conditions (from Eq. (9), using Eq. (7) for ξ).

	ν=0	0.05	0.1	0.15	0.2
γ=0	0	0	0	0	0
0.5	0.5923 (0.5923)	0.5491 (0.5570)	0.5135 (0.5259)	0.4834	0.4573 (0.4315)
1	4.0602 (4.0602)	3.2800 (4.3256)	2.8218 (3.6496)	2.5485	2.3136
1.5	24.370	12.195	9.4296	7.9975	7.0652
2	192.640	35.713	25.530	20.920	18.140
3	43.090	239.68	163.17	130.85	112.10
4	6.30×10^7	1888.5	1286.2	1032.2	884.7

Table 2. Values of M_{tether}/M_{tip}

The figures in parenthesis in Table 2 are calculated according to Eq. (10), for comparison. These results are presented graphically in Fig. 1 (for $\gamma < 1.1$) and Fig. 2 (for higher γ).

For purposes of calibration, let us assume the following properties (appropriate for Kevlar tethers):

$$\rho = 1.44\ g/cm^3 = 1440\ Kg/m^3$$

$$\sigma = 1/4\ \ 140\ Kg/mm^3 = 1/4\ \ 1.4\times10^9 N/m^2$$

and also $R_{LEO} = R_E + 400\ Km = 6.77\times10^6 m$. We then calculate

$$\gamma = 19.5 \frac{L}{R_{LEO}} = \frac{L(Km)}{347}$$

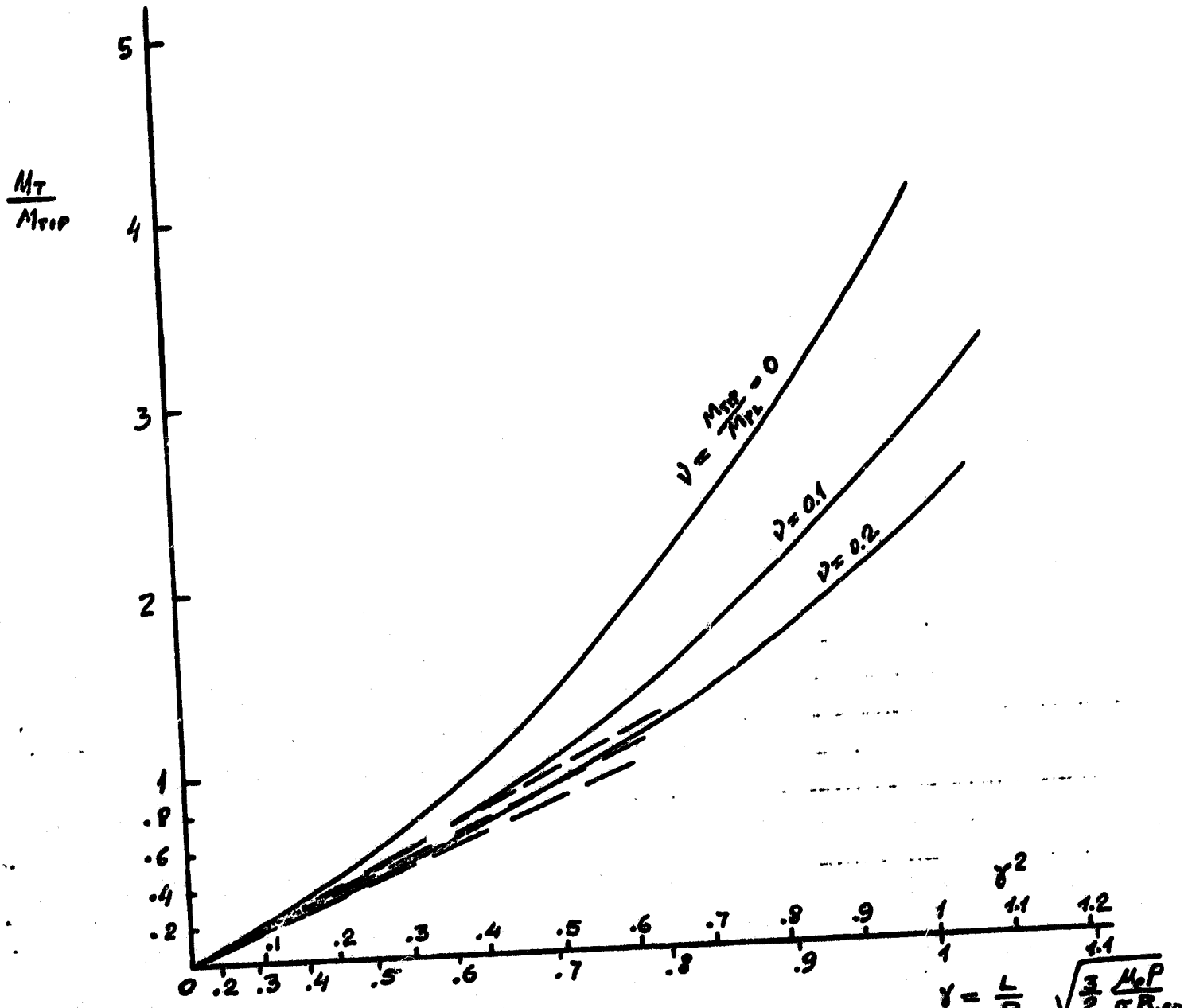

FIG. 1 . RELATIVE TETHER MASS

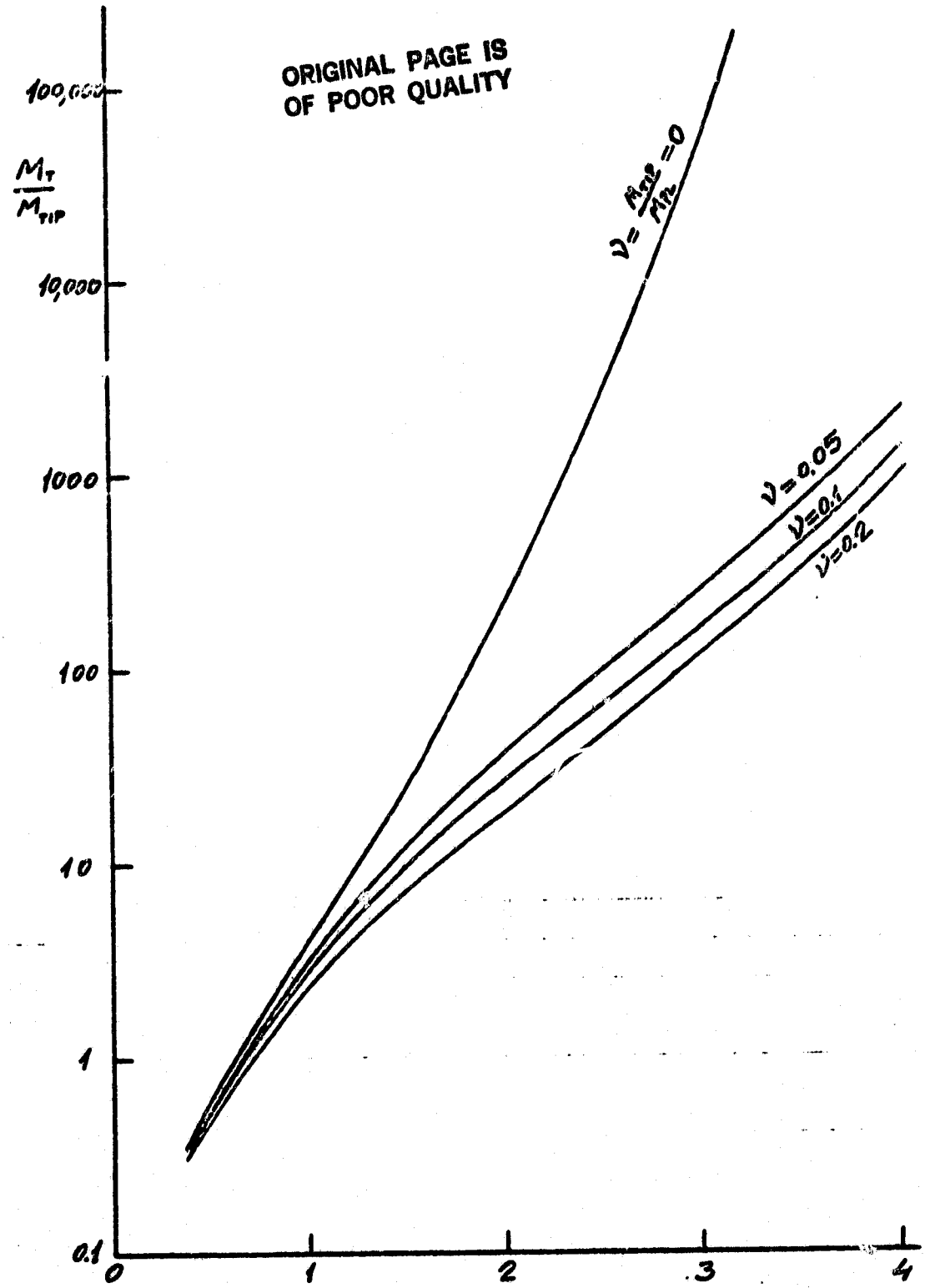

FIG. 2 RELATIVE TETHER MASS FOR LONG TETHERS

$$\gamma = \frac{L}{R_{LEO}} \sqrt{\frac{3}{2} \frac{\mu_e \rho}{\sigma R_{LEO}}}$$

$$\left(\gamma_{LEO} \simeq \frac{L(Km)}{347}\right)$$

From Fig. 1 we see now that the tether mass increases like L^2 for $L \lesssim$ 200 - 300 Km; for longer tethers in LEO, the mass escalates rapidly, as shown in Fig. 2. For L ≃ 1200 Km, as required for no-propulsion transfer to GEO, we see that $M/M_{tip} \simeq 200$, while if this length is reduced to 600 Km by use of partial propulsion, then $M/M_{tip} \simeq 15$. A similar reduction occurs if the working strength could be doubled (see discussion below).

If R_{LEO} is replaced by R_{GEO} = 42200 Km, then

$$\gamma_{GEO} \simeq \frac{L(Km)}{5500}$$

showing that much longer tethers can be deployed in GEO orbits.

Properties of Tether Materials.

The single most important property of a desirable material for our application is a high specific stress (σ/ρ). Fig. 3 compares the σ/ρ data of many high-strength materials, including steel, fiberglass, boron and graphite fibers and the fibers known under the trade name of Kevlar 29 and Kevlar 49 (Dupont). The latter are clearly the best candidates, unless high modulus is important to minimize stretch (in which case boron or graphite fibers are superior). A similar comparison, this time in terms of the direct stress-strain curves for several fibers, is shown in Fig. 4. Values of σ up to $3.6 \times 10^9 N/m^2$ are shown for Kevlar in the form of impregnated strands (360 Kg/mm^2).

Physically, these strands are made if a bundle of very thin fibers (diameter ~12 μm), and the values quoted refer to tests made on samples of a few inches in length. Clearly, the probability of a flaw increases with

FIGURE 3. SPECIFIC* TENSILE STRENGTH AND SPECIFIC* TENSILE MODULUS OF REINFORCING FIBERS

* TENSILE STRENGTH OR MODULUS DIVIDED BY DENSITY

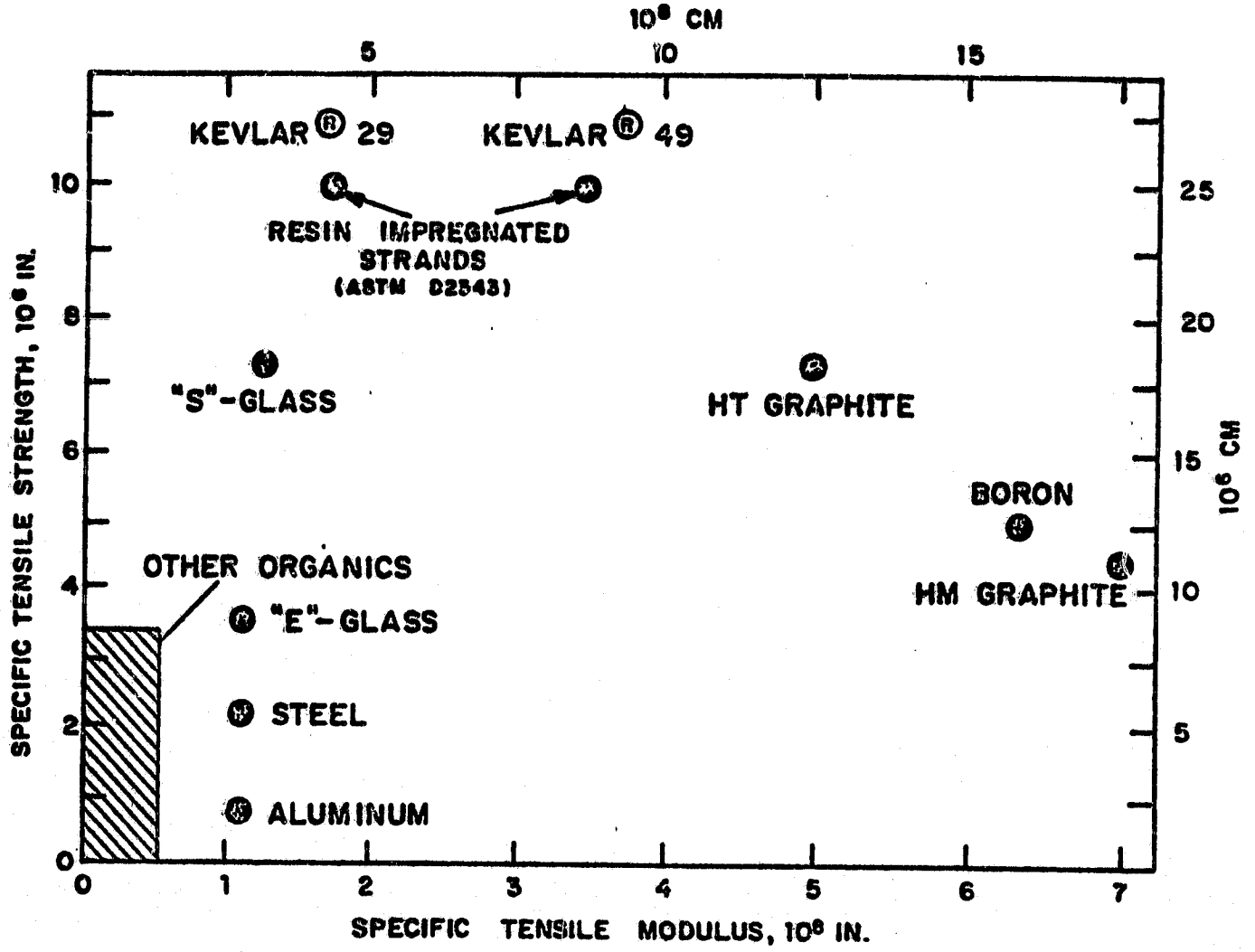

FIGURE 4. STRESS-STRAIN BEHAVIOR OF REINFORCING FIBERS

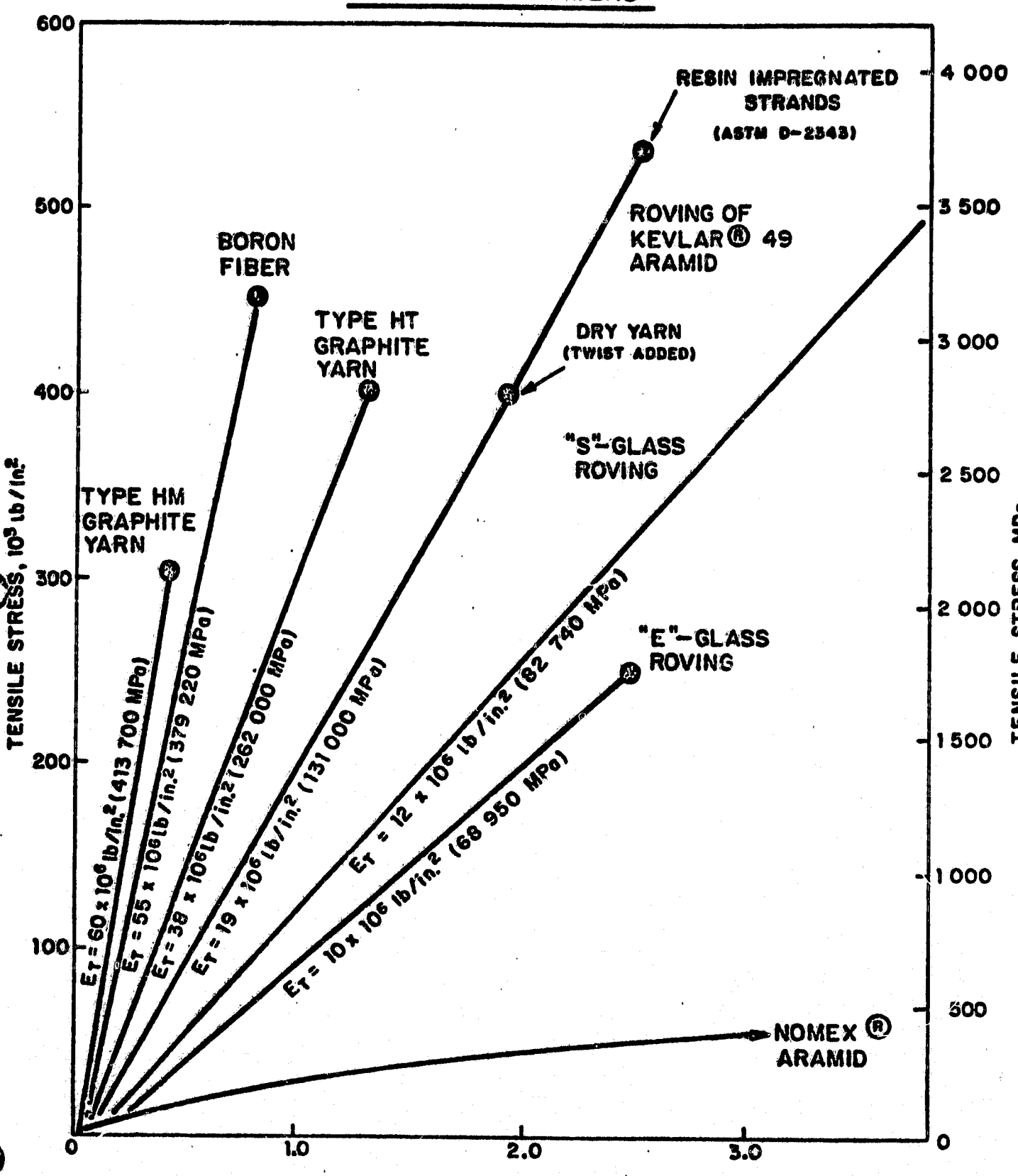

ASTM D2343-67 RESIN IMPREGNATED STRAND TEST

(REV 12/77)

the length of the fiber, and this is reflected in a lower expected strength for longer tethers. Some data for a limited range of L/D fiber values are shown in Fig. 5. For Kevlar 49, the data can be represented as

$$\sigma = 340 \left(\frac{0.06}{L(m)}\right)^{0.051}$$

and if we tentatively extrapolate to the very long lengths contemplated, we calculate the results shown in Table 3:

L(m)	0.06	1	10	100	1 Km	10 Km	100 Km	1000 Km
$\sigma_{n\ell}$(Kg/mm^2)	340	295	262	233	207	184	164	146

Table 3. Extrapolated Fiber Strength for Kevlar-49

Clearly, the extrapolation used is questionable, and much more experience with long tethers is required before a firm design strength value can be identified. For most of the calculations in this report we have adopted 140 Kg/mm^2 as the ultimate (break) strength, and used a factor of safety of 4.

Other relevant properties of Kevlar-49 are listed in Tables 4a and 4b. Note in particular the relatively small elongation (2.5% to break, or about 0.6% at the design strength used here).

Finally, one area of some concern is the observed UV degradation of Kevlar-49 fibers. Here, again, the data are inadequate. Table 5 shows a few examples. The data for the 1/2" rope indicate partial self-screening, with the outer layers protecting the inner ones from the UV radiation. This also hints at the possibility of protective layers, which could also serve as a matrix for enhancing inter-fiber friction.

By contrast, electron radiation damage is minimal.

FIGURE 5. TENSILE STRENGTH UNIFORMITY OF REINFORCING FIBERS

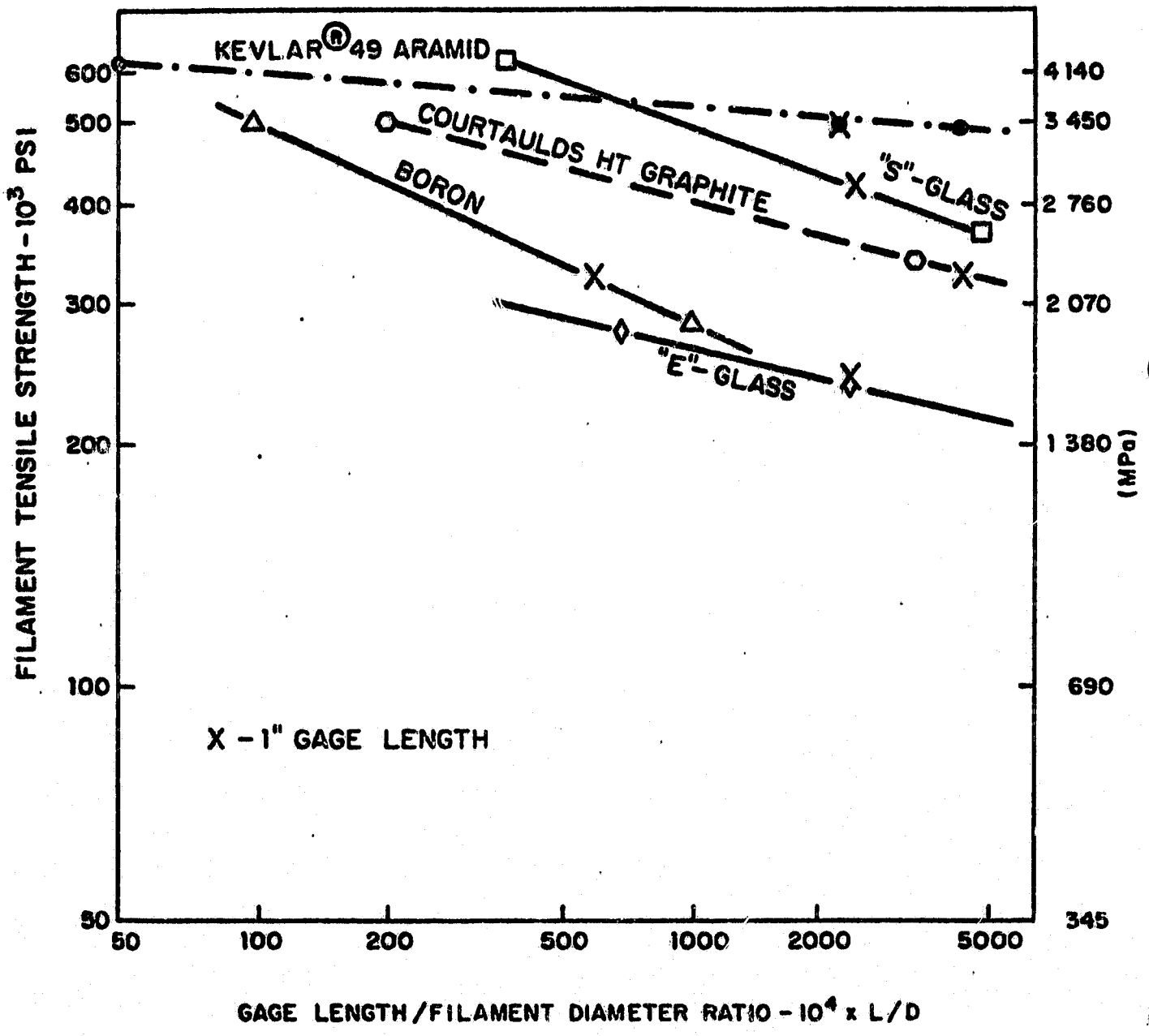

YARN AND ROVING OF KEVLAR® 49

MECHANICAL PROPERTIES

PROPERTY	VALUE	REFERENCE
TENSILE STRENGTH, S_T		II-1
RESIN IMPREGNATED STRANDS (ASTM D2343)	525,000 LB/IN^2 3 620 MPA	II-2
DRY YARN (TWISTED TEXTILE TEST)	400,000 LB/IN^2 2 760 MPA	
VARIABILITY	C.V. = 4	
TENSILE MODULUS, E_T	18 x 10^6 LB/IN^2 124 000 MPA	II-1 II-2
VARIABILITY	C.V. = 5	
UNIFORMITY	---	II-3
ELONGATION-TO-BREAK	2.5%	II-1
DENSITY	0.052 LB/IN^3 1.44 G/CM^3	II-4
FILAMENT DIAMETER	0.00047 IN 0.00119 CM	II-5
CROSS-SECTION	ROUND	
SPECIFIC TENSILE STRENGTH, S_T/DENSITY	10 x 10^6 IN 25.4 x 10^6 CM	II-6
SPECIFIC TENSILE MODULUS, E_T/DENSITY	3.5 x 10^8 IN 8.8 x 10^8 CM	II-6

TABLE 4a.

	PROPERTY	VALUE	REF.	
YARN AND ROVING OF KEVLAR® 49	KNOT STRENGTH	35% TENSILE STRENGTH		MECHANICAL PROPERTIES
	FLEXURAL FATIGUE RESISTANCE	200 CYCLES AT 56,000 PSI OVER 3 MIL DIA. PIN (386 MPA; 0.08 MM)		
	CREEP, 90% ULTIMATE TENSILE STRENGTH	0.0011 IN/IN, INITIAL 0, SECONDARY	II-7	
	COEFFICIENT OF FRICTION			
	YARN-YARN	0.46		
	YARN-METAL	0.41		
FABRIC OF KEVLAR® 49	FABRIC STRIP TENSILE TONGUE TEAR TRAPEZOIDAL TEAR	DEPENDENT ON FABRIC STYLE	II-8	

TABLE 4b.

ULTRAVIOLET STABILITY OF "KEVLAR" 49

MATERIAL	EXPOSURE	BREAK LOAD (LB)	STRENGTH LOSS (%)
770 DENIER TWISTED CORD (530 FILAMENTS)	CONTROL	37.8	--
	FADEOMETER		
	100 HRS	22.2	41
	200 HRS	20.1	47
	WEATHEROMETER		
	100 HRS DRY	21.3	44
	100 HRS WET	22.2	41
	200 HRS DRY	18.1	52
	200 HRS WET	18.3	51
1/8" DIAMETER CABLE*	CONTROL	1322	--
	WEATHEROMETER		
	100 HRS DRY	1030	22
1/2" DIAMETER 3-STRAND ROPE*	CONTROL	11,400	--
	WEATHEROMETER		
	200 HRS DRY	10,600	7
	FLORIDA SUN		
	6 MONTHS	10,260	10
	12 MONTHS	9,240	19

TABLE 5.

WEATHEROMETER EXPOSURE - SUNSHINE CARBON ARC
FADEOMETER EXPOSURE - XENON LAMP
FLORIDA EXPOSURE - HIALEAH

*data indicates self-screening influence of outer layers of "Kevlar" 49

Appendix 2

Platform Orbit Recovery Using Impulsive Thrust

Consider a platform of mass M carrying a satellite of mass m, both of them in an orbit at R_L (orbital speed $v_L = \sqrt{\frac{\mu_e}{R_L}}$). If the satellite is deployed on a light tether of length L, the platform descends to

$$R_a = R_L(1 - \lambda_p) \quad ; \quad \lambda_p = \frac{L}{R_L}\,\frac{m}{m+M}$$

and it travels there at

$$V_a = V_L(1 - \lambda_p)$$

If the payload is now released, R_a and V_a become the apogee radius and speed for the platform in its new elliptic orbit. Since the apogee velocity is

$$V_a = \sqrt{\frac{\mu_e}{R_a}\,\frac{2R_p}{R_a+R_p}}$$

we can now solve for the perigee radius R_p. To first order in λ_p, we find $R_p \simeq 1 - 7\,\lambda_p$. The velocity at this perigee is

$$V_p = V_a\,\frac{R_a}{R_p} \simeq V_L\,(1 + 5\,\lambda_p)\ .$$

In order to return the platform to its original orbit using impulsive thrust, we apply first a perigee impulse

$$\Delta V_p = V_p' - V_p$$

where $V_p' = \sqrt{\frac{\mu_e}{R_p}\,\frac{2R_L}{R_L+R_p}}$ is the speed at the perigee of the new (transfer) orbit that will reach apogee at the intended radius $R = R_L$.

Approximately, then, $V_p' \simeq V_L(1 + \frac{21}{4}\lambda_p)$, and

$$\Delta V_p \simeq \frac{1}{4} V_L \lambda_p$$

When the platform reaches apogee at R_L, a circularization impulse $\Delta V_a = V_L - V_a'$ is needed, where $V_a' = V_p' \frac{R_p}{R_L}$. We find

$$\Delta V_a \simeq \frac{7}{4} V_L \lambda_p$$

The total ΔV required is therefore

$$\Delta V = 2V_L \lambda_p = 2V_L \frac{L}{R_L} \frac{m}{m+M}$$

and the total impulse is

$$M\Delta V = 2V_L \frac{L}{R_L} \frac{Mm}{M+m}$$

It is of interest to compare this impulse to that which would be required to place the satellite in its post-release orbit with no tether assist. Such an orbit has as its perigee the release radius

$$R_p = R_L(1 + \lambda_s) \quad ; \quad \lambda_s = \frac{L}{R_L} \frac{M}{M+m}$$

and as its perigee velocity, $V_p = V_L(1 + \lambda_s)$.

In order to raise the satellite impulsively from R_L, V_L to this elliptic orbit, the optimum impulsive maneuver consists of two firings, the first one applied at the point in the circular orbit opposite the eventual perigee, and such as to produce a transfer orbit tangent to the final orbit at that perigee (which is itself the transfer orbit apogee).

This firing is found to be

$$\Delta V_p = \frac{1}{4} V_L \lambda_s$$

The second firing is applied at the point of tangency of transfer and final orbits; it is found to be

$$\Delta V_a = \frac{7}{4} V_L \lambda_s$$

for a total ΔV of $2V_L \lambda_s$, and a total impulse

$$m\Delta V = \frac{L}{R_L} \frac{Mm}{M+m}$$

This is exactly the same value found for the impulse spent in re-establishing the platform orbit after satellite release, a result perhaps not unexpected on the basis of along-the-orbit overall momentum conservation.

Appendix 3

Platform Orbit Recovery Using Low Thrust

In this appendix we examine the orbital dynamics of platform orbital restoration by means of high specific impulse, low thrust engines. The results will be of use in calculations of power and propellant requirements for these platforms.

1. Orbital Perturbations of the Platforms. For the LEO platform releasing a payload/engine combination, the sequence of operations can be as follows:

(a) The Shuttle docks with an orbiting platform which has a radial outward tether deployed. Payload and OTV are transferred to the platform (including Hg for the upper platform).

(b) The payload/engine combination travels along the tether to its top. Travelling rate must be controlled to ensure radial position at the end and to minimize oscillations. The platform loses altitude, but, to first order, the system c.g. remains in the original orbit.

(c) The payload/engine combination is released. The platform (plus tether) enter a perturbed elliptic orbit with apogee at the release point. The platform mass must be sufficient to prevent reentering at the perigee.

(d) Low thrust engines on the platform are activated to slowly raise and circularize the platform orbit to its original configuration.

Let R_a be the apogee of the platform perturbed orbit, h the tether length and M and m the platform and payload/engine masses. The radius of the original (and eventual) platform orbit is then

$$a_1 = R_a + \frac{m}{m+M} h = R_a \left(1 + \frac{\lambda\nu}{1+\nu}\right) \tag{1}$$

where

$$\lambda = \frac{h}{R_a} \quad , \quad \nu = \frac{m}{M} \tag{2}$$

Some simple dynamical calculations show that, for small λ , the perigee R_p of the perturbed orbit is given by

$$\frac{R_p}{R_a+R_p} = \frac{1}{2} - \frac{3}{2}\frac{\lambda\nu}{1+\nu} \tag{3}$$

Thus, the eccentricity is

$$e = \frac{R_a-R_p}{R_a+R_p} \simeq \frac{3\lambda\nu}{1+\nu} \tag{4}$$

and the semimajor axis is

$$a_o = \frac{R_a+R_p}{2} \simeq R_a\left(1-\frac{3\lambda\nu}{1+\nu}\right)$$

or, combining with (1),

$$\frac{a_1}{a_o} \simeq 1 + 4\frac{\lambda\nu}{1+\nu} \tag{5}$$

A very similar development can be made for the upper (GEO) tether manauvers. The sequence is now

(a) The station with a radially inward deployed tether is initially in GEO orbit. The payload (after separation from the OTV last stage) docks with the tether lower end.

(b) The c.g. of the system is now in an elliptic orbit with apogee somewhat below GEO (by $\frac{m}{m+M} H$, where H is the tether length). The payload is made to climb along the tether at a controlled rate. At the end of the climb, both, the payload and the platform are in the same orbit occupied by the c.g. after docking (to 1st order).

(c) Low thrust engines on the platform are activated to raise and circularize the platform-payload combination to GEO.

It can be shown that equations (4) and (5) still describe the perturbed orbit in this case, with the obvious redefinitions

$$\lambda = \frac{H}{R_{GEO}} \quad , \quad \nu = \frac{m \text{ (payload)}}{M \text{ (GEO platform)}}$$

2. Low Thrust Steering Law. Since the action of the platform engines is quite gradual, we will describe their effect using the orbital perturbation equations (Ref. 1). If f_t is the applied tangential acceleration and no normal acceleration is applied, the rates of change of semimajor axis a, eccentricity e and periapsis azimuth w are

$$\frac{da}{dt} = f_t \, v \, \frac{2a^2}{\mu} \tag{7}$$

$$\frac{de}{dt} = \frac{2f_t}{v} (e + \cos \theta) \tag{8}$$

$$\frac{dw}{dt} = \frac{2f_t}{ev} \sin \theta \tag{9}$$

Ref. 1 Modern Spacecraft Dynamics and Control, by M.H. Kaplan, J. Wiley & Sons (1976), Ch. 8.

where θ is azimuth from periapsis. The vehicle is in a slowly evolving elliptical path described instantaneously by

$$\frac{1}{r} = \frac{1+e\cos\theta}{a(1-e^2)} \tag{10}$$

and such that

$$r^2 \frac{d\theta}{dt} = \sqrt{\mu a(1-e^2)} \tag{11}$$

For small eccentricity e, we can use (11) to eliminate time from (7), (8) and (9):

$$\frac{da}{d\theta} = \frac{2a^3}{\mu} f_t (1-e\cos\theta) \tag{12}$$

$$\frac{de}{d\theta} = \frac{2a^2}{\mu} f_t[\cos\theta + e(1-3\cos^2\theta)] \tag{13}$$

$$\frac{dw}{d\theta} = \frac{2a^2}{e\mu} f_t \sin\theta\,(1-e\cos\theta) \tag{14}$$

The simplest steering law allowing simultaneous control of eccentricity and orbital energy is a modulated acceleration law of the form

$$f_t = f_o + f_1 \cos(\theta-\theta_o) \tag{15}$$

Substituting into (12) to (14) and averaging over one period of θ, we obtain (for long times, neglecting products of e and f_o or f_1):

$$\frac{da}{d\theta} = \frac{2a^3 f_o}{\mu} \tag{16}$$

$$\frac{de}{d\theta} = \frac{a^2 f_1 \cos\theta_o}{\mu} \tag{17}$$

$$\frac{dw}{d\theta} = \frac{a^2}{e\mu} f_1 \sin\theta_o \tag{18}$$

For fastest reduction of eccentricity, and in order to avoid periapsis rotation, we chose $\theta_o = 0$. Eqs. (16) and (17) integrate immediately to

$$a = \frac{a_o}{\sqrt{1 - \frac{4f_o a_o^2}{\mu}\theta}} \tag{19}$$

$$e = e_o + \frac{f_1}{4f_o} \ln\left(\frac{1}{1 - \frac{4f_o a_o^2}{\mu}\theta}\right) \tag{20}$$

If at a certain azimuth θ, we impose <u>both</u> $a = a_1$ and $e = 0$, we obtain the condition

$$\frac{f_1}{f_o} = \frac{-2e_o}{\ln(\frac{a_1}{a_o})} \tag{21}$$

So that, using equations (4) and (5) for e_o and a_1/a_o, we find to 1st order

$$\frac{f_1}{f_o} = -\frac{3}{2}$$

and so, the acceleration law is

$$f_t = f_o\left(1 - \frac{3}{2}\cos\theta\right) \tag{22}$$

This indicates retrofiring at perigee ($f_t = -\frac{1}{2} f_o$) and maximum forward thrust at apogee ($f_t = \frac{5}{2} f_o$).

3. Propellant Consumption. The usual law

$$\frac{m_{final}}{m_{initial}} = e^{-\frac{\Delta V}{c}}$$

applies, with

$$= \int_0^{t_{final}} |f_t| dt \qquad (23)$$

where the absolute value of the applied acceleration is used, since propellant consumption is independent of thrust orientation. Eq. (11) is used again to eliminate dt in favor of dθ. To first order in e, the velocity increment per turn is then found to be

$$\Delta V_1 = f_o \sqrt{\frac{a^3}{\mu}} \left[(2\sqrt{5} + 2\pi - 4 \cos^{-1} \tfrac{2}{3}) + e(\tfrac{4}{3}\sqrt{5} + 3\pi - 6 \cos^{-1} \tfrac{2}{3}) \right]$$

$$= f_o \sqrt{\frac{a^3}{\mu}} (7.391 + 7.360\, e) \qquad (24)$$

Also, to the lowest order in e, the number of turns in time t is $N = \frac{1}{2\pi} \sqrt{\frac{\mu}{a^3}}\, t$, so that, to that order

$$\Delta V \simeq 1.176\, f_o t \qquad (25)$$

The product $f_o t$ can be related to the mission characteristics by integration of the time equation (Eqs. (11) and (10), combined with Eq. (19) for a). Ignoring the cyclic part and retaining only the secular term, we obtain:

$$\frac{dt}{d\theta} = \frac{a_o^{3/2}}{\sqrt{\mu}\left(1 - \frac{4 f_o a_o^2}{\mu} \theta\right)^{3/4}}$$

ORIGINAL PAGE IS
OF POOR QUALITY

which integrates to

$$f_o t = \sqrt{\frac{\mu}{a_o}} \left[1 - \left(1 - \frac{4 f_o a_o^2}{\mu}\theta\right)^{1/4}\right] = \sqrt{\frac{\mu}{a_o}} \left[1 - \sqrt{\frac{a_o}{a}}\right] \qquad (26)$$

where (19) has been used once more. Thus, if t refers to the final time, when $a = a_f$ (and $e = 0$), we obtain

$$f_o t = \sqrt{\frac{\mu}{a_o}} \left(1 - \sqrt{\frac{a_o}{a_1}}\right) = v_{c_o} - v_{c_1} \qquad (27)$$

where v_{c_1} is the final orbital velocity, while v_{c_o} would be the velocity in a circular orbit with the same energy as the initial (elliptic) orbit. Using now Eq. (5) for $\frac{a_o}{a_1}$, we obtain finally (to lowest order in e)

$$\Delta V = 1.176\, v_{c_1} \frac{2\lambda\nu}{1+\nu} \qquad (28)$$

It can be seen by comparison to the results of Appendix 2 that the ΔV required with low thrust is 1.176 times that required with the optimal combination of impulsive firings. However, since the specific impulse can be quite high using ion or other electric thrustors, the propellant use can still be significant.

APPENDIX 4

Dynamics of the tether system during ferry transfer.

1. Formulation of the Problem

We consider in this section the dynamical effects that occur during ascent of a loaded ferry which translates along a tether line deployed from an orbiting platform. A terminal handling facility is also assumed to exist at the upper end of the tether; this upper platform also serves to provide tension for the tether, due to the gravity gradient force acting on it.

The system to be studied is shown in Fig. 1. We will assume small angular deflections from the vertical, and ignore the mass of the tether itself. The latter assumption implies tether lengths below some 200 Km, while the small deflection assumption will be well satisfied for sufficiently small ferry velocity (v), provided no dynamical instability is encountered. These are precisely the issues to be clarified by the analysis.

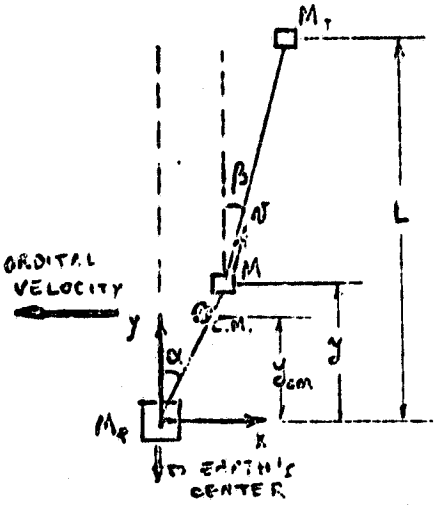

FIG. 1

The gravity gradient forces on the three masses depend on orbital angular speed, Ω and distance to the overall center of mass CM.

With the origin of coordinates fixed at the lower platform, as shown, these distances are

$$x_{cm} = \nu x + \nu_T x_T \quad ; \quad y_{cm} = \nu y + \nu_T L \tag{1}$$

$$x - x_{cm} = (1-\nu)x - \nu_T x_T \quad ; \quad y - y_{cm} = (1-\nu)y - \nu_T L \tag{2}$$

$$x_T - x_{cm} = (1-\nu_T)x_T - \nu x; \quad L - y_{cm} = (1-\nu_T)L - \nu y \tag{3}$$

where

$$\nu \equiv \frac{M}{M+M_p+M_T} \quad , \quad \nu_T \equiv \frac{M_T}{M+M_p+M_T} \tag{4a, b}$$

and $$\nu_p \equiv 1 - \nu - \nu_T = \frac{M_p}{M+M_p+M_T} \tag{5}$$

The gravity gradient forces are then (positive upwards)

$$F_p^{GG} = -3\Omega^2 M_p y_{cm} \tag{6}$$

$$F_m^{GG} = 3\Omega^2 M(y - y_{cm}) \tag{7}$$

$$F_T^{GG} = 3\Omega^2 M_T(L - y_{cm}) \tag{8}$$

In addition to these forces, the Coriolis forces must be considered, since the axes rotate at speed Ω. When the ferry is travelling upwards at speed $\dot{y}$ relative to the platform, since the center of mass must remain (to first order) at a fixed altitude, the other masses (and the tether) must travel downwards to compensate. The absolute velocities are then $(1-\nu)\dot{y}$ (ferry) and $-\nu\dot{y}$ (upper and lower platforms). The corresponding Coriolis forces are then (positive backwards)

$$F_p^c = -2\Omega M_p \nu \dot{y} \tag{9}$$

$$F_m^c = 2\Omega M (1-\nu) \dot{y} \tag{10}$$

$$F_T^c = -2\Omega M_T \nu \dot{y} \tag{11}$$

We will assume the vertical accelerations are small enough that the tensions T_{upper} and T_{lower} of the upper and lower tether segments respectively are equal to their quasi-static values:

$$T_{upper} = F_T^{GG}$$

$$T_{lower} = -F_p^{GG}$$

With the small-angle assumptions

$$\sin\alpha \approx \alpha \approx x/y \quad ; \cos\alpha \approx 1$$

$$\sin\beta \approx \beta \approx \frac{x_T - X}{L-y} \; ; \cos\beta \approx 1$$

the horizontal components of these tensions contribute forces

$$F_p^T = -F_p^{GG}\frac{x}{y} \tag{12}$$

$$F_m^T = F_p^{GG}\frac{x}{y} + F_T^{GG}\frac{x_T - x}{L - y} \tag{13}$$

$$F_T^T = F_T^{GG}\frac{x_T - x}{L - y} \tag{14}$$

The equations of motion for the three masses are then

$$M_p(\nu\ddot{x} + \nu_T\ddot{x}_T) = -3\Omega^2\left\{M[(1-\nu)y - \nu_T L] + M_T[(1-\nu_T)L-\nu y]\right\}\frac{x}{y} - 2\Omega M_p\nu\dot{y} \tag{15}$$

$$M[(1-\nu)\ddot{x}-\nu_T\ddot{x}_T] = -3\Omega^2\left\{M[1-\nu)y-\nu_T L] + M_T[(1-\nu_T)L-\nu y]\right\}\frac{x}{y} + 3\Omega^2 M_T[(1-\nu_T)L-\nu y]\frac{x_T-x}{L-y} \tag{16}$$

$$M_T[(1-\nu_T)\ddot{x}_T-\nu\ddot{x}] = -3\Omega^2 M_T[(1-\nu_T)L-\nu y]\frac{x_T-x}{L-y} - 2\Omega M_T\nu\dot{y} \tag{17}$$

It must be noticed that only two of these equations are independent, since the linear combination representing the motion of the CM must be satisfied. The motions of ferry and upper mass relative to the lower platform can be extracted by the combinations (16)/M - (15)/M_p and (17)/M_T - (15)/M_p respectively. After simplification,

$$\ddot{x} = -3\Omega^2\frac{1-\nu_T}{\nu}(\nu y+\nu_T L)\frac{x}{y} + 3\Omega^2\frac{\nu_T}{\nu}[(1-\nu_T)L-\nu y]\frac{x_T-x}{L-y} - 2\Omega\dot{y} \tag{18}$$

$$\ddot{x}_T = -3\Omega^2(\nu y+\nu_T L)\frac{x}{y} - 3\Omega^2[(1-\nu_T)L - \nu y]\frac{x_T-x}{L-y} \tag{19}$$

A useful variation is obtained by difference of these equations. Defining

$$\delta = x_T - x \tag{20}$$

this equation is

$$\ddot{\delta} = 3\Omega^2\frac{\nu_p}{\nu}(\nu y+\nu_T L)\frac{x}{y} - 3\Omega^2\frac{1-\nu_p}{\nu}[(1-\nu_T)L - \nu y]\frac{\delta}{L-y} \tag{21}$$

There are at least two characteristic times involved in this problem: the first is the transit time T of the ferry; the second is $1/\Omega$, the inverse of the orbital angular velocity (of the same order as the period of the gravity gradient oscillations). Typically, in the situation being considered, T ~ 1 - 3 days, while $1/\Omega \approx 14$ min. Hence, the non-dimensional parameter

$$\varepsilon = \frac{1}{\Omega T} \tag{22}$$

is very small, and can be used as an expansion parameter for an approximate solution. We make this parameter explicit by introducing a dimensionless time

$$\theta = \frac{t}{T} \tag{23}$$

and rewriting Eqs. (18) and (21) as

$$\varepsilon^2 \frac{d^2x}{d\theta^2} = -3 \frac{1-\nu_T}{\nu} (\nu y + \nu_T L) \frac{x}{y} + 3 \frac{\nu_T}{\nu} [(1-\nu_T)L - \nu y] \frac{\delta}{L-y} + 2\varepsilon \frac{dy}{d\theta} \tag{24}$$

$$\varepsilon^2 \frac{d^2\delta}{d\theta^2} = 3 \frac{\nu_p}{\nu} (\nu y + \nu_T L) \frac{x}{y} - 3 \frac{1-\nu_p}{\nu} [(1-\nu_T)L - \nu y] \frac{\delta}{L-y} - 2\varepsilon \frac{dy}{d\theta} \tag{25}$$

In addition to the two widely different time scales, which indicates the likelihood of a slowly modulated gravity gradient oscillation, Eqs. (24) and (25) contain the factors $\frac{1}{y}$ and $\frac{1}{L-y}$. These will cause singularities near the initial and final times. Physically, such singularities arise because of the high frequency of relative oscillations when two of the masses come close to each other; for the condition $y \to L$, there is the possibility of a divergence of δ as the ferry approaches the upper platform.

Although Eqs. (24) and (25) are linear in (x,δ), their complex structure (particularly since $\dot{y}(t)$ is arbitrary), indicates the necessity of approximate methods of solution. The plan of attack will be to use a WKB solution away from y=0 and y=L, and to match it asymptotically to "inner" solutions valid near each end.

2. The WKB solution (ferry not near the ends).

Except for the very fast oscillations near the ends of the trip, we anticipate the solution to consist of slowly modulated (on a scale $\theta \sim 1$) gravity gradient oscillations (of period $\sim \varepsilon$). There should be actually two gravity gradient "modes," roughly corresponding to a collective, near straight-line oscillation of the three masses, and a "bending" oscillation with x opposing x_p and x_T. The WKB method is well suited to this linear problem; we represent the homogeneous approximate solutions as exponentials of truncated series in ε, the leading term (of order $1/\varepsilon$) being imaginary to represent the oscillatory behavior:

$$x = e^{\left[i\,\frac{K(\theta)}{\varepsilon} + A(\theta) + \varepsilon C(0) + \ldots\right]} \tag{26}$$

$$\delta = e^{\left[i\,\frac{K(\theta)}{\varepsilon} + B(\theta) + \varepsilon D(\theta) + \ldots\right]} \tag{27}$$

where the functions K, A, B, C, D are presumed to be smooth on the scale of θ. Differentiating and substituting into Eqs. (24), (25) we obtain

$$\varepsilon^2\left[-\frac{\dot K^2}{\varepsilon^2} + 2i\,\frac{\dot K}{\varepsilon}\,(\dot A+\varepsilon\dot C+\ldots) + i\,\frac{\ddot K}{\varepsilon} + \ddot A + \varepsilon\ddot C + \ldots + (\dot A + \varepsilon\dot C + \ldots)^2\right] =$$

$$= -3\,\frac{1-\nu_T}{\nu}\,(\nu y+\nu_T L)\,\frac{1}{y} + 3\,\frac{\nu_T}{\nu}\,\frac{(1-\nu_T)L-\nu y}{L-y}\,e^{B-A}\,e^{(B-C)\varepsilon}\ldots \tag{28}$$

$$\varepsilon^2\left[-\frac{\dot K^2}{\varepsilon^2} + 2i\,\frac{\dot K}{\varepsilon}\,(\dot B+\varepsilon\dot D+\ldots) + i\,\frac{\ddot K}{\varepsilon} + \ddot B + \varepsilon\ddot D + \ldots + (\dot B + \varepsilon\dot D + \ldots)^2\right] =$$

$$= 3\,\frac{\nu_p}{\nu}\,\frac{\nu y+\nu_T L}{y}\,e^{A-B}\,e^{(C-B)\varepsilon}\ldots - 3\,\frac{1-\nu_p}{\nu}\,\frac{(1-\nu_T)L-\nu y}{L-y} \tag{29}$$

where the inhomogeneous terms $\pm 2\varepsilon\,\frac{dy}{d\theta}$ have been omitted, in the understanding that a particular solution will have to be added later in order to obtain the general solution. Here a dot is meant to represent $d/d\theta$.

We first observe that these two equations can be compatible to order ε^0 only if the two right hand sides are identical (with the $\exp((C-B)\varepsilon)$ terms omitted). This condition leads to a second order algebraic equation for $X \equiv e^{A-B}$:

$$\frac{\nu_p}{\nu} e^{2(A-B)} + \left[\frac{1-\nu_T}{\nu} - \frac{y}{L-y}\frac{(1-\nu_T)L-\nu y}{\nu y + \nu_T L}\frac{1-\nu_p}{\nu}\right] e^{A-B} - \frac{y}{L-y}\frac{(1-\nu_T)L-\nu y}{\nu y + \nu_T L}\frac{\nu_T}{\nu} = 0 \quad (30)$$

which has the two solutions

$$X^+ \equiv e^{A^+-B^+} = \frac{y}{L-y} \quad (31)$$

$$X^- \equiv e^{A^--B^-} = \frac{-\nu_T}{\nu_p}\frac{(1-\nu_T)L-\nu y}{\nu_T L + \nu y} \quad (32)$$

If this condition is satisfied, the zero'th order part of, for instance, Eq. (29), reduces to

$$\dot{K}^2 = -3\frac{\nu_p}{\nu}\frac{\nu y+\nu_T L}{y} e^{A-B} - 3\frac{1-\nu_p}{\nu}\frac{(1-\nu_T)L-\nu y}{L-y} \quad (33)$$

Substitution of either Eq. (31) or Eq. (32) here, leads to the two possible instantaneous frequencies:

$$\dot{K}^+ = \pm\sqrt{3} \quad (34)$$

$$\dot{K}^- = \pm\sqrt{\frac{3}{\nu}\left[(1-\nu_T)L-\nu y\right]\frac{\nu y+\nu_T L}{y(L-y)}} \quad (35)$$

These expressions are valid for arbitrary climbout laws. The phases K^+, K^- are obtained by time integration, and depend, therefore, on the particular choice of climbing law:

$$K^+ = \pm\sqrt{3}\ \theta \quad (36)$$

$$K^- = \int_0^\theta \sqrt{\frac{3}{\nu}\left[(1-\nu_T)L-\nu y\right]\frac{\nu y+\nu_T L}{y(L-y)}}\ d\theta \quad (37)$$

The first of these modes is recognizable as the ordinary gravity gradient oscillation, at frequency $\sqrt{3}\,\Omega$; we expect both X and X_T to

be in phase in this mode. The second one has a more complex structure, with frequency increasing as $\frac{1}{\sqrt{y}}$ near y = 0 and as $\frac{1}{\sqrt{L-y}}$ near y = L; as will be seen in the next section, these "inner limits" of the "outer solution" indeed match the outer limits of the inner solutions near each extreme. This second mode, therefore, can be expected to be the bending mode, and X and ξ should be in counterphase.

To continue the solution, we write down the order-ε parts of Eqs. (28) and (29):

$$2i\dot{K}\dot{A} + i\ddot{K} = 3\,\frac{\nu_T}{\nu}\,\frac{(1-\nu_T)L-\nu y}{L-y}\;e^{B-A}(B-C) \tag{38}$$

$$2i\dot{K}\dot{B} + i\ddot{K} = 3\,\frac{\nu_p}{\nu}\,\frac{\nu y+\nu_T L}{y}\;e^{A-B}(C-B) \tag{39}$$

By division, we can eliminate (B-C) and obtain the required connection between A and B:

$$\frac{2\dot{K}\dot{B}+\ddot{K}}{2\dot{K}\dot{A}+\ddot{K}} = -\,\frac{\nu_p}{\nu_T}\,\frac{L-y}{y}\,\frac{\nu y+\nu_T L}{(1-\nu_T)L-\nu y}\;e^{2(A-B)} \tag{40}$$

For the collective (+) mode, $\ddot{K}^+ = 0$ (see Eq. (34)), and e^{A-B} is given by Eq. (31), from which

$$\dot{A}^+ = \dot{B}^+ + \frac{L\ddot{y}}{y(L-y)} \tag{41}$$

substituting in (40), we can solve for $\frac{dB^+}{dy}$ (after cancelling dt) as

$$\frac{dB^+}{dy} = -\nu_p\,\frac{(\nu y+\nu_T)L}{(L-y)S(y)}\;;\; S(y) \equiv \nu_T(1-\nu_T)L^2 - 2\nu_T\nu Ly + \nu(1-\nu)y^2 \tag{42}$$

which integrates to

$$e^{B^+} = (L-y)\sqrt{\frac{\nu_T(1-\nu_T)}{S(y)}} \tag{43}$$

and, after Eq. (31),

$$e^{A^+} = y\,\sqrt{\frac{\nu_T(1-\nu_T)}{S(y)}} \tag{44}$$

This shows that in the collective gravity gradient mode, the amplitude of the oscillations of X increases nearly linearly with y (α amplitude about constant), while those of X_T-X decrease in amplitude about linearly in L-y (β about constant). The X-amplitude approaches a finite limit as $y \to L$, and since $X(y = 0) = 0$, δ approaches the same limit as $y \to 0$. X and X_T-X oscillate in phase.

For the "bending" (-) mode, for which $\dot{K}^-$ is given by Eq. (35) and $\ddot{K}^-$ does not vanish, a somewhat more elaborate procedure is required. Notice that the left hand side of Eq. (40) can be written as

$$\frac{\dot{2K}\dot{B}+\ddot{K}}{\dot{2K}\dot{A}+\ddot{K}} = \frac{2\dot{K}^2\dot{B}+\ddot{K}\dot{K}}{2\dot{K}^2\dot{A}+\ddot{K}\dot{K}} = \frac{2\dot{B}+\frac{1}{2}\frac{d\ell n}{d\theta}\dot{K}^2}{2\dot{A}+\frac{1}{2}\frac{d\ell n}{d\theta}\dot{K}^2} = \frac{\frac{d}{dy}(2B+\ell n|\dot{K}|)}{\frac{d}{dy}(2A+\ell n|\dot{K}|)}$$

$$2A^- + \ell n|\dot{K}^-| = F \quad ; \quad 2B^- + \ell n|\dot{K}^-| = G \tag{45}$$

so that we have, from Eqs. (40) and (32)

$$\left(\frac{dG}{dy}\right)/\left(\frac{dF}{dy}\right) = -\frac{\nu_T}{\nu_p}\,\frac{L-y}{y}\,\frac{(1-\nu_T)L-\nu y}{\nu_T L+\nu y} \tag{46}$$

and, from (32) and (45)

$$F - G + 2(A^- - B^-) = 2\,\ell n\left[-\frac{\nu_T}{\nu_p}\,\frac{(1-\nu_T)L-\nu y}{\nu_T L+\nu y}\right]$$

$$\frac{dF}{dy} - \frac{dG}{dy} = \frac{-2\nu L}{[(1-\nu_T)L-\nu y](\nu_T L+\nu y)} \tag{47}$$

Equations (46) and (47) can be solved for $\frac{dF}{dy}$ and $\frac{dG}{dy}$, which can then be integrated to obtain F and G. A^- and B^- then follow from Eq. (45), using (35) for $|\dot{K}^-|$. The result of this calculation is

$$e^{A^-} = + \left(\frac{\nu}{3}\right)^{1/4} \frac{[(1-\nu_T)L-\nu y]^{3/4} y^{1/4} (L-y)^{1/4}}{(\nu_T L+\nu y)^{1/4} \sqrt{S(y)}} \tag{48}$$

$$e^{B^-} = - \frac{\nu_p}{\nu} \left(\frac{\nu}{3}\right)^{1/4} \frac{(\nu_T L+\nu y)^{3/4} y^{1/4} (L-y)^{1/4}}{[(1-\nu_T)L-\nu y]^{1/4} \sqrt{S(y)}} \tag{49}$$

where $S(y)$ is as defined in Eq. (42). These formulae show that X and X_T-X indeed oscillate in counterphase ("bending" mode). Both variables have amplitudes varying roughly as $[y(L-y)]^{1/4}$, which indicate angular amplitude for α like $1/y^{3/4}$ (near $y = 0$) and for β like $1/(L-y)^{3/4}$ (near $y = L$). Although this looks like a divergent behavior, matching to the near-end solutions will show that at least one finite angle solution exists at each end.

Having determined e^A, e^B and $e^{i\,K/\varepsilon}$ for each of the two gravity gradient modes, we have a good approximation to the homogeneous solution and can truncate the expansion in powers of ε. The remaining task is to generate a particular solution of the complete equations; none can be identified by inspection, and so, the method of variation of parameters must be resorted to. To this end, let us represent the homogeneous solution in the form

$$X = C_1 f_1 + C_2 f_2 + C_3 f_3 + C_4 f_4 \tag{50}$$

$$\delta = C_1 g_1 + C_2 g_2 + C_3 g_3 + C_4 g_4 \tag{51}$$

where

$$f_1 = e^{A^+ + i\frac{K+}{\varepsilon}} \; ; \quad f_2 = e^{A^+ - i\frac{K^+}{\varepsilon}} \; ; \quad f_3 = e^{A^- + i\frac{K^-}{\varepsilon}} \; ; \quad f_4 = e^{A^- - i\frac{K^-}{\varepsilon}} \tag{52}$$

$$g_1 = e^{B^+ + i\frac{K^+}{\varepsilon}} \; ; \quad g_2 = e^{B^+ - i\frac{K^+}{\varepsilon}} \; ; \quad g_3 = e^{B^- + i\frac{K^-}{\varepsilon}} \; ; \quad g_4 = e^{B^- - i\frac{K^-}{\varepsilon}} \tag{53}$$

If C_1 , C_2 , C_3 , C_4 are regarded now as functions of time, the usual process of differentiation, enforcement of auxiliary conditions and substitution into the complete equations (Eqs. (24), (25) leads to a system of equations for $\dot{C}_1$, $\dot{C}_2$, $\dot{C}_3$, $\dot{C}_4$:

$$\left.\begin{aligned} f_1\dot{C}_1 + f_2\dot{C}_2 + f_3\dot{C}_3 + f_4\dot{C}_4 &= 0 \\ g_1\dot{C}_1 + g_2\dot{C}_2 + g_3\dot{C}_3 + g_4\dot{C}_4 &= 0 \\ \dot{f}_1\dot{C}_1 + \dot{f}_2\dot{C}_2 + \dot{f}_3\dot{C}_3 + \dot{f}_4\dot{C}_4 &= 2\frac{\dot{\gamma}}{\varepsilon} \\ \dot{g}_1\dot{C}_1 + \dot{g}_2\dot{C}_2 + \dot{g}_3\dot{C}_3 + \dot{g}_4\dot{C}_4 &= -2\frac{\dot{\gamma}}{\varepsilon} \end{aligned}\right\} \qquad (54)$$

Notice, from Eqs. (52), (53) that $g_1/f_1 = g_2/f_2 = e^{B^+-A^+}$, and similarly $g_3/f_3 = g_4/f_4 = e^{B^--A^-}$; thus, the first two equations of (54) admit the single solution

$$\left.\begin{aligned} f_1\dot{C}_1 + f_2\dot{C}_2 &= 0 \\ f_3\dot{C}_3 + f_4\dot{C}_4 &= 0 \end{aligned}\right\} \qquad (55)$$

Elimination of $\dot{C}_2$ and $\dot{C}_4$ between these equations and the bottom two equations of (54) then gives

$$\left.\begin{aligned} \left(\frac{\dot{f}_1}{f_1} - \frac{\dot{f}_2}{f_2}\right) f_1\dot{C}_1 + \left(\frac{\dot{f}_3}{f_3} - \frac{\dot{f}_4}{f_4}\right) f_3\dot{C}_3 &= 2\frac{\dot{\gamma}}{\varepsilon} \\ \left(\frac{\dot{g}_1}{f_1} - \frac{\dot{g}_2}{f_2}\right) f_1\dot{C}_1 + \left(\frac{\dot{g}_3}{f_3} - \frac{\dot{g}_4}{f_4}\right) f_3\dot{C}_3 &= -2\frac{\dot{\gamma}}{\varepsilon} \end{aligned}\right\} \qquad (56)$$

Noting that

$$\left(\frac{\dot{g}_1}{f_1} - \frac{\dot{g}_2}{f_2}\right) = \left(\frac{\dot{g}_1}{g_1} - \frac{\dot{g}_2}{g_2}\right) e^{B^+-A^+} = \left(\frac{\dot{f}_1}{f_1} - \frac{\dot{f}_2}{f_2}\right) e^{B^+-A^+}$$

and, similarly,

$$\left(\frac{\dot{g}_3}{f_3} - \frac{\dot{g}_4}{f_4}\right) = \left(\frac{\dot{f}_3}{f_4} - \frac{\dot{f}_4}{f_4}\right) e^{B^--A^-} \quad ,$$

Eqs. (56) can be solved to

$$\dot{C}_1 = \frac{-2}{\varepsilon}\,\dot{y}\,\frac{1 - 1/X^-}{f_1\left(\frac{d\ \ell n\ f_1/f_2}{d\theta}\right)\left(\frac{1}{X^+} - \frac{1}{X^-}\right)} \tag{57}$$

$$\dot{C}_3 = \frac{2}{\varepsilon}\,\dot{y}\,\frac{1/X^+ - 1}{f_3\left(\frac{d\ \ell n\ f_3/f_4}{d\theta}\right)\left(\frac{1}{X^+} - \frac{1}{X^-}\right)} \tag{58}$$

where X^+, X^- are as in Eqs. (31), (32). Also, then

$$\dot{C}_2 = -\frac{f_1}{f_2}\,\dot{C}_1 \quad ; \quad \dot{C}_4 = -\frac{f_3}{f_4}\,\dot{C}_4 \tag{59}$$

From Eqs. (52), (53) it follows that $\frac{d\ \ell n\ f_1/f_2}{d\theta} = \frac{2i}{\varepsilon}\,\dot{K}^+$

and $\frac{d\ \ell n\ f_3/f_4}{d\theta} = \frac{2i}{\varepsilon}\,\dot{K}^-$. Also, f_2 is the complex conjugate of f_1

and, similarly, $f_4 = f_3^*$. Therefore, Eqs. (57) and (59) imply

$$C_2 = C_1^* \tag{60}$$

and, similarly, $C_4 = C_3^*$. (61)

Using the expressions found before for X, K, etc., one can now calculate

$$C_1 = K_1 + \frac{i\nu}{\sqrt{3\nu_T(1-\nu_T)}}\int_0^y e^{-i\,\frac{3}{\varepsilon}\,\theta}\,\frac{\nu_T L - (1-\nu)y}{\sqrt{S(y)}}\,dy \tag{62}$$

where K_1 is an arbitrary (complex) constant and θ is to be regarded for integration as a function of y, which implies specification of

a particular climbout law. Similarly,

$$C_3 = K_3 - i\nu_T L \int_0^y e^{-i\frac{|K^-(\theta)|}{\varepsilon}} \left[\frac{\nu}{3} \frac{y(L-y)}{(\nu_T L+\nu y)[(1-\nu_T)L-\nu y]}\right]^{1/4} \frac{dy}{\sqrt{S(y)}} \qquad (63)$$

where $K^-(\theta)$ is given by Eq. (37).

Finally, since $C_2 f_2 = (C_1 f_1)^*$ and $C_4 f_4 = (C_3 f_3)^*$,

$$x = 2\, R_e(C_1 f_1) + 2\, R_e(C_3 f_3) \qquad (64)$$

$$\delta = \frac{2\, R_e(C_1 f_1)}{X^+} + \frac{2\, R_e(C_3 f_3)}{X^-} \qquad (65)$$

or, after some reduction,

$$X = \frac{2\nu}{\sqrt{S(y)}} \left\{P \cos\left(\frac{\sqrt{3}}{\varepsilon}\theta + \phi\right) + \frac{\nu L}{\sqrt{3}} \int_0^y \sin\frac{\sqrt{3}}{\varepsilon}(\theta'-\theta) \frac{L-Q(y')}{\sqrt{S(y')}} dy' \right\} +$$

$$+ 2 \frac{(L-Q(y))^{3/4}}{\sqrt{S(y)}} \left[\frac{\nu}{3} \frac{y(L-y)}{Q(y)}\right]^{1/4} \left\{R \cos\left(\frac{K^-(\theta)}{\varepsilon} + \psi\right) - \nu_T L \int_0^y \sin\left(\frac{K^-(\theta')-K^-(\theta)}{\varepsilon}\right) x \right.$$

$$\left. x \left[\frac{\nu}{3} \frac{y'(L-y')}{Q(y')(L-Q(y'))}\right]^{1/4} \frac{dy'}{\sqrt{S(y')}} \right\} \qquad (66)$$

$$\delta = \frac{2(L-y)}{\sqrt{S(y)}} \left\{P \cos\left(\frac{\sqrt{3}}{\varepsilon}\theta\ \phi\right) + \ldots\ldots\ldots\ldots\ldots\ldots\ldots\right\} -$$

$$- 2 \frac{\nu_p}{\nu_T} \frac{(Q(y))^{3/4}}{\sqrt{S(y)}} \left[\frac{\nu}{3} \frac{y(L-y)}{L-Q(y)}\right]^{1/4} \left\{R \cos(\quad) \ldots\ldots\ldots\ldots\ldots\right\} \qquad (67)$$

Here we have defined

$$Q(y) = \nu_j L + \nu y \tag{68}$$

and P, R, ϕ and ψ are a new set of arbitrary (real) constants, to be found by imposing the correct boundary conditions.

3. Boundary conditions. Behavior when the ferry is near one end.

For our problem, we will assume the tether is initially deployed along the radial direction, and that the ferry starts out from the lower platform with a relative velocity $\dot{y}(0) = v_0$, in a direction making an angle $\alpha_0 = \lim_{t\to 0} \left(\frac{\dot{x}}{\dot{y}}\right)$ to the local vertical. Thus, the initial conditions are

$$X(0) = 0 \qquad \frac{dx}{dt}(0) = \alpha_0 v_0$$

$$\delta(0) = 0 \qquad \frac{d\delta}{dt}(0) = -\alpha_0 v_0 \tag{68b}$$

We first notice that, from Eq. (67), for $\delta(0) = 0$ we need $P\cos\phi = 0$, and since $P \neq 0$ is required for later matching, we take

$$\phi = -\frac{\pi}{2} \tag{69}$$

such that $\cos\left(\frac{\sqrt{3}}{\varepsilon}\theta + \phi\right) = \sin\left(\frac{\sqrt{3}}{\varepsilon}\theta\right)$. The limiting behavior of the solution for small θ is then

$$x = \frac{2y}{\sqrt{\nu_T(1-\nu_T)}}\left\{\frac{P}{L}\sin\frac{\sqrt{3}}{\varepsilon}\theta + \frac{\nu}{\sqrt{3}}\sqrt{\frac{1-\nu_T}{\nu_T}}\int_0^y \sin\frac{\sqrt{3}}{\varepsilon}(\theta'-\theta)\,dy'\right\} +$$

$$+ \frac{2}{\nu_T^{3/4}} \left[\frac{\nu}{3}\left(\frac{1-\nu_T}{L}\right)\right]^{1/4} y^{1/4} \left\{R \cos\left(\frac{K^-(0)}{3} + \psi\right) - \right.$$

$$\left. - \frac{\left(\frac{\nu\nu_T}{3L}\right)^{1/4}}{\left[1-\nu_T\right]^{3/4}} \int_0^y (y')^{1/4} \sin \frac{K^-(0')-K^-(\theta)}{\varepsilon}\, dy' \right\} \qquad (69b)$$

$$\delta \simeq \frac{2L}{\sqrt{\nu_T(1-\nu_T)}} \left\{ \ldots\ldots\ldots\ldots\ldots \right\} -$$

$$- 2 \frac{\nu_p}{\nu_T^{3/4}(1-\nu_T)^{3/4}} \left(\frac{\nu}{3}\right)^{1/4} \left(\frac{y}{L}\right)^{1/4} \left\{ \ldots\ldots\ldots\ldots\ldots\ldots \right\} \qquad (70)$$

Here, the limiting form of $K^-(\theta)$ can be found from Eq. (37) as

$$K^- \underset{\theta \to 0}{\to} 2\sqrt{\frac{3}{\nu}\, \nu_T\, (1-\nu_T) \left(\frac{L}{v_{0T}}\right)} \sqrt{\theta} \qquad (71)$$

The integral in the first bracket is simply $-v_{0T} \frac{\varepsilon}{\sqrt{3}} (1-\cos \frac{\sqrt{3}}{\varepsilon} \theta)$, and vanishes like θ^2 for small θ. Thus the whole first term in the expression for x (the collective mode) is at least of order θ^2, and does not contribute either to x or to $\frac{dx}{dt}$ near $\theta = 0$. The integral in the second bracket is more involved. As suggested by Eq. (71), we can define a time scale for the fast "bending" oscillations near $y = 0$ as

$$\tau_0 = \frac{\nu}{3\nu_T(1-\nu_T)} \frac{v_0}{\Omega^2 L} \qquad (72)$$

Such that $\frac{K^-(0)}{\varepsilon} = 2\sqrt{\frac{t}{\tau_0}} = 2\sqrt{\frac{y}{v_0\tau_0}}$. The integral is then

$$I = \int_0^y (y')^{1/4} \sin \left[\frac{2}{\sqrt{v_0\tau_0}} \left(\sqrt{y'} - \sqrt{y}\right)\right] dy' \qquad (73)$$

The time τ_0 is much shorter than even the "fast" gravity gradient time $\sim 1/\Omega$, since, from (72), $\Omega\tau_0 = \frac{\nu}{3\nu_T(1-\nu_T)}\left(\frac{v_0}{L}\right)\varepsilon \sim \varepsilon$. Therefore, an intermediate time scale exists such that $\frac{t}{\tau_0} \to \infty$ but still $\theta = \frac{t}{T} \to 0$. We are thus justified in evaluating (73) in an asymptotic form, for large values of $\eta = \frac{y}{v_0\tau_0}$:

$$I = (v_0\tau_0)^{5/4}\int_0^{\eta}(\eta')^{1/4}\sin(2\sqrt{\eta'} - 2\sqrt{\eta})d\eta' \underset{\eta\to\infty}{\to} -(v_0\tau_0)^{5/4}\eta^{3/4} =$$

$$= -v_0^{5/4}\tau_0^{1/2}t^{3/4} \qquad (74)$$

We thus obtain

$$x \underset{t\to 0}{\to} \frac{2}{\nu_T^{3/4}}\left[\frac{\nu}{3}(1-\nu_T)\frac{v_0}{L}\right]^{1/4}Rt^{1/4}\cos\left(2\sqrt{\frac{t}{\tau_0}} + \psi\right) + 2\frac{\nu}{3\nu_T(1-\nu_T)}\frac{v_0^2}{\Omega L}t \qquad (75)$$

and

$$\delta \underset{t\to 0}{\to} \frac{2P}{\sqrt{\nu_T(1-\nu_T)}}\sin\sqrt{3}\,\Omega t + \frac{2\nu L}{3\nu_T\Omega T}(1-\cos\sqrt{3}\,\Omega t) -$$

$$- \frac{2\nu_p}{[\nu_T(1-\nu_T)]^{3/4}}\left(\frac{\nu}{3}\frac{v_0}{L}\right)^{1/4}t^{1/4}R\cos\left(2\sqrt{\frac{t}{\tau_0}} + \psi\right) - \frac{2\nu_p\nu}{3\nu_T(1-\nu_T)^2}\frac{v_0^2 t}{\Omega L} \qquad (76)$$

Now, to complete the determination of constants, we need to examine the behavior on the very short time scale $\tau_0 \sim \varepsilon^2 T$, where our WKB approximation must fail. For this purpose, we go back to the basic equations (24) and (25). In (24), for very short time after the start of the climb, we can replace $\delta \simeq 0$, $\frac{dy}{d\theta} \simeq \frac{v_0}{T}$, $y \simeq 0$:

$$\varepsilon^2\frac{d^2x}{d\theta^2} + 3\frac{\nu_T(1-\nu_T)}{\nu}\frac{x}{v_0T} \simeq 2\varepsilon\frac{v_0}{T} \qquad (77)$$

The homogeneous part of (77) is a Bessel equation in the variable $\sqrt{t}$. A particular solution is obtained by inspection, with $x \sim 0$. altogether, then, one obtains the solution

$$x = 2\Omega v_0 \tau_0 t + D\sqrt{t}\, J_1\left(2\sqrt{\frac{t}{\tau_0}}\right) + E\sqrt{t}\, Y_1\left(2\sqrt{\frac{t}{\tau_0}}\right) \tag{78}$$

where τ_0 is as defined in Eq. (72). Near the origin, $\sqrt{t}\, Y_1\left(2\sqrt{\frac{t}{\tau_0}}\right) \to \frac{1}{\pi}\sqrt{\tau_0}$, while $\sqrt{t}\, J_1\left(2\sqrt{\frac{t}{\tau_0}}\right) \to \frac{t}{\sqrt{\tau_0}}$. Thus, to ensure $x = 0$ at $t = 0$, E must be zero, and we have

$$x = 2\Omega v_0 \tau_0 t + D\sqrt{t}\, J_1\left(2\sqrt{\frac{t}{\tau_0}}\right) \underset{t\to 0}{\to} \left(2\Omega v_0 \tau_0 + \frac{D}{\sqrt{\tau_0}}\right) t \tag{79}$$

Equating the coefficient of t in Eq. (79) to $v_0\alpha_0$ (See Eq. (68)) gives

$$D = \sqrt{\tau_0} v_0 (\alpha_0 - 2\Omega\tau_0) \tag{80}$$

Now, in the intermediate limit $\frac{t}{\tau_0} \to \infty$ (but still $\frac{t}{T} \to 0$), valid for very small ε, we can use the known asymptotic expansion of the Bessel function J_1 to obtain from Eq. (79)

$$x \underset{t/\tau_0 \to \infty}{\sim} 2\Omega v_0 \tau_0 t + \frac{D}{\sqrt{\pi}} (t\tau_0)^{1/4} \cos\left(2\sqrt{\frac{t}{\tau_0}} - \frac{3\pi}{4}\right) \tag{81}$$

This is the outer limit of the inner solution (Eq. (79)), and it must coincide with the inner limit (Eq. (75)) of the outer solution. It can be seen that the term linear in t is already matched; matching of the oscillatory term requires the two conditions

$$\psi = -\frac{3\pi}{4} \tag{82}$$

and

$$R = \frac{D}{2\sqrt{\pi\Omega}} \sqrt{\frac{\nu_T}{1-\nu_T}} \tag{83}$$

or, using Eqs. (80) and (72),

$$R = -\frac{L}{\sqrt{12\pi}} \frac{\sqrt{\nu}}{1-\nu_T} \left(\frac{v_0}{\Omega L}\right)^{3/2} \left(\alpha_0 - \frac{2}{3} \frac{\nu}{\nu_T(1-\nu_T)} \frac{v_0}{\Omega L}\right) \tag{84}$$

Only the constant P remains to be determined, and this must be done using the remaining initial condition $\frac{d\delta(0)}{dt} = -\alpha_0 v_0$. Starting from Eq. (76) one can follow a matching procedure similar to that which led to (84). The result, after some algebra, is

$$P = \frac{\nu}{2\sqrt{3}} \sqrt{\frac{\nu_T}{1-\nu_T}} \frac{v_0 \alpha_0}{\Omega} \tag{85}$$

The final expressions for x and $\delta = x_T - x$ are therefore

$$x = \frac{\nu L}{\sqrt{3}} \frac{y}{\sqrt{S(y)}} \left\{ -\sqrt{\frac{\nu_T}{1-\nu_T}} \frac{v_0 \alpha_0}{\Omega L} \sin(\sqrt{3}\Omega t) + 2 \int_0^y \sin\left[\sqrt{3}\Omega(t'-t) \frac{L-Q(y')}{S(y')} dy'\right] \right\} +$$

$$+ \nu_T L \frac{[1-Q(y)]^{3/4}}{\sqrt{S(y)}} \left[\frac{\nu}{3} \frac{y(L-y)}{Q(y)}\right]^{1/4} \times$$

$$\times \left\{ \frac{1}{\sqrt{3\pi}} \frac{\sqrt{\nu}}{\nu_T(1-\nu_T)} \left(\frac{v_0}{\Omega L}\right)^{3/2} \left(\alpha_0 - \frac{2}{3} \frac{\nu}{\nu_T(1-\nu_T)} \frac{v_0}{\Omega L}\right) \cos\left(\Omega T K^-(\theta) - \frac{3\pi}{4}\right) - \right.$$

$$\left. - 2 \int_0^y \sin\left[\Omega T (K^-(0') - K^-(\theta))\right] \left[\frac{\nu}{3} \frac{y'(L-y')}{Q(y')(L-Q(y'))}\right]^{1/4} \frac{dy'}{\sqrt{S(y')}} \right\} \tag{86}$$

$$\delta = x_T - x = \frac{\nu L}{\sqrt{3}} \frac{L-y}{\sqrt{S(y)}} \left\{ -\sqrt{\frac{\nu_T}{1-\nu_T}} \quad \cdots\cdots\cdots\cdots\cdots \right\} -$$

$$- \nu_p L \frac{(Q(y))^{3/4}}{\sqrt{S(y)}} \left[\frac{\nu}{3} \frac{y(L-y)}{L-Q(y)}\right]^{1/4} \left\{ \frac{1}{\sqrt{3\pi}} \quad \cdots\cdots\cdots\cdots\cdots \right\} \tag{87}$$

4. Discussion of the results.

Examination of these expressions for y approaching L shows that (a) the lag x of the ferry approaches some finite limit, with gravity gradient collective oscillations, also of finite amplitude. The "bending" mode oscillations decay as $(L-y)^{1/4}$.

(b) The differential lag $x_T - x$ has a linearly vanishing component corresponding to gravity gradient oscillations which tend to a constant angular (δ) amplitude. It also has a "bending" mode oscillation which decays in amplitude as $(L-y)^{1/4}$; as we have found from the similar analysis near y = 0, these constitute the asymptotic "tail" of a near-end behavior characterized by either a J_1 or a Y_1 Bessel function.

While near y = 0 the Y_1 component was absent due to the finite initial conditions, there is no guarantee of a similar absence near y = L. A detailed analysis shows solutions of the same sort as near y = 0, i.e.,

$$\delta = \left(\frac{X_T}{L} V_T - 2\Omega V_T \tau_T\right)(T-t) + F\sqrt{T-t}\, J_1\left(2\sqrt{\frac{T-t}{\tau_T}}\right) + G\sqrt{T-t}\, Y_1\left(2\sqrt{\frac{T-t}{\tau_T}}\right) \qquad (88)$$

where x_T and V_T are the values approached by x and $\frac{dy}{dt}$ near y = L, and, similar to the definition of τ_0, the fast local time scale is

$$\tau_T = \frac{\nu}{3\nu_p(1-\nu_p)} \frac{V_T}{\Omega^2 L} \qquad (89)$$

The values of the constant F and G would now be entirely determined by asymptotic matching to the known solution given by Eqs. (86) and (87), and would therefore depend on the climbout law y(t) adopted. While the J_1 part leads to oscillations of finite angular amplitude, the Y_1 part would give a finite limit for the amplitude of δ oscillations, and hence an angular divergence. The object of speed control in the terminal phase of ascent should be to ensure the absence of this divergence. We can easily match (87) and (88) in their common region of validity, by noting that

$J_1(X) \underset{X\to\infty}{\to} \sqrt{\frac{2}{\pi X}} \cos\left(X - \frac{3\pi}{4}\right)$ while $Y_1(X) \underset{X\to\infty}{\to} \sqrt{\frac{2}{\pi X}} \sin\left(X - \frac{3\pi}{4}\right)$. Thus, by comparison to Eq. (86), in order to ensure the absence of the Y_1 term, the phase $\Omega T\, K^{-}(T)$ must approach an integer number of cycles:

$$\Omega\, T\, K^{-}(T) = 2\,\pi\, n \tag{90}$$

or

$$\Omega \int_0^T \sqrt{\frac{3}{\nu} \frac{[L-Q(y)]Q(y)}{(L-y)y}}\, dt = 2\,\pi\, n \tag{91}$$

Since this phase is varying rapidly near the end, fine control of y(t) in that phase should be sufficient to ensure this condition, and hence to prevent wraparound.

It may also be noted that even the <u>bounded</u> fast oscillations may be avoided altogether near both ends if the angle of departure, α_0, and of arrival β_T are related in the appropriate way to the corresponding velocities v_0 and v_T. For the departure phase, this is obvious by inspection of Eq. (80); the condition for smooth take-off is

$$\alpha_0 = 2\,\Omega\,\tau_0 = \frac{2}{3} \frac{\nu}{v_T(1-v_T)} \frac{v_0}{\Omega L} \tag{92}$$

For the arrival phase, a similar simple expression can be arrived at: fast terminal oscillations are avoided if

$$\beta_T = \frac{X_T}{L} - \frac{2}{3} \frac{\nu}{v_p(1-v_p)} \frac{v_T}{\Omega L} \tag{93}$$

5. <u>Some numerical estimates</u>.

The order of magnitude of the various quantities involved can best be appreciated by means of a representative numerical example. Consider the following case:

$L = 200$ Km

$\Omega = 1.158 \times 10^{-3}$ rad/sec (300 Km orbit)

$\nu = \nu_T = 0.1$, $\nu_p = 0.8$

$T = 2.592 \times 10^{5}$ sec (3 days)

$\epsilon = \frac{1}{\Omega T} = 3.332 \times 10^{-3}$

Mean ascent velocity $\bar{V} = 0.7716$ m/sec

Angle α_0 for smooth starting (at $\bar{V}$) : $\alpha_0 = 2.468 \times 10^{-3}$ rad $= 0.141°$

Fast initial time scale τ_0 (at $\bar{V}$) : $\tau_0 = 1.066$ sec

Gravity gradient period $\frac{2\pi}{\sqrt{3\Omega}} = 3133$ sec $= 52.2$ min